UNIVERSITAT ROVIRA I VIRGILI

# SYNTHESIS OF HECTORITES AND SAPONITES WITH MICROWAVES AND THEIR APPLICATION IN CATALYSIS AND COMPOSITES

**Isabel Vicente Valverde**

**ISBN:**
**Dipòsit Legal: T. 1033-2011**

UNIVERSITAT ROVIRA I VIRGILI
SYNTHESIS OF HECTORITES AND SAPONITES WITH MICROWAVES AND THEIR APPLICATION IN CATALYSIS AND COMPOSI
Isabel Vicente Valverde
ISBN:/DL:T. 1033-2011

Isabel Vicente Valverde

# Synthesis of Hectorites and Saponites with Microwaves and their Application in Catalysis and Composites

PhD Thesis

Directed by

Dr. Pilar Salagre Carnero

Dr. Yolanda Cesteros Fernández

Department of Physical and Inorganic Chemistry

UNIVERSITAT ROVIRA I VIRGILI

UNIVERSITAT ROVIRA I VIRGILI
SYNTHESIS OF HECTORITES AND SAPONITES WITH MICROWAVES AND THEIR APPLICATION IN CATALYSIS AND COMPOSI
Isabel Vicente Valverde
ISBN:/DL:T. 1033-2011

UNIVERSITAT ROVIRA I VIRGILI
DEPARTAMENT DE QUÍMICA FÍSICA I INORGÀNICA
Campus Sescelades
Marcel·lí Domingo, s/n
43007 Tarragona
Tel. +34 977 55 81 37
Fax +34 977 55 95 63
www.quimica.urv.es

Dra. Pilar Salagre Carnero y Dra. Yolanda Cesteros Fernández, profesoras titulares del del Departamento de Química Física e Inorgánica de la Universidad Rovira i Virgili,

HACEMOS CONSTAR:

Que este trabajo titulado “Synthesis of Hectorites and Saponites with Microwaves and their Application in Catalysis and Composites”, que presenta Isabel Vicente Valverde, ha sido realizado bajo nuestra dirección en el Departamento de Química Física e Inorgánica de esta Universidad y que cumple los requisitos para poder optar a Mención Europea.

Tarragona, diciembre de 2010

Dra. Pilar Salagre Carnero

Dra. Yolanda Cesteros Fernández

UNIVERSITAT ROVIRA I VIRGILI
SYNTHESIS OF HECTORITES AND SAPONITES WITH MICROWAVES AND THEIR APPLICATION IN CATALYSIS AND COMPOSI
Isabel Vicente Valverde
ISBN:/DL:T. 1033-2011

# Agradecimientos

Quisiera agradecer a las doctoras Pilar Salagre y Yolanda Cesteros por haberme aceptado en su grupo, y por la dirección de esta tesis.

A Pilar gracias por ayudarme a descubrir que tengo paciencia y que de todo se puede sacar algo bueno. A Yolanda, gracias por esa capacidad para los detalles, por tener esa puerta tan cerca.

No sólo mis supervisoras me han transmitido conocimiento, gracias al grupo de Organometálicos y Catálisis Homogénea y también a la Dra. Angels Serra a la que agradezco sus comentarios.

Muchas, muchísimas horas en el laboratorio…
A las gatitas verdes, Dolores, Tatiana y Elena, gracias por hacer tan fácil el trabajo y todos esos momentos compartidos ¡Qué buen verano! A Olga, por haberme introducido en esa maraña de tubos y reactivos en los que nunca faltaron los momentos kit-kat. A Xavi, aunque hubiera que aberroncharse para hacerles hueco, esos cafés valen su peso en trans-trans ¡Plegatín!

Otro tanto en el seminario…
Algunos hace mucho que se hicieron doctores y abandonaron el nido, a ellos gracias porque me enseñaron que los compañeros de trabajo también podían ser amigos: Bianca, Clara, Rosa, Cyril, Eva, Eduardo y Jesús ¡Ah! También Marta, Vanesa e Yvette ¿Chicas, para cuándo la próxima?
Otros muchos siguen allí o casi, hemos compartido tanto…gracias por los muchos buenos ratos pasados, y aunque no lo sepáis, por lo mucho que me habéis enseñado: Alí (te has ganado el cielo mr.), Vero, Ariadna, Angélica y Mercè (venga va ¡Que ya no os queda nada!), Martha (ya lo lograste doctora, ¡Felicidades!). Amadeu, Oriol y Javi: trío de ansiosos ¡Qué miedo! ¡Os deseo prosperidad en vuestras ligas! ¡ A Cristina P(..aulova, nunca el fútbol tuvo tanto estilo), Cristina Solé (o la PDA, multitareas), Sabina (¡Recúperate pronto!), Bernabé (sé que debería ponerte en este párrafo, pero como no te quejarás), Carolina (Ídem) y a Eli, Jessica, Raquel, y Tatiana (las nuevas, ánimos y…¡Suerte!).
Uno se hizo doctor y aún no se va del seminario, gracias Aitor, nunca lo pasé tan bien con el payaso triste.

A ratitos en ingeniería…
Gracias Anna, Antón, Alvarito, Adriana, Alex, Beteley, Chimen, Iuliana, Kaveh, Mayra, Noe, Luis, María, Sandra y Susana por vuestra ayuda ¡Qué bien lo pasamos!

UNIVERSITAT ROVIRA I VIRGILI
SYNTHESIS OF HECTORITES AND SAPONITES WITH MICROWAVES AND THEIR APPLICATION IN CATALYSIS AND COMPOSI
Isabel Vicente Valverde
ISBN:/DL:T. 1033-2011

A veces no es posible hacerlo todo por uno mismo. Es, en esos momentos, que se agradece contar con algunos recursos como los de Jordi o Mª José, las "secres" o los del "Servei de Recursos científics i tècnics" de la Universidad. Gracias a todos.

Cuando me propusieron hacer una estancia en Salamanca, no lo pensé dos veces. Gracias a los Doctores Vicente Rives, Raquel Trujillano y Miguel Ángel Vicente, por haberme acogido en el departamento y haberme enseñado con tanto mimo el mundo de hidrotalcitas y arcillas apilaradas. Gracias Vicente, Raquel, Miguel Ángel, Mar, Dani, Sole, Silvia, Paco, Santis, porque me hicisteis sentir como en casa.

In order to apply for the doctor Europeus Mention I had to spend three months abroad. The destination was the Materials and Engineering Research Institute in Sheffield Hallam University. I want to thank Prof. Chris Breen for accepting me in his group, and for introducing me in the composites world. I also would like to thank Dr. Francis Clegg for his continuous supervision. I met many lovely people there... Thanks to Deeba, Bob, Indira and the rest of the people there for making things easier. Thanks to Khairuddin, Ganesh and all the guys at the office since you made me feel like a little princess. And thank-you Vicky, Fabio and Mike, for all we shared.

Lo que tiene ser aspirante a rata de laboratorio es que en ocasiones olvidas que existe un más acá, menos mal que tienes amigos para recordártelo. Algunas son de hace tantos años que asusta: Gracias Gemma (¡Ay moza, ya eres más gallega que yo!) y Montse (¡Perro ladrador! ¡Gracias por pegarme el tirón de orejas cuando más falta hace!). Poco a poco se fueron uniendo otros: Miriam & Cía (¡Mucha suerte!), Anna y Rubén (Quiero utilizar comas para referirme a vosotros asap), Yolanda (bueno es tener un médico cerca, al otro lado del mundo), Diana (sin vacaciones pero con F1), Fernando (¡Qué bueno haberte conocido! Llamaré a un tuno para que amenice el momento), Idoia (Blu Bambu, Anita Verano, éxtasis de chocolate, las Midlands temblaron y nos echan de menos), Sarah (¡Aún no me creo que sólo hace dos años que nos conocemos!)…Gracias por estar allí ¡Siempre!

A veces dicen que no tengo abuela, sí las tengo, un poco lejos, al igual que el resto de la familia: en Zaragoza, al otro lado de la Península o del charco... Gracias a todos, también a los que os habéis marchado un poco más lejos, por todo el esfuerzo invertido y amor que me habéis dado, es bonito formar parte de algo ¡TAN GRANDE!

Por último y no por ello menos importante, gracias mami y papi (lo seguirán siendo cuando tenga 50 años), por dejar que desarrolláramos nuestra curiosidad científica sin explotar la casa (y aún no sé como lo lograron), Daniela, César ¡Os quiero mucho!

Seguramente habrá alguien que no salga, en ese caso disculpas y gracias porque aunque sin saberlo, me habrás ayudado de algún modo.

UNIVERSITAT ROVIRA I VIRGILI
SYNTHESIS OF HECTORITES AND SAPONITES WITH MICROWAVES AND THEIR APPLICATION IN CATALYSIS AND COMPOSI
Isabel Vicente Valverde
ISBN:/DL:T. 1033-2011

Por largo que sea el camino
siempre empieza con un paso

A journey of a thousand
miles begins with a single step.

*Confucio/Confucius*

UNIVERSITAT ROVIRA I VIRGILI
SYNTHESIS OF HECTORITES AND SAPONITES WITH MICROWAVES AND THEIR APPLICATION IN CATALYSIS AND COMPOSI
Isabel Vicente Valverde
ISBN:/DL:T. 1033-2011

"…But you don't understand, Osgood?
I'm a man!
Well, nobody is perfect."

Some like it hot, 1959.

## Table of contents

# Chapter 3

# Chapter 4

## Saponites and hectorites as catalytic supports for the hydrogenation of styrene oxide

# Chapter 1

## General Introduction & Scope

## 1.1. General Introduction

Clay minerals are widespread materials not only on the Earth but also on Mars (McKeown et al., 2009). There are signs that people already used them many thousands of years ago to create pottery and decorative items. There are references 4500 years old from Mesopotamia in which clays were told to be used for therapeutic purposes like the treatment of wounds and the inhibition of haemorrhages. (Carretero et al., 2006). Nowadays, millions of tons of these minerals are used because of their applications, not only as ceramics in building, abrasive materials, in foundry moulds, in pharmaceuticals and beauty treatments, but also as catalysts, adsorbents or catalytic supports, depending on their properties. Even in nature, they play an important role since their amount determines key parameters in soils (structure, texture, water retention, fertility), because of their important capacity of adsorption and water retention.

Clays are phyllosilicates the layers of which consists of $M(O, OH)_6$ octahedral sheets (where $M=Al^{3+}$, $Mg^{2+}$, $Fe^{3+}$ o $Fe^{2+}$) and tetrahedral sheets mainly composed by Si(O, OH). In both sheets, isomorphic substitution by less charged cations is possible. A couple of examples can be, the hectorite, where $Mg^{2+}$ is partially replaced by $Li^{+}$ in the octahedral positions, or the saponite, where the $Si^{4+}$ from the tetrahedral sheet, can be partially replaced by $Al^{3+}$. This substitution provokes negative charge of layers, which is compensated by cations located in the interlayer space (Vaccari, 1999).

The combination of one tetrahedral sheet and one octahedral sheet (TO), results in layers which form 1:1 clays like kaolinites and serpetinites, while in 2:1 clays, layers are formed by a TOT combination (Figure 1.1-1).

UNIVERSITAT ROVIRA I VIRGILI
SYNTHESIS OF HECTORITES AND SAPONITES WITH MICROWAVES AND THEIR APPLICATION IN CATALYSIS AND COMPOSI
Isabel Vicente Valverde
ISBN:/DL:T. 1033-2011

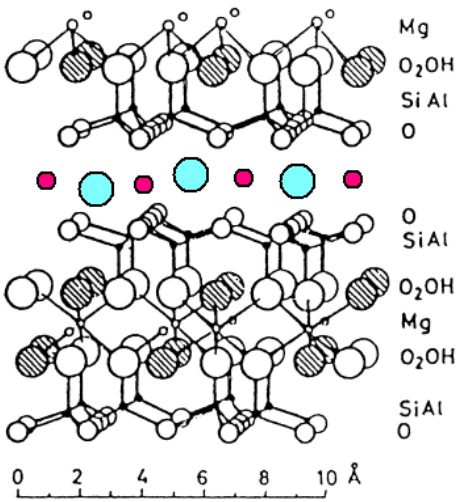


**Figure 1.1-1.** Smectite as example of 2:1 clay structure.

TOT mineral clays can be dioctahedral or trioctahedral depending on the quantity of occupied octahedral positions: that is 2/3 or all the positions, respectively (Pinnavaia, 1983).

General formulae for dioctahedral and trioctahedral mineral clays are:

$$(Si_{8-x}M_x)^T[Al_{4-y}M'_y]^0(OH)_4O_{20}M''^{n+}_{(x+y)/n}\cdot mH_2O$$

$$(Si_{8-x}M_x)^T[Mg_{6-y}M'_y]^0(OH)_4O_{20}M''^{n+}_{(x+y)/n}\cdot mH_2O$$

Where $^T$ and $^O$ refers to tetrahedral and octahedral positions, M and M' have one unit of charge less than the substituted cation and M'', which has an oxidation estate n, is the exchangeable cation located in the interlayer space. Table 1.1-1 summarises general formulae and examples of different 2:1 clays.

UNIVERSITAT ROVIRA I VIRGILI
SYNTHESIS OF HECTORITES AND SAPONITES WITH MICROWAVES AND THEIR APPLICATION IN CATALYSIS AND COMPOSI
Isabel Vicente Valverde
ISBN:/DL:T. 1033-2011

**Table 1.1-1.** Classification of some 2:1 clay minerals. (Kloprogge et al., 1999).

| Mineral group | Dioctahedral | Trioctahedral |
|---|---|---|
| Pyrophillite Talc | Pyrophillite: $(Si_{8.0})\ [Al_{4.0}]\ (OH)_4O_{20}$ | Talc: $(Si_{8.0})\ [Mg_{6.0}]\ (OH)_4O_{20}$ |
| Smectites X: 0.4-1.2 | Montmorillonite: $(Si_{8.0})\ [Al_{4.0-x}Mg_x]\ (OH)_4O_{20}M^{n+}_{x/n}\cdot mH_2O$ | Hectorite: $(Si_{8.0})\ [Mg_{6.0-x}Li_x]\ (OH.F)_4O_{20}M^{n+}_{x/n}\cdot mH_2O$* |
| | | Stevensite: $(Si_{8.0})\ [Mg_{6.0-x}Vacancy_x]\ (OH)_4O_{20}M^{n+}_{x/n}\cdot mH_2O$ |
| | Beidellite: $(Si_{8.0-x}Al_x)\ [Al_{4.0}](OH)_4O_{20}M^{n+}_{x/n}\cdot mH_2O$ | Saponite: $(Si_{8.0-x}Al_x)\ [Mg_{6.0}]\ (OH)_4O_{20}M^{n+}_{x/n}\cdot mH_2O$ |
| | Nontronite: $(Si_{8.0-x}Al_x)\ [Mg_{4.0}](OH)_4O_{20}M^{n+}_{x/n}\cdot mH_2O$ | |
| Micas | Muscovite: $[Al_{4.0}](Si_{6.0}Al_{2.0})(OH)_4O_{20}K_2$ | Flogopite: $[Mg_{6.0}](Si_{6.0}Al_{2.0})(OH)_4O_{20}K_2$ |

*In this clay some hydroxyl groups can be replaced by $F^-$

Properties of clay minerals depend on their composition and particle size. The specific surface area decreases as the particle size increases. The typical properties of smectites are the interlayer swelling (Stepkowska et al., 2004), and the cation exchange, which can be quantified as cation exchange capacity (CEC) (Bergaya and Vayer, 1997; Czímerová et al., 2006). Clays can present Brønsted and Lewis acidity. Brønsted acid sites are related to –OH groups, whereas Lewis acidity comes from interlayer cations and cations from deficiently coordinated layers.

Smectites have been extensively applied in adsorption processes (Vico and Acebal, 2006; Zielke and Pinnavaia, 1988) from the early years of twentieth century. Afterwards, smectites were also applied in catalytic processes. (Aggarwal et al., 2006; Moreno et al. 1996; Varma, 2002). Nowadays, their use has risen because it is possible to design the material for a specific purpose.

Smectites have been applied to:

- Organic synthesis as catalyst or catalytic supports of the following reaction types: condensation, oxidation, acylation, addition, isomerisation, oligomerisation, esterification, Friedel-Crafts, Diels-Alder, Heck, Suzuki or asymmetric reactions (Békássy et al., 2000, 2007; Cseri et al., 1996; Farkas et al., 2000, 2002; Guidotti et al., 2009; Kawasaki et al., 2009; Nagendrappa, In press; Sento et al., 1999).

- Photocatalysis, by using them with metal salts or metal oxides such as zinc oxide (Robertson and Bandosz, 2006), copper oxide (Chmielarz et al., 2006), titania (Spagnuolo et al., 2004; Ma et al., 2010) or iron (II) acetylacetonate (Herney-Ramirez et al., In press).

- Radiactive waste treatment, by adsorption of Th (IV), U (VI) and Eu (III) radioactive cations of contaminated waters. (Guerra et al., 2010; Pshinko et al., 2010; Schlegel and Descostes, 2009).

- In the pharmaceutical industry, as excipients or for controlled drug delivery. (Carretero and Pozo, 2009; Viseras et al., 2010).

- The preparation of nanocomposites with polymers because of the improvements in the stiffness and the toughness, the enhancement of barrier properties, and the resistance to fire and ignition of resulting materials. (Alexandre and Dubois, 2000; Liff et al., 2007; Liu and Breen, 2005;Seydibeyoğlu et al., 2010).

UNIVERSITAT ROVIRA I VIRGILI
SYNTHESIS OF HECTORITES AND SAPONITES WITH MICROWAVES AND THEIR APPLICATION IN CATALYSIS AND COMPOSI
Isabel Vicente Valverde
ISBN:/DL:T. 1033-2011

In order to have reproducible mineral clay for these applications, smectites must be synthesised. However, their synthesis often involves long hydrothermal treatments. The use of microwaves during the clay synthesis could decrease the synthesis time and confer special features to the obtained materials.

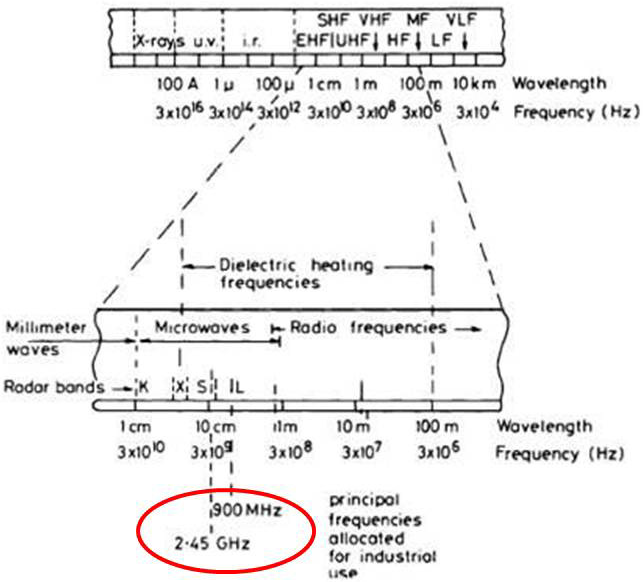


**Figure 1.1-2.** Electromagnetic spectrum. The main frequencies for the heating are indicated in red.

Microwaves are electromagnetic waves with wavelengths ranging from as long as one meter to as short as one millimetre, or equivalently, with frequencies between 300 GHz and 300 MHz (0.3 GHz, Figure 1.1-2). The magnetron device, which generates fixed-frequency microwaves, was designed during the XX War World as part of RADAR development. At that time it was observed that microwaves could heat water very fast. First microwave ovens appeared in the fifties of former century but it was not until 30 years later that their home application become usual. In order not to interfere with RADAR and radio

frequencies, microwaves ovens use a fix frequency of 5100, 2450 and 900 MHz, (Figure 1.1-2) (Kingston et al., 1997).

The great potential of this technique applied to the preparation of materials is the decrease of the synthesis time or temperature and the introduction of structural modifications in the obtained compounds. Microwaves have been extensively used for organic synthesis (Calvino-Casilda et al., 2003, 2009; Kappe, 2004; Martín-Aranda et al., 1997; Perozo-Rondon et al., 2006), in the preparation of zeolites (Romero et al., 2004), hydrotalcites (Benito et al., 2006, 2009; Bergadà et al., 2007a, 2007b) and mesoporous materials (Tompsett et al., 2006) but there are very few references about the use of microwaves in the synthesis of clay minerals (Trujillano et al., 2010, In press).

## 1.2. Scope

There is an increasing interest in mineral clays due to their important technological applications such as for nanocomposites preparation or in catalysis. The use of natural clays for these applications has significant limitations due to the non-uniformity of their chemical composition. However, conventional clays preparation methods often involve hard hydrothermal treatments (pressure, temperature) at long preparation times (from hours to days). The use of microwaves for the synthesis of materials can contribute to decrease the temperature and time of preparation, with the subsequent energy saving, and can involve the obtention of different properties in the solids.

The main objective of this thesis was to synthesise hectorite and saponite with microwaves and apply them to catalysis and composites. Our partial objectives were:

- To synthesise hectorite using microwaves radiation. Study of the influence of using microwaves, the aging time, the temperature of microwave aging and the crystallinity of brucite.

- To study different ways to obtain purer hectorite and to check the influence of these procedures on the properties of purified samples. Obtention of purer hectorite by decantation or treatment of impure hectorite with $Na_2CO_3$, and by decreasing the $SiO_2$ content with respect to the rest of reagents in the starting slurry.

- To synthesise saponite using microwave radiation. Study of some preparation parameters, such as the heating time, the pH of the initial slurry by using different reactants sources and the presence of fluorides, to establish their influence on the resulting saponites.

- To evaluate the catalytic behaviour of hectorite-supported nickel and saponite-supported nickel catalysts for the hydrogenation of styrene oxide to 2-phenylethanol. Study of the influence of microwave or conventional aging during clay synthesis, the presence of amorphous silica in clays and the presence of acid sites, in competition with metal sites.

  Ni/hectorite and Ni/saponite catalysts were obtained by impregnation with different nickel contents or by cation exchange.

- To study the feasibility of using microwaves synthesised hectorite in the formation of composites with commercial polyurethane compared to the behaviour using commercial hectorite (Laponite). Study of the interaction of clays with soft and hard segments of polyurethane.

- To characterise all samples by X-ray diffraction (XRD), $N_2$ adsorption, cation exchange capacity (CEC) determination, magic angle spinning-nuclear magnetic resonance (MAS-NMR), infrared spectroscopy (FTIR), UV/Vis spectroscopy, X-ray fluorescence (XRF), energy dispersive X-ray (EDX), inductively coupled plasma (ICP), scanning electron microscopy (SEM), transmission electron microscopy (TEM), thermogravimetric analysis (TGA), temperature-programmed reduction (TPR) and thermo mechanical dynamic analysis.

# Chapter 2

Experimental section

In this chapter, the basis and the experimental conditions of the techniques used to synthesise and characterise the samples are indicated. The preparation conditions of hectorites, saponites, clay supported nickel catalysts, and composites will be displayed in the corresponding chapters.

## 2.1. Microwaves technology

When applying microwaves, the heating of watery samples is mainly produced through two mechanisms: Dielectric polarisation and dipolar polarisation. The heating by dielectric polarisation is due to the inability of partially bound charges to follow the rapid changes in a high frequency electric field. In the dipolar polarisation mechanism, the polar molecules rotate to get oriented with the electromagnetic field produced by the microwaves radiation resulting in frictions among them that generate an increase in the temperature of the sample (Kingston and Haswell, 1997, Figure 2.1-1). For a typical frequency of 2450 MHz the alignment of molecules followed by their relaxation occur 4.9 x $10^9$ times/s, resulting in a fast heating. Because of the high rate of heating, hot spots may occur.

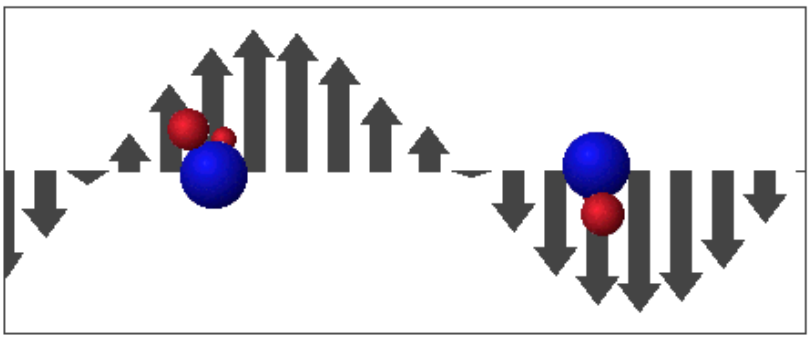

**Figure 2.1-1.** Water molecule rotation through the dipolar rotation mechanism because of the electric field generated by the microwaves.

UNIVERSITAT ROVIRA I VIRGILI
SYNTHESIS OF HECTORITES AND SAPONITES WITH MICROWAVES AND THEIR APPLICATION IN CATALYSIS AND COMPOSI
Isabel Vicente Valverde
ISBN:/DL:T. 1033-2011

In this study the aging procedure during hectorites and saponites synthesis were performed in laboratory microwave equipment Milestone Ethos Touch Control (Figure 2.1-2). 6 autoclaves of 85 mL capacity, containing 50 mL of slurry each one, were placed in a 6-positions rotor. Temperature was controlled with a thermowell placed in one of the autoclaves. Maximum microwave power used was 600 W. In order to maximise the homogeneity of heating, all the autoclaves were magnetic stirred and the rotor turned while the equipment was working.

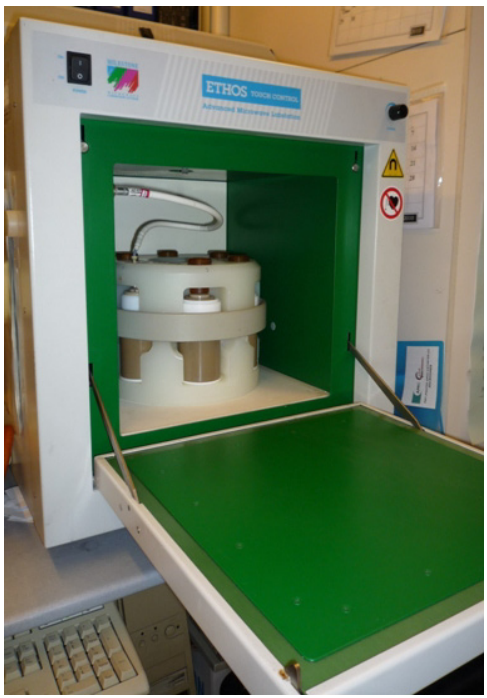


**Figure 2.1-2.** Microwave equipment (Milestone Ethos Touch control).

UNIVERSITAT ROVIRA I VIRGILI
SYNTHESIS OF HECTORITES AND SAPONITES WITH MICROWAVES AND THEIR APPLICATION IN CATALYSIS AND COMPOSI
Isabel Vicente Valverde
ISBN:/DL:T. 1033-2011

## 2.2. Characterisation techniques

### *2.2.1. X-ray diffraction (XRD).*

X-ray diffraction is widely used to identify bulk phases and to estimate crystallite sizes (Cohen and Schwartz, 1977). X-rays have wavelengths in the Å range, which are sufficiently energetic to penetrate solids and well suited to probe their internal structure.

XRD measurements of synthesised clays and clay-supported nickel catalysts were made using a Siemens D5000 diffractometer (Bragg–Brentano parafocusing geometry and vertical θ–θ goniometer) fitted with a curved graphite diffracted-beam monochromator and diffracted-beam Soller slits, a 0.06° receiving slit, and scintillation counter as a detector. The angular 2θ diffraction range was between 2 and 70°. Sample was dusted on to a low background Si(510) sample holder. The data were collected with an angular step of 0.05° at 3 s per step and sample rotation. $Cu_{k\alpha}$ radiation was obtained from a copper X-ray tube operated at 40 kV and 30 mA.

The X-ray diffraction patterns of powder clay samples were analysed using the Fundamental Parameters Approach convolution algorithm (Cheary and Coelho, 1992) as implemented in the program TOPAS 3.0 (Coelho, 2005). This approach calculates the contribution to the peak width produced by a specific instrument configuration.

Crystallite sizes were calculated from the net integral breadth of the peaks, βi, (Stokes and Wilson, 1942) according to the following formula that comes from the Scherrer expression: $\beta i=\lambda/\varepsilon\cos\theta$ were λ is the X-ray wavelength, ε is the

crystallite size and θ is the Bragg angle. 001 reflection was selected to determine the basal spacing of the samples, and to estimate the crystallite size in the stacking direction. 060 reflection was used to calculate the crystallite size of the sample sheets. Moreover through the d(060) value it was possible to determine whether a clay was dioctahedral (0.148 nm < d(060) < 0.152 nm)) or trioctahedral when d(060)≥0.152 nm. Nickel crystallite size was calculated from reflection 111 of metallic nickel phase for clay supported nickel catalysts.

In order to evaluate the amount of amorphous silica in hectorite samples, the starting cell parameters of hectorite used were a: 5.2401 Å, b: 9.0942 Å, c: 10.7971 Å andβ: 99.207° with the space group C2/m (Breu et al., 2003). The crystal structure of hectorite was not used for quantitative analysis because it was described with heavy cations that are not present in the current samples. For brucite, we took the cell parameters of ICDD card 44-1482: a: 3.1442 Å and c: 4.777 Å with the space group P-3m1. For amorphous $SiO_2$, we used an isolated broad peak located at ~22.8° 2θ. The 2θ position of this amorphous halo was previously adjusted with a pure sample of amorphous $SiO_2$.

The reflections of smectites present an anisotropic peak broadening due to the plate shape of smectites particles: (00l) reflections usually present different width that those (hk0) reflections.

The refined parameters that were allowed to vary with the individual profiles included cell parameters, constrained peak position of amorphous $SiO_2$, linear background function, zero error, and the integral breadth of a Lorentzian profile to describe the extent of particle size induced broadening. The anisotropic peak broadening of hectorite was modelled fitting a spherical harmonic function

implemented in the software. Figure 2.2-1 shows one example of refined diffraction pattern.

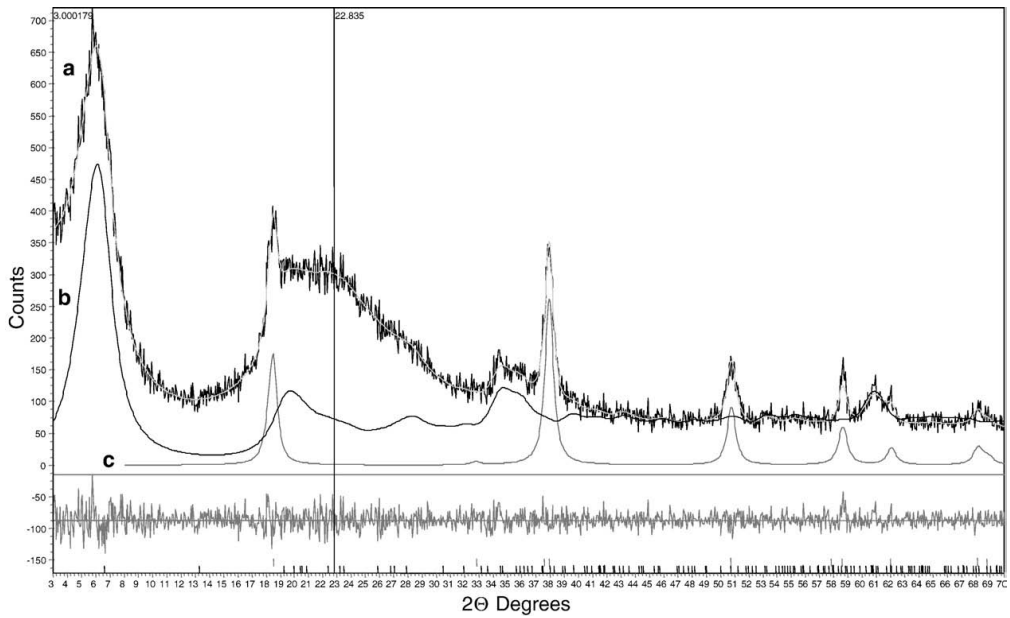


**Figure 2.2-1.** (a) XRD pattern of one hectorite sample, b) hectorite contribution, (c) brucite contribution and amorphous $SiO_2$ (vertical line at 2θ =22.8°).

The mass fraction of hectorite, brucite and $SiO_2$ was indirectly derived from the integrated intensity of all reflections that appear in the 2-theta range measured. We related the relative integrated intensity of hectorite and amorphous $SiO_2$ to previous chemical analysis in such a way that a direct relationship was found between intensity and chemical analysis.

In the case of clay samples dispersed in polyethylene glycol 600 (PEG 600) and the composite samples, XRD measurements were made using a Panalytical Philips diffractometer (Bragg–Brentano parafocusing geometry and vertical θ–θ goniometer) fitted with ½º divergence slit, 1º anti-scatter slit, gold mask of 15º and a curved graphite diffracted-beam monochromator. The angular 2θ

diffraction range was between 2 and 35°.

Swollen samples with PEG600 were obtained by preparing a suspension containing: 4 g of water, 0.1 g of PEG 600 and 0.2 g of clay. This suspension was stirred for 24 h. Approximately 1 mL of this suspension was poured onto a glass slide. Regarding composite samples, approximately 1 mL of suspension was poured onto a glass slide. The data were collected with an angular step of 0.05° at 2 s per step and sample rotation. $Cu_{k\alpha}$ radiation was obtained from a copper X-ray tube operated at 40 kV and 40 mA.

### *2.2.2. $N_2$ adsorption*

$N_2$ physisorption is one of the oldest techniques in surface characterisation. Continued addition of nitrogen gas molecules at 77 K after the monolayer formation leads to the gradual stacking of multiple layers (or multilayer) on top pores become completely filled with adsorbate (Van Santen et al., 2000).

Adsorption isotherms (graphic representation of the volume of adsorbed $N_2$ vs. $N_2$ relative pressure) describe the macroscopic consequence of these interactions.

The majority of isotherms, which result from physical adsorption, may conveniently be grouped into five classes originally proposed by Brunauer, Deming, and Teller. The essential features of these types are indicated in Figure 2.2-2.

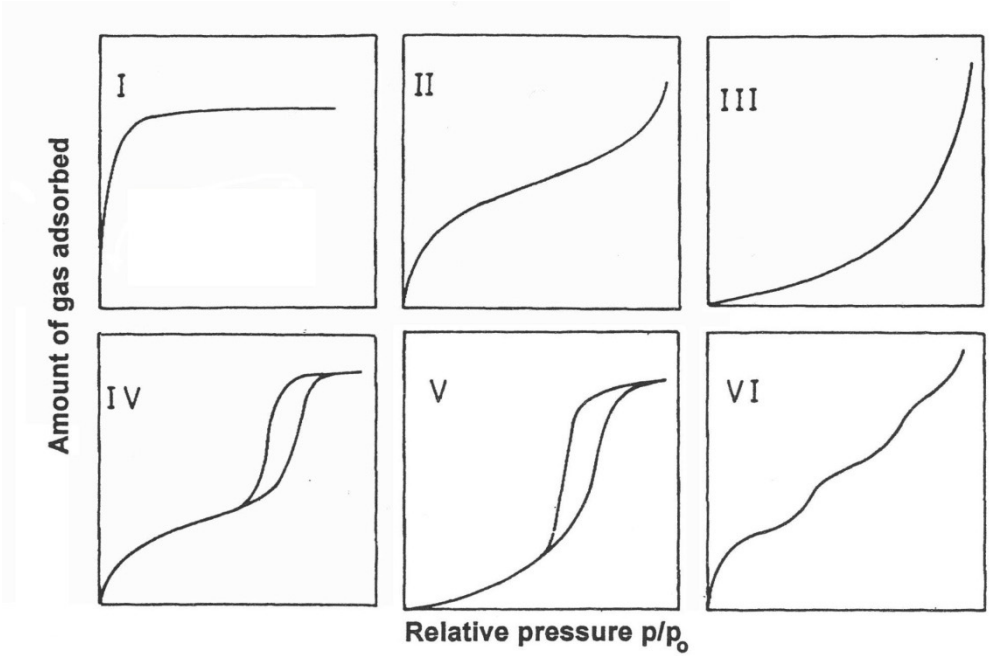


**Figure 2.2-2.** The six types of adsorption isotherms following the Brunauer, Deming, and Teller notation.

- Isotherm I is typical of microporous solids with very low external surface. (molecular sieves and activated carbons).

- Isotherm II represents multilayer physisorption on a flat surface (nonporous or macroporous solids).

- Isotherm III is characteristic of weak gas solid interactions.

- Isotherm IV is characteristic of multilayer adsorption accompanied by capillary condensation in mesopores.

- Isotherm V is similar to that of isotherm III but it reflects the existence of mesoporous in the sample.

UNIVERSITAT ROVIRA I VIRGILI
SYNTHESIS OF HECTORITES AND SAPONITES WITH MICROWAVES AND THEIR APPLICATION IN CATALYSIS AND COMPOSI
Isabel Vicente Valverde
ISBN:/DL:T. 1033-2011

- When the surface of a nonporous adsorbent is energetically uniform, the isotherm may have a step-like shape (Isotherm VI).

Hysteresis between adsorption and desorption is typical of isotherms IV and V. According to de Boer, there are 5 different types of hysteresis depending on the pore shape (Figure 2.2-3).

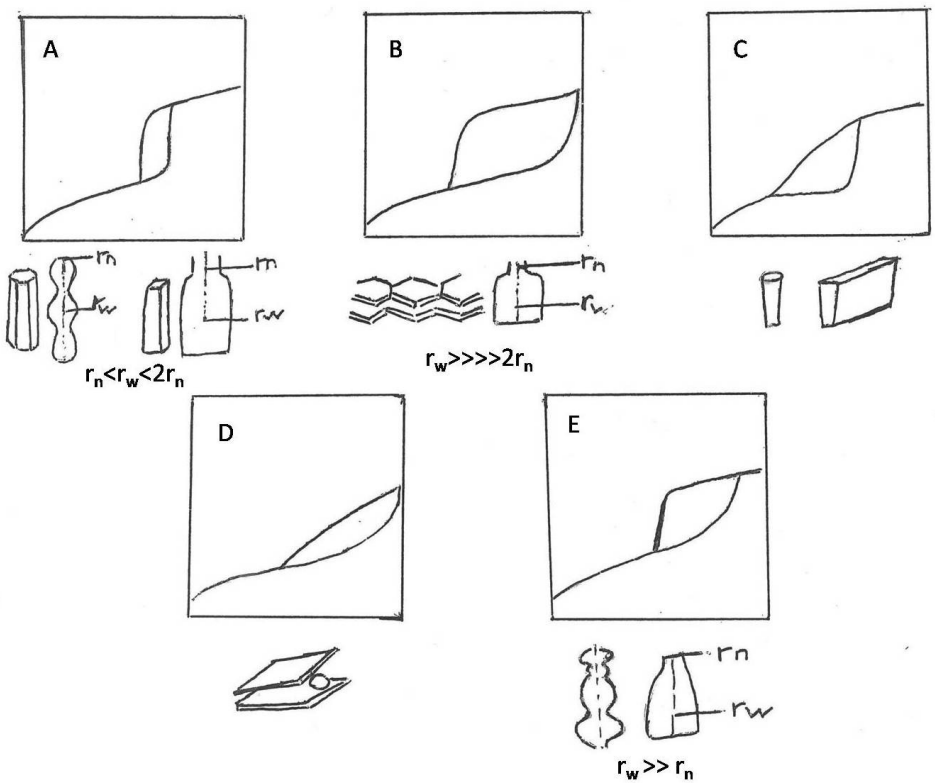


**Figure 2.2-3.** The five types of hystheresis of adsorption isotherms following the Boer notation.

ISBN:/DL:T. 1033-2011

- Hysteresis A is related to, open on both sides, tubular pores.

- Hysteresis B is related to pores formed by parallel crystalline layers separated by small particles or by crystalline defects.

- Hysteresis C and D come from type A and B, respectively. Type C is related to conic pores and type D is related to pores formed by non parallel layers. Both are quite difficult to be found.

- Hysteresis E indicates the presence of neck bottle shaped pores. This means that pores are wide but with a narrow neck.

On the basis of the well-known Brunauer, Emmett and Teller (BET) theory, one can estimate the sample's surface area from the monolayer volume (Vm):

$$V/Vm= c(p/po)/[(1-p/po)(1-(1-c))(p/po)]$$

Where V is the volume of gas adsorbed, Vm is the volume of the gas adsorbed in the monolayer and po is the vapour pressure above the macroscopically thick layer of the pure liquid on the surface. The c value approximates to $\exp -(\Delta H_d - H_{vap})/RT$, in which the $\Delta H_d$ is the enthalpy of adsorption on the first adsorbed layer and $H_{vap}$ is the heat of vaporisation.

For these measurements we used a Micromeritics ASAP 2000 apparatus. Samples were first activated in vacuum at 353 K. Analysed quantity was that one enough to have an absolute area ≥ 10 $m^2$.

### *2.2.3. Cation exchange capacity (CEC)*

Cation exchange capacity (CEC) gives information about the number of interlayer exchangeable cations. The magnitude of cation exchange capacity (CEC) is commonly measured in terms of milliequivalents of exchangeable cations per 100 g of solid.

Cation exchange capacity (CEC) of hectorites and saponites was determined by the method reported by Bergaya and Vayer (1997) as follows: 200 mg of clay mineral were poured in 25 mL of a 0.01 M $[Cu(ethylenediamine)_2]^{2+}$ solution. The suspension was stirred for 2 h. Afterwards the supernatant was separated by centrifugation for twice. The concentration of $[Cu(ethylenediamine)_2]^{2+}$ remaining in the solution was determined by UV-Vis spectroscopy at λ=547 nm. The same method was followed for silica (CEC < 5 meq/ 100 g sample).

### *2.2.4. Magic angle spinning-nuclear magnetic resonance MAS–NMR*

Since nuclear magnetic resonance (NMR) was discovered, it has emerged as one of the most powerful tools in research for characterising structure. The observation of the transition frequency measured in the NMR spectrum for an atomic nucleus is a very sensitive probe of its environment (Kloprogge et al., 1994a; Levin et al., 2004; Pruski et al., 1976).

Magnetic nuclei can absorb radio frequency energy when placed in a magnetic field of a strength specific to the identity of the nuclei. When this absorption occurs, the nucleus is described as being in resonance. Different atomic nuclei within a molecule resonate at different (radio) frequencies for the same magnetic field strength.

High-resolution solid NMR spectra can be achieved when line broadening phenomena due to chemical shift, dipolar paramagnetic and quadrupolar interactions are removed or reduced. This can be done by Dipolar Decoupling (DD), Multiple Pulse Sequences (MPS), and Magic Angle Spinning (MAS). This last technique, discovered by Andrew et al. (1959) and Lowe (1959), is now the one that is most commonly used because line broadenings due to dipolar interactions and chemical shift anisotropy can be reduced to their isotropic values by rotating the sample quickly about an axis inclined at the angle =54º44' (magic angle spinning). Thus, application of MAS is sufficient to remove the chemical shift anisotropy and any small dipolar interaction, and to narrow quadrupolar broadened lines.

$^{27}$Al-MAS-NMR spectra of clays can provide direct information on Al coordination: A signal around 60 ppm is observed for tetrahedral aluminium and a signal around 0 ppm is observed for tetrahedral aluminium that can be in layer or interlayer positions (Sanz, 2006).

$^{27}$Al-MAS-NMR spectra of saponites were obtained on a Bruker AV400 spectrometer. A 4mm BL4 MAS probe was used with the samples spun at 10 kHz at the magic angle, using pulses < PI/12 with a time between pulses of 1 s. Chemical shits are given in ppm relative to $[Al(H_2O)_6]^{3+}$ (0 ppm).

### *2.2.5. Infrared spectroscopy (FTIR)*

Fourier transform infrared (FTIR) technique is one of the most commonly used surface characterisation tools basically because of its low cost and simplicity. When structural units and groups of solids absorb infrared radiation, they experiment a variation in their dipolar momentum, which is a consequence of

their vibration and rotation movements. Infrared spectra wavelengths range from 0.78 to 1000 μm, however FTIR spectroscopy has been mainly used in the middle infrared region (MIR) where the fundamental vibrational models appear and corresponds to wavelengths between 2.5 to 25 μm or to 4000 and 400 $cm^{-1}$, respectively (Rusell and Fraser, 1994; Petit, 2006).

Transmission Infrared spectra of clays were recorded on a Bruker-Equinox-55 FTIR spectrometer. The spectra were acquired by accumulating 32 scans at 4 $cm^{-1}$ resolution in the range of 400–4000 $cm^{-1}$. Samples were prepared by mixing the powdered solids with FTIR grade KBr in pellets in a weight ratio of 1:250, and dried in an oven before measurements.

Diffuse reflectance infrared Fourier transform spectra (DRIFTS) of clays were recorded on a Nicolet Magna 860 FTIR spectrometer using DRIFTS accessory. Samples were dispersed at 5 % wt. in FTIR grade KBr (Aldrich). (0.015 g+ 0.285 g KBr). The system was purged with air. The number of scans was set at 60 with a resolution of 4 $cm^{-1}$, in the range 4000–600 $cm^{-1}$.

### *2.2.6. UV/Vis spectroscopy*

UV/VIS spectroscopy is a technique for determining the chemical species of a dissolution. A light beam of a certain wavelength range interacts with the sample and the intensity of the transmitted or reflected signal is recorded as a function of the wavelength. Because of the interaction with the sample, at certain frequencies the light is absorbed resulting in absorption peaks in the spectrum. The absorption frequencies are specific for certain chemical compounds and associated with their electron transitions. The chemical composition of the sample can therefore be determined by analysing the spectrum using standards

that allow quantitative measurement. The basis of this theory is the Lamber-Beer law:

$$A=\varepsilon bc$$

Where A is absorbance, Ɛ is the molar absorbtivity (L $mol^{-1}$ $cm^{-1}$), b is the path length of the sample (cm) and c is the concentration of the compound in solution ($L^{-1}$).

Absorbance of $[Cu(ethylenediamine)_2]^{2+}$ solutions were analysed using a Shimadzu spectrometer at 547 nm.

### *2.2.7. X-ray fluorescence (XRF)*

X-ray fluorescence (XRF) is the characteristic emission of secondary electrons from a material that has been excited by bombarding with high-energy X-rays or gamma rays (Van Santen et al., 2000). The phenomenon is widely used for elemental analysis and chemical analysis, particularly in the investigation of metals, glass, ceramics and building materials, and for research in geochemistry, forensic science and archaeology.

In order to determine the content of Si, Mg, N or Al of clay samples, X-ray fluorescence (XRF) experiments were obtained with a Philips PW-2400 sequential XRF analyser with Phillips Super Q software. Analyses were made by triplicate for each sample.

### *2.2.8. Inductively coupled plasma (ICP)*

Inductively coupled plasma atomic emission spectrometry (ICP-AES, or ICP), often referred to simply as ICP, is a multi-element analysis technique that uses an inductively coupled plasma source to dissociate the sample into its constituent atoms or ions, exciting them to a level where they emit light of a characteristic wavelength. A detector measures the intensity of the emitted light, and calculates the concentration of that particular element in the sample.

When undergoing ICP analysis, the sample experiences temperatures as high as 10000 K, where even the most refractory elements are atomised with high efficiency. As a result, detection limits for these elements can be orders of magnitude lower with ICP than with FAAS techniques, typically at the 1-10 parts-per-billion level.

In order to determine the content of Li or F of clay samples, experiments were obtained with a Perkin Elmer Optima 4300 D analyser. Analyses were made by triplicate for each sample.

### *2.2.9. Scanning electron microscopy (SEM), energy dispersive X-ray (EDX)*

Electron microscopy is a rather straightforward technique to determine the size and shape of materials (Van Santen et al., 2000).

When a beam of electrons hits the sample, electrons can pass through or gradually lose their energy until absorbed. In this process, low secondary electrons are ejected. Furthermore, a portion of incident electrons are back-scattered.

Scanning electron microscopy (SEM) is carried out by rastering a narrow electron beam over the surface and detecting the yield of either secondary or back-scattered electrons.

Contrast is caused by the orientation: parts of the surface facing the detector appear brighter than parts of the surface normal pointing away from the detector. The secondary electrons have low energies (10-50 eV) and originate from the surface of the sample. Back-scattered electrons come from deeper and carry information on the composition of the sample, because heavy elements are more efficient scatterers and appear brighter in the sample.

Scanning electron micrographs of clays were obtained with a JEOL JSM-35C scanning microscope operating at an accelerating voltage of 20 kV, work distance (wd) of 8 mm, and magnification values in the range 20,000–50,000×.

An electron microscope offers additional possibilities for analysing the sample. When a focused beam of electrons irradiates the sample, x-rays are emitted which have an energy characteristic of the parent element.

The difference between EDX and XRF is the type of radiation hitting the sample. EDX uses an electron beam while XRF uses an x-ray beam. Due to the small beam size possible with electrons, elemental analysis can be obtained for volumes as small as one μm in diameter.

Si, Mg, N or Al contents on synthesised-clay surface were quantified by energy dispersive X-ray experiments (EDX) were performed on a scanning electron microscope, JEOL JSM6400, operating at accelerating voltage of 15 kV and work distances of 15 mm. All samples were covered with a graphite layer. Accumulating time was 120 seconds.

### *2.2.10. Transmission electron microscopy (TEM)*

Electrons have characteristic wavelengths in the range 0.1-1 nm (visible light: 400-700 nm), and come close to seeing the atomic detail (Van Santen et al., 2000).

Transmission electron microscopy (TEM) uses transmitted electrons. A TEM instrument is very similar to an optical microscope, if one replaces optical by electromagnetic lenses.

In a TEM, a high intensity primary electron beam passes through a condenser to produce parallel rays, which impinge on the sample. When a beam of electrons hits the sample, electrons can pass through or gradually lose their energy until absorbed. Furthermore, a portion of incident electrons are back-scattered. An objective aperture placed on the through side of the material filters out the scattered electrons so that only those electrons that passed through the sample are imaged. Consequently, those materials composed of light atoms like carbon allow a lot of electrons to pass through without scatter and appear as bright fields, while heavy elements are more efficient scatterers and appear as dark fields.

The transmission electron microscopy of clays and clay-supported nickel catalysts was performed on a JEOL 1011 operated at an accelerating voltage of 80 kV and magnification values of 200-800 k. Samples were dispersed in ethanol, and a drop of resultant suspensions were poured on carbon coated-copper grids.

### *2.2.11. Thermogravimetric analysis (TGA)*

The fundamental of this technique is the variation of weight when a sample is subjected to thermal treatment in a particular environment ($O_2$, $N_2$). The decomposition steps of samples can be observed throughout the graphic representation of weight variation vs. temperature. The first derivative of this curve permits to better differentiate these steps (Van Santen et al., 2000).

Experiments of clays and composites films were performed using a thermoanalyser Mettler Toledo TG 500. In each case, a 15 mg sample was heated under a nitrogen flow rate of 100 mL/min at a heating rate of 20 K/min from room temperature to 1273 K.

### *2.2.12. Temperature-programmed reduction (TPR)*

Temperature-programmed reduction (TPR) is a useful technique for the characterisation of metal oxide catalysts. During a TPR experiment the solid under investigation is placed in a fixed-bed reactor and exposed to a reducing mixture (5% $H_2$/Ar) that continuously perfuses the catalyst bed, while the temperature is increased according to a linear temperature programme. The difference between the inlet and outlet concentration of the gas mixture is measured as a function of time using a thermal conductivity detector. The resulting TPR contains qualitative information on the oxidation state of the reducible species present allowing the researchers to better know about the reducibility and surface properties of the catalyst (Van Santen et al., 2000).

TPR experiments of several clay-supported NiO precursors were carried out using a TPD/R/O 1100 (Thermo Finnigan) equipped with a programmable temperature furnace and a calibrated TCD detector. Experiments were

performed with 5 % $H_2$/Ar flowing through the sample, that was heated from 303 K to 1173 K at 10 K/min.

### *2.2.13. Thermo mechanical dynamic analysis*

Thin film dynamic mechanical analysis was performed to determine the effect of hectorite concentration on the nanocomposite thermomechanical properties.

Dynamic mechanical analysis (DMA) is performed on polymers in order to determine the elastic energy storage and viscous energy dissipation properties of the polymer as a function of time and temperature. In thin-film DMA a composite film is held in tension with its top end connected to a stationary clamp and the other end attached to a clamp on an oscillating, retractable drive shaft. The entire assembly sits within a furnace. The oscillating stress or strain amplitude, oscillating frequency, and temperature can all be controlled and the thin-film thermomechanical properties, i.e. the flexural storage modulus, the flexural loss modulus, and the loss tangent, are determined whereas material thermal transitions are inferred (Liff et al., 2007).

The stress, a, is defined as

$\sigma = \sigma_o \sin(\omega t)$ or $\sigma^* = \sigma, \exp(i\omega t)$.

where $\sigma^*$ is the complex stress, $\sigma_o$ is the stress amplitude, $\omega$ is the frequency of oscillation in rad/ s, and *t* is time. Similarly, the strain, $\varepsilon$, is defined as

$\varepsilon = \varepsilon_o \sin(\omega t - \delta)$ or $\varepsilon^* = \varepsilon_o \exp\{i(\omega t - \delta)\}$

where $\varepsilon^*$ is the complex strain, $\varepsilon_o$ is the strain amplitude and $\delta$ is the phase angle which describes the lag time between the stress and strain oscillations.

The complex flexural modulus, E*, is the ratio of the complex stress to the complex strain,

$$E^{*}=\frac{\sigma^{*}}{\varepsilon^{*}}=\frac{\sigma o}{\varepsilon o}\cos(\delta)+i\frac{\sigma}{\varepsilon o}\sin(\delta)=E^{'}+iE^{''}$$

The complex flexural modulus can be broken into real and imaginary components where $E'$ represents the flexural storage modulus and $E''$ represents the flexural loss modulus. The storage modulus quantifies the elastic behaviour of the material while the loss modulus quantifies the viscous behaviour of the material. The ratio of the elastic behaviour to the viscous behaviour is the loss tangent (tan $\delta$). Peaks in the tan δ curve correspond to glass transition temperatures (Nielsen and Landel, 1994).

Mechanical analysis (DMA) were performed using a PerkinElmer DMA 8000, Dynamic Mechanical Analyser over a temperature range of 223-423 K at a frequency of 1Hz, a ramp rate of 2 K/min, and an initial strain of 0%. Thin films were typically 10 x 9.5 x 0.1 $mm^3$.

## 2.3. Catalytic tests

Figure 2.3-1 illustrates the assembly used to perform the catalytic test in the reaction of hydrogenation of styrene oxide (SO) to selectively obtain 2-phenylethanol (2-PEA).

Catalytic hydrogenation of styrene oxide was performed in the liquid phase, using for all tests 1 g of catalyst, 150 mL of absolute ethanol (Panreac, 96 %) and 2 mmol of styrene oxide (Aldrich, 97 %) with a hydrogen flow of 2 mL/s and mechanic stirring of 500 rpm. The reaction was performed at room temperature. Sample was taken at 1, 2 and 6 h of reaction.

**Figure 2.3-1.** Assembly used in the catalytic tests for the hydrogenation of styrene oxide.

ISBN:/DL:T. 1033-2011

The reaction products were analysed by gas chromatography, using a chromatograph model Shimadzu GC-2010 equipped with a 30 m capillary column DB-1 coated with phenylmethylsilicon and a FID detector. They were quantified by adding an internal standard (cyclohexanol) and by using calibrated lines.

# Chapter 3

## Synthesis of Clays with Microwaves

UNIVERSITAT ROVIRA I VIRGILI
SYNTHESIS OF HECTORITES AND SAPONITES WITH MICROWAVES AND THEIR APPLICATION IN CATALYSIS AND COMPOSI
Isabel Vicente Valverde
ISBN:/DL:T. 1033-2011

## 3.1. Introduction

In order to obtain reproducible smectites due to their multiple applications, the synthesis of these clay minerals has been studied since 1940's but it has not stopped yet. The most noteworthy methods to synthesise hectorite and saponite will be now displayed.

### *3.1.1. Synthesis of hectorites* $(Si_{8.0})\ [Mg_{6.0-x}Li_x]\ (OH.F)_4O_{20}M^{n+}_{x/n}\cdot mH_2O$

Hectorite is one of the most synthesised clay mineral by hydrothermal treatment. Its synthesis usually starts with the preparation of slurries containing the necessary reagents (Si, Mg, Li, F, etc.) that are aged under reflux or in autoclave at 333-573 K resulting in the desired hectorite. No references about synthesis of hectorites using microwaves were found. This is the reason why the most interesting conventional methods to synthesise hectorites are summarised in Table 3.1.1-1 and will be commented below.

*Hofmann and Stresse*

In 1941 Stresse and Hofmann studied the synthesis of hectorite at low temperatures (373 K, Table 3.1.1-1). They obtained a low crystalline hectorite in an amorphous silica matrix (Kloprogge et al., 1999).

*Caillère, Henin and Robichet*

Caillère et al. and Henin and Robichet (1954, Table 3.1.1-1), prepared a very crystalline hectorite by mixing much more diluted solutions. Indeed, the yield was very low. They also proposed a crystallisation mechanism: the brucite sheets may act as a stencil on which the silicate sheets would incorporate (Kloprogge et

al., 1999).

**Table 3.1.1-1.** Summary of hectorite synthesis methods (Kloprogge et al., 1999).

| Authors | Year | Final product | Reagents | Conditions and remarks |
|---|---|---|---|---|
| Strese &, Hoffmann | 1941 | Amorphous hectorite | Silicic acid, $MgCl_2$ ($Na^+$, $K^+$ and $Ca^{2+}$) hydroxides. | Refluxing at 373 K, at least 20 h. |
| Caillere et al., Robichet | 1954 | Hectorite | $SiO_2$, $FeCl_2$, $Mg^{2+}$ and $Al^{3+}$ salts. | Add a 10-20 ppm reagents solution to a 2 L of $H_2O$. Boiling. Optimum pH 8-9. |
| Granquist & Pollack | 1959 | Hectorite | $SiO_2$ gel; $Mg(OH)_2$; LiF; LiOH/NaOH. | 10 % wt. Solids reagents slurry; Reflux treatment at 373 K for 1-7 days. |
| Decarreau | 1980 | Hectorite | $Na_2SiO_3$, $MgCl_2$, LiF, acid. | Mixture metasilicate + metal salts; aging at T<373 K. |
| Laporta | 1971 | Hectorite with vacancies | $Na_2SiO_3$, $Na_2CO_3$, Mg salts and NaOH. | Refluxing at 373 K for 10-20 h. |
| Barrer & Jones | 1970 | Fluorhectorite Quartz $Li_2SiO_3$ | Silica, MgO, $MgF_2$, NaF, LiF $Na_2CO_3$ and $Li_2CO_3$ | Treatment at 1073 K for 24 h (solid reagents) or at 1123 K for 2 h (fused reagents). |

*Granquist and Pollack*

Granquist and Pollack (1959,Table 3.1.1-1) synthesised hectorite by refluxing at 373 K a 10 wt. % solids slurry consisting of silica gel ($SiO_2 \cdot nH_2O$), fresh prepared brucite ($Mg(OH)_2$), obtained by precipitation of $MgCl_2$ with ammonia, and variable amounts of NaOH, LiOH or LiF. After aging for 7 days, they

obtained a synthetic hectorite that had similar crystallinity (Figure 3.1.1-1), similar composition, and similar CEC value than those observed for a natural hectorite. They also reported that the use of $Na^+$ instead of $Li^+$ decreased the crystallisation rate whereas the addition of $F^-$ improved the crystallinity of the hectorite.

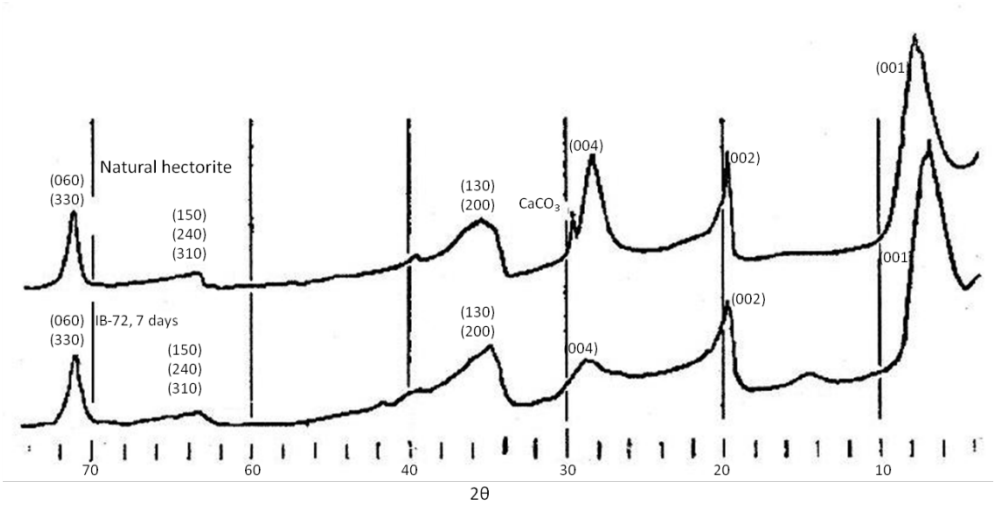


**Figure 3.1.1-1.** XRD patterns from natural hectorite (above) and the synthetic one obtained by Granquist and Pollack (below).

In later studies Baird et al (1971-1973, Table 3.1.1-1), studied the crystallisation method using the same synthetic procedure than Granquist and Pollack. They proposed a multi-step formation mechanism. First, silica monomers condense over the brucite sheets forming pseudo-smectite nuclei (Figure 3.1.1-2). In a second step some of brucite nuclei dissolve resulting in a “doughnut” structure, and finally these structures condense forming hectorite nuclei.

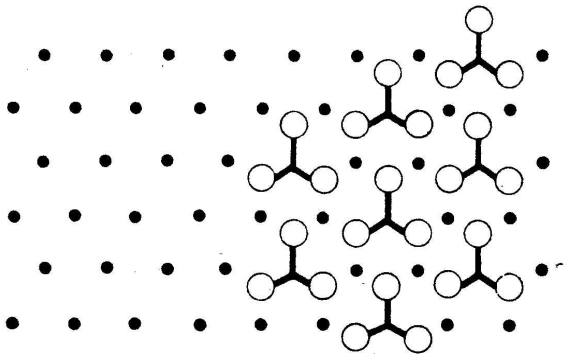

**Figure 3.1.1-2.** Pseudo-smectite structure. Maximum substitution of $Si(OH)_3O^-$ by $OH^-$ is 1 to 3. • Brucite hydroxil surface.

*Decarreau*

In 1980, Decarreau (Table 3.1.1-1) developed a method to synthesise high amounts of reproducible hectorite at lower temperature than Granquist and Pollack (333-363 K) by the precipitation of sodium silicate and magnesium chloride in acid medium and later addition of LiF. However, the aging time was even higher (2-3 weeks). From these results, Decarreau supposed that groups of small layers or “crayons” were formed, and afterwards they got ordered and grow in the extension of the layer but not in the stacking.

*Laporta industries*

By definition, hectorite should not have any vacant in octahedral positions. However Laporta industries (Table 3.1.1-1) synthesised clay minerals with this feature to control the rheology of paints. After 10-20 h of aging, an hectorite with formula $(Si_{8.0})$ $[Mg_{5.1}Li_{0.6}Vac_{0.3}]$ $(OH)_{4.6}O_{19.4}Na_{0.6}$ was obtained. It had impurities, low crystallinity and a sligthly lower interlayer charge because of silanol groups (Kloprogge et al., 1999).

*Barrer and Jones*

Barrer and Jones (1970, Table 3.1.1-1) focused their study in introducing $F^-$ in the hectorite structure, because of its high stability, to be used as catalyst in organic syntheses. They obtained fluorhectorite (Figure 3.1.1-3) but, additional quartz and $Li_2SiO_3$ phases also appeared.

**Figure 3.1.1-3.** SEM image of Na-fluorhectorite.

## *3.1.2. Synthesis of saponites $(Si_{8.0-x}Al_x)\,[Mg_{6.0}]\,(OH)_4O_{20}M^{n+}_{x/n}\cdot mH_2O$*

Because of the high tendency of $Al^{3+}$ to be in an octahedral environment, one of the most important challenges when synthesising saponites is to avoid the isomorphic substitution of $Al^{3+}$ in:

- Octahedral positions in such a way that the layer charge decreases or disappears.
- The interlayer space that may affect the features of the saponite (swelling, acidity…) and its possible catalytic applications.

UNIVERSITAT ROVIRA I VIRGILI
SYNTHESIS OF HECTORITES AND SAPONITES WITH MICROWAVES AND THEIR APPLICATION IN CATALYSIS AND COMPOSI
Isabel Vicente Valverde
ISBN:/DL:T. 1033-2011

Table 3.1.2-1 summarises some conventional methods to synthesise saponite. They will be commented below.

**Table 3.1.2-1.** Summary of methods to synthesise saponite (Kloprogge et al., 1999).

| Authors | Year | Final product | Reagents | Conditions and remarks |
|---|---|---|---|---|
| Liyama, Roy | 1963 | Saponite | Silica solution (LUDOX), $Mg^{2+}$, $Al^{3+}$ and $Na^{+}$ nitrates. | Hydrothermal treatment at 848 K. |
| Kloprogge, Vogels | 1994 | $NH_4$Saponite with $Al^{3+}$ in 2/3 of Oh positions | Amorphous silica, $Al^{3+}$ isopropoxide. $(CH_3COO)_2Mg$,$NH_3$. | Hydrothermal treatment at 473 K, 72 h. |
| Jaber | 2005 | Saponite | Amorphous silica, $Mg^{2+}$, $Al^{3+}$ and $Na^{+}$ nitrates, acetates or hydroxides. | Hydrothermal treatment at 493 K, 48 h. |
| Vogels | 2005 | Saponite-like material | Silica solution,$GaCl_3$ or $Na_2B_4O_7$, $Mg(NO_3)_2$, NaOH, urea. | Treatment at 363 K for 20-48 h. |
| Cheshire | 2005 | Saponite | Crisolite, formic acid, NaOH. | 1.-Treatment with formic acid; 2.-Treatment with NaOH; Both at 473 K for 48-96 h. |

*Liyama and Roy*

In a first attempt to synthesise saponite, high temperature treatments were used. By aging a gel with the appropriate reagents ratio at 873-1123 K and 1 kbar, Liyama and Roy (1963, Table 3.1.2-1) obtained a pure and very stable saponite. On the counterpart, it had some $Al^{3+}$ in octahedral positions. When the aging pressure increased or the aging temperature decreased, a mixture of talc

and saponite was obtained (Kloprogge et al., 1999).

*Kloprogge and Vogels*

The synthesis of saponite at medium-low temperature has been widely studied by Klopproge et al. (1994b) and Vogels et al. (1997), who suggested a crystallisation mechanism and studied the applications of saponites in catalysis (Table 3.1.2-1).

One of the objectives was to minimise the amount of $Al^{3+}$ in the octahedral positions by using $F^-$ as reagent or by increasing the $NH_4^+/Al^{3+}$ reagents ratio. The best result was obtained with the highest $NH_4^+/Al^{3+}$ studied ratio. However, some $Al^{3+}$ got into the interlayer space. From these results, they suggested a mechanism in which tetrahedral layers containing Si and Al grew in the ab axis while bayerite forming the saponite.

Using the same method than Kloprogge et al., Jaber and Miéhé-Brendlé (2005, Table 3.1.2-1), studied the influence of the initial pH of the reagents slurry by changing reagents. They observed that the saponite synthesised at pH=12.5 was not the most crystalline but the one with the most similar composition with respect to the natural clay and with less content of tetrahedral $Al^{3+}$.

They proposed two different crystallisation mechanisms depending on the initial pH of the reagents slurry.

- At alkaline pH: Si and Al are in tetrahedral soluble species $Na_4SiO_4$ and $Na[Al(OH)_4]$ whereas magnesium is in brucite form, $Mg(OH)_2$, which is octahedral and not much soluble. There is an equilibrium among the solubilised magnesium species and the precipitated

brucite in which small amounts of $Al^{3+}$ got into. In this way, the brucite sheet acquires a positive charge that attracts $Si(OH)_3O^-$ and $Al(OH)_4^-$ resulting in the formation of the saponite.

- At acid pH: Al and Mg are in soluble acetate form whereas Si is in a low soluble form (polisilicic acid). There is an equilibrium among the precipitate and the solubilised species of silicic acid in which small amounts of $Al^{3+}$ get into, creating some negative charge that attracts the $Mg^{2+}$ and $Al^{3+}$ species, resulting in the formation of the saponite.

*Vogels*

In most cases the saponite synthesis involves a hydrothermal treatment. However in some applications a saponite –like material (in which there is $B^{3+}$ or $Ga^{3+}$ instead of $Al^{3+}$) can be used. This saponite-like material was synthesised to be used as acid catalyst, at low temperature (363 K) in quite short time (1-2 days) using urea as crystallising agent (Vogels et al., 2005).

As we can observe, long times or high aging temperatures are necessary in order to synthesise saponite or hectorite. The introduction of the microwave technology could mean an improvement in the synthesis of these materials. Recently, Trujillano et al. (2010, In press) reported the synthesis of saponite-like materials with microwave aging, but no more references were founded.

## 3.2. Fast Microwave Synthesis of Hectorite

### Abstract

Hectorite has been synthesised by aging the gel precursor by microwave–hydrothermal treatment at 393 K for 16 h. This hectorite had higher purity (60%) than hectorite prepared by conventional heating (45%). The effect of brucite used, aging temperature and time under microwaves on the resulting hectorite has been studied by XRD, $N_2$ adsorption, and SEM techniques. Higher proportions of hectorite with higher crystallinity were achieved at longer aging time, higher temperature, and by using a more crystalline brucite.

### *3.2.1. Introduction*

In hectorite $M_x[Li_xMg_{6-x}Si_8O_{20}(OH)_4]$ (M=Na, Li, $NH_4$) all octahedral sites are occupied with either $Mg^{2+}$ or $Li^+$. Hectorites used in many important fields such as catalysis (Korösi et al., 2004), synthesis of polymer-based nanostructured materials (Alexandre & Dubois 2000), adsorption (Zielke & Pinnavaia 1988), ionic Exchange (Laudelout 1987), and environmental issues (Pieper et al. 2006). Smectites can be extracted from natural resources; however they must be synthesised to obtain an impurity-free reproducible solid. Classical methods of synthesis involve the use of high temperatures (623 K) or long aging times (from several days to several weeks) (Granquist & Pollack 1959; Decarreau 1980; Kloprogge et al. 1999; Higashi et al. 2002).

Microwave technology has been used from 80's in different research fields, such as solid dehydration, and promotion of both organic and inorganic reactions (Komarneni et al., 1992; Kingston and Haswell,1997). In the last years, there is an increasing interest in using microwaves to synthesise mesoporous materials (Newalkar et al., 2001), not only due to the particular characteristics that the synthesised solids can achieve, but also to decreased synthesis time with the subsequent energy saving. Therefore, microwave reactions constitute valuable processes in Green Chemistry. Microwaves have never been used to synthesise hectorite (or other smectites), but the noteworthy amount of publications reporting synthesis of hydrotalcites (Bergadà et al., 2007a, 2007b; Komarneni et al., 1996; Rivera et al., 2006; Tichit et al., 2002), or synthesis of zeolites (Pilter et al., 2000; Romero et al., 2004), motivated us to take into account this new method. We report a faster synthesis of hectorite by microwave–hydrothermal treatment.

### *3.2.2. Experimental*

Hectorite was prepared according to the method reported by Granquist and Pollack (1959) in which brucite sheets are proposed to act as crystallisation nuclei of hectorite. Preparation was carried out as follows: 50 ml of a slurry composed by 0.8 g of $SiO_2$ (Aerosil 380 from Degussa), 0.3 g of freshly prepared brucite $Mg(OH)_2$ and 46 mg of LiF was vigorously stirred for 1 h. The slurry contained 3 wt.% solids and the molar ratio of the reactants was $SiO_2$:$Mg(OH)_2$:LiF=5.5:3:1. The samples were aged by autoclaving in laboratory microwave equipment (Milestone Ethos Touch Control), at 373 K for 4 and 8 h (samples H1–H2, Table 3.2.2-1) or at 393 K for 4, 8 and 16 h (samples H3–H6, Table 3.2.2-1). One hectorite sample was aged in an autoclave inside a conventional oven, to compare conventional aging with microwave hydrothermal treatment (sample H7). Brucite was synthesised by two different ways: the first consisted on rehydrating commercial magnesia by refluxing for 2 h (sample Brh); the second by precipitation from an aqueous solution of $MgCl_2$ with ammonia (Brp).

**Table 3.2.2-1.** Preparation conditions of samples.

| Sample | Aging method | Aging time (h) | Aging temperature (K) | Brucite used in the synthesis |
|---|---|---|---|---|
| H1 | MW | 4 | 373 | Brp |
| H2 | MW | 8 | 373 | Brp |
| H3 | MW | 4 | 393 | Brp |
| H4 | MW | 8 | 393 | Brp |
| H5 | MW | 8 | 393 | Brh |
| H6 | MW | 16 | 393 | Brp |
| H7 | Conventional | 192 | 393 | Brp |

UNIVERSITAT ROVIRA I VIRGILI
SYNTHESIS OF HECTORITES AND SAPONITES WITH MICROWAVES AND THEIR APPLICATION IN CATALYSIS AND COMPOSI
Isabel Vicente Valverde
ISBN:/DL:T. 1033-2011

Samples were characterised by X-ray diffraction (XRD), X-ray fluorescence (XRF), $N_2$ adsorption, Scanning Electron Microscopy (SEM), and determination of cation exchange capacity (CEC). The experimental conditions are indicated in the Experimental Section (2.2).

### *3.2.3. Results and Discussion*

*Influence of using microwaves*

X-ray diffractions patterns of samples H4 (under microwaves) and H7 (conventional preparation) showed only one crystalline phase corresponding to hectorite (Figure 3.2.3-1). A very broad peak with a maximum at 2θ=22.8°was assigned to amorphous silica. The particles of hectorite H4 are larger (9.3 nm) than those of the hectorite aged in a conventional oven (H7, 7.9 nm) (Table 3.2.3-1).

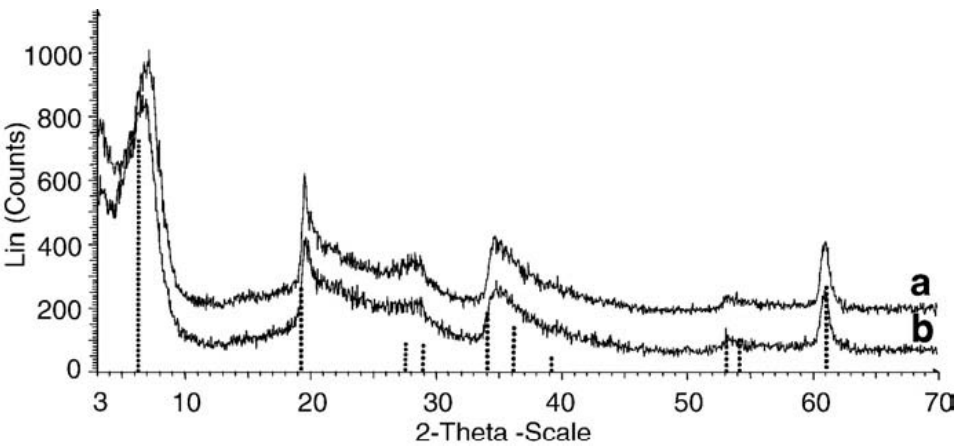


**Figure 3.2.3-1.** XRD patterns of (a) H7 aged during 8 days by conventional heating at 393 K, and (b) H4 aged during 8 h by microwave treatment at 393 K. Dotted lines refer to hectorite.

**Table 3.2.3-1.** Characterisation data from XRD patterns

| Sample | 001 Hectorite crystallite size (nm) | 060 Hectorite crystallite size (nm) | Basal spacing (Å) |
|---|---|---|---|
| H1 | 2 | 5.8 | 14.4 |
| H2 | 2.4 | 6.2 | 14.4 |
| H3 | 2.5 | 9.2 | 13.3 |
| H4 | 2.5 | 9.3 | 13.3 |
| H5 | 2.8 | 8 | 12.8 |
| H6 | 2.2 | 10.5 | 12.7 |
| H7 | 2.4 | 7.9 | 12.6 |

The basal spacing was slightly higher for H4 (13.4 Å) than for H7 (12.6 Å) (Table 3.2.3-1). For conventional prepared hectorites, a higher basal spacing has been attributed to the presence of some residual brucite in the interlayer space (Srodon, 2006). However, we think that the higher basal spacing observed for H4 could also be related to the presence of higher amounts of interlamellar cations, which may mean a higher layer charge. Nevertheless, the presence of $Mg(OH)_2$ layers cannot be completely discarded although this phase cannot be detected by XRD.

The microwave aged sample (H4) has higher CEC (0.68 meq/g) than H7 (0.53 meq/g). A contribution of amorphous silica or residual brucite to the CEC has been discarded, as commented in the experimental section. The higher CEC of H4 may be attributed to the presence of lower amounts of silica in this sample or due to a higher layer charge.

From atomic absorption results, Si/Mg and Mg/Li ratios were determined (Table 3.2.3-2). The Si/Mg ratios of samples H4 and H7 are higher than that found in the literature (Levin et al., 2004) for a natural hectorite (San Bernadino hectorite, Si/Mg=1.52). They are also higher than that expected for a theoretical pure hectorite (Si/Mg=1.67, when x=1.2) due to the presence of the amorphous silica.

**Table 3.2.3-2.** Characterisation data from different techniques

| Sample | % $SiO_2$[a] | % MgO[a] | %Li[b] | Si/Mg ratio | Mg/Li ratio | % Amorphous silica | % Hectorite | CEC (meq/g sample) | BET surface area ($m^2/g$) |
|---|---|---|---|---|---|---|---|---|---|
| H1 | 62.4 | 16.2 | 0.40 | 2.6 | 7.0 | – | 39[c] | – | 108 |
| H2 | 66.6 | 19.1 | 0.46 | 2.3 | 7.3 | – | 43[c] | – | 145 |
| H3 | 64.1 | 15.2 | 0.41 | 2.8 | 6.3 | – | 45[c] | 0.47 | 132 |
| H4 | 65.5 | 16.5 | 0.47 | 2.7 | 6.1 | 54 | 46[d] | 0.68 | 156 |
| H5 | 67.4 | 18.8 | 0.54 | 2.4 | 5.9 | 60 | 40[d] | 0.61 | 172 |
| H6 | 69.2 | 18.4 | 0.68 | 2.5 | 4.6 | 40 | 60[d] | 0.67 | 170 |
| H7 | 65.5 | 18.0 | 0.85 | 2.3 | 3.6 | 55 | 45[d] | 0.53 | 165 |

[a]From XRF [b]From ICP. To reach 100% it is necessary to add %Lost in ignition mass.

[c]Calculated using a representation of relative integrated intensity in % of the hectorite phase for samples H4, H5, H6 and H7, obtained from XRD patterns versus content of hectorite calculated from CEC and XRF.

[d]Calculated from Si/Mg, Mg/Li, and CEC.

The proportion of hectorite and amorphous silica in H4 and H7 were estimated from Si/Mg, Mg/Li, and CEC (Table 3.2.3-2). The content of hectorite and amorphous silica in H4 and H7 are very similar (45% of hectorite and 55% of amorphous silica).

H4 has much higher Mg/Li ratio (6.1) than sample H7 (3.6) (Table 3.2.3-2). Assuming that magnesium and lithium are in the hectorite structure (in the layers or in the interlamellar space), the higher Mg/Li ratio of H4 could be attributed to the presence of higher amounts of magnesium ions in the interlamellar space.

H4 has slightly lower specific BET surface area (156 $m^2/g$) than H7 (165 $m^2/g$) (Table 3.2.3-2). The slightly lower surface area may be related to the higher crystallinity of H4.

*Influence of type of brucite*

The brucite prepared by precipitation (Brp) was more crystalline (crystallite size=14.6 nm) than rehydrated magnesia (Brh) (crystallite size=7.3 nm).

In the X-ray diffraction patterns of H4 and H5 crystalline brucite was not observed, appearing crystalline hectorite and amorphous silica. Hectorite H4 has higher crystallinity (larger particles) and slightly higher basal spacing than hectorite H5 (Table 3.2.3-1).

Both samples present similar CEC (Table 3.2.3-2, 0.68 meq/g for H4, 0.61 meq/g for H5). H4 also has a higher Si/Mg ratio and similar Mg/Li ratio compared to H5 (Table 3.2.3-2). The estimated amount of amorphous silica, calculated from the CEC and Si/Mg ratio values, was higher for sample H5 (60% in H5, 54% in H4).

Therefore, a more crystalline brucite yielded higher amounts of more crystalline hectorite. This is in agreement with the lower specific BET surface area obtained for H4 (156 $m^2/g$, Table 3.2.3-2).

*Influence of temperature during microwave aging*

The influence of the temperature during microwave aging has been studied by comparing samples H2 and H4.

Crystalline brucite was detected as an associated phase in H2. The higher basal spacing of the hectorite phase for sample H2 (14.8 Å, Table 3.2.3-1) could be explained by the presence of $Mg(OH)_2$ layers in the interlamellar space. Particles of H4 hectorite are larger (9.3 nm) than those of H2 (6.2 nm), indicating the higher crystallinity of the hectorite aged at higher temperature.

The quantification of the hectorite phase, from CEC and atomic absorption results, was not possible for sample H2 due to the presence of brucite. For samples with brucite, another quantification method has been developed. First, we made a representation of the relative integrated intensity in % of the hectorite phase, obtained from XRD patterns, for samples H4, H5, H6 and H7 (samples without brucite) versus content of hectorite calculated from CEC and XRF. Then, from the straight line obtained in this representation, we applied the relative integrated intensity in % of hectorite H2, calculated from XRD, obtaining a value of 43% of hectorite content. This value is slightly lower than for H4 (46%).

The presence of crystalline brucite in H2 also explains its higher Mg/Li ratio (Table 3.2.3-2), and also could be responsible for its lower specific BET surface area (145 $m^2/g$) when compared to H4 (156 $m^2/g$). Thus, formation of higher amounts of more crystalline hectorite is faster at higher temperature.

UNIVERSITAT ROVIRA I VIRGILI
SYNTHESIS OF HECTORITES AND SAPONITES WITH MICROWAVES AND THEIR APPLICATION IN CATALYSIS AND COMPOSI
Isabel Vicente Valverde
ISBN:/DL:T. 1033-2011

*Influence of time under microwave aging*

XRD patterns of the samples prepared under microwaves at different temperatures and times are shown in Figure 3.2.3-2. We can observe the presence of crystalline hectorite and amorphous silica for all samples. Crystalline brucite was also detected for the samples aged at 373 K (H1 and H2), and 393 K for 4 h (H3). The amount of the brucite phase gradually decreases with time and with temperature (Figure 3.2.3-2). In fact, the amount of brucite in sample H3 is very small. At 393 K, conversion of brucite into hectorite was promoted. The crystallinity of hectorite (Table 3.2.3-1) increases with increasing the aging time for both temperatures. The higher basal spacing observed for H1 and H2 (Table 3.2.3-1) can be related to the presence of higher amounts of interlayer $Mg(OH)_2$ layers.

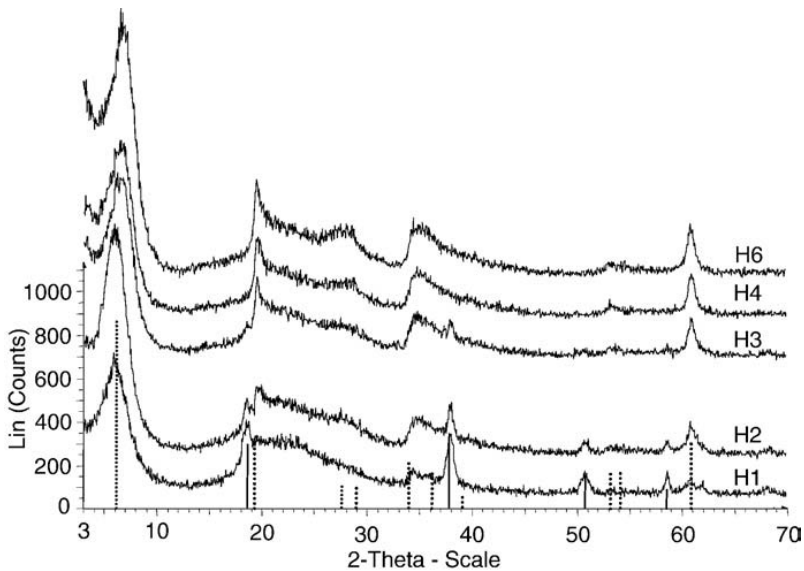


**Figure 3.2.3-2.** XRD patterns of H1 and H2 aged at 373 K, and H3, H4, and H6 aged at 393 K. Dotted lines refer to hectorite, and solid lines refer to brucite.

Although there is an increase of the CEC between H3 (0.47 meq/g) and H4 (0.68 meq/g), a further increase of time to 16 h did not increase the CEC (Table 3.2.3-2, H6, 0.67 meq/g).

There is a decrease of the Si/Mg ratios at increasing aging time (Table 3.2.3-2). This is in agreement with the expected decrease of amorphous silica with time. The Mg/Li ratio is very high in samples H1 (7.0) and H2 (7.3) probably due to the presence of higher amounts of brucite in these samples. The higher Mg/Li value of H2 compared with H1 can be related to the presence of higher amounts of magnesium ions in the interlamellar space.

The proportion of the hectorite phase increases with time, and was always higher for samples prepared at higher temperature (Table 3.2.3-2).

Specific BET surface area increases with time for each group of samples (Table 3.2.3-2). For the samples aged at 373 K (H1 and H2), the increase can be related to the smaller amount of crystalline brucite.

For the samples prepared at 393 K (H3, H4 and H6), the amount of brucite also explains the increase of area between H3 and H4. However, the increasing of specific surface area from H4 to H6, which do not have brucite, may be related to a certain disaggregation of hectorite particles with time, probably as a consequence of the continuous action of microwaves. This is in agreement with the decrease of the stacking degree of H6 (Table 3.2.3-1) and with SEM pictures. H6, obtained at longer aging times (Figure 3.2.3-3b), shows less agglomerated particles than H4 (Figure 3.2.3-3a).

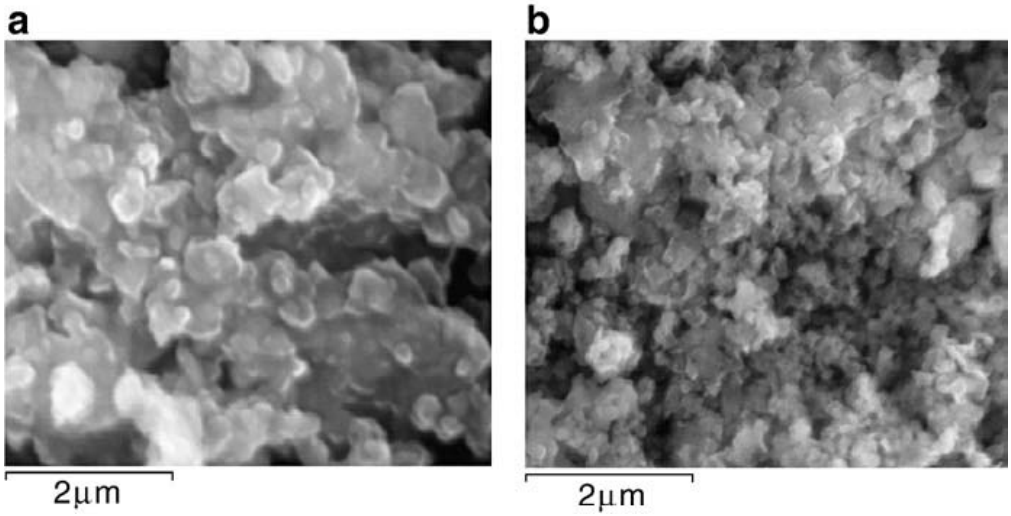


**Figure 3.2.3-3.** SEM micrographs of: a) H4 (×20,000) and b) H6 (×20,000).

### *3.2.4. Conclusions*

In summary, the hydrothermal microwave treatment provides a faster synthesis of hectorites.

### *3.2.5. Acknowledgments*

The authors are grateful for the financial support of the Ministerio de Educación y Ciencia of Spain and FEDER funds (CTQ2005-02384/ PPQ) and for the FPU grant (AP2006-00835) also financed by the Ministerio de Educación y Ciencia of Spain.

UNIVERSITAT ROVIRA I VIRGILI
SYNTHESIS OF HECTORITES AND SAPONITES WITH MICROWAVES AND THEIR APPLICATION IN CATALYSIS AND COMPOSI
Isabel Vicente Valverde
ISBN:/DL:T. 1033-2011

## 3.3. Preparation of pure hectorite using microwaves

### Abstract

Hectorite, $(Si_{8.0})[Mg_{6.0-x}\ Li_x](OH.F)_4\ O_{20}\ M^{n+}_{x/n}{\cdot}mH_2O$ is a triocahedral smectite that can be used in multiple fields. Our objective in this work is to obtain pure hectorite by different ways (decantation, treatment with a solution of $Na_2CO_3$, change of the reactants ratio) and to study the influence of these procedures on the properties of purified samples. Samples were characterised by XRD, FTIR, $N_2$ physisorption, TEM techniques and determination of CEC. Pure hectorite samples were obtained by different procedures, resulting in hectorites with different features. The choice of one or other would depend on the application of hectorite.

### *3.3.1. Introduction*

Clay minerals are widely spread on the Earth surface. The layer of these phyllosilicates is formed by $M(O, OH)_6$ octahedral sheets (where $M=Al^{3+}$, $Mg^{2+}$, $Fe^{3+}$ o $Fe^{2+}$) and tetrahedral sheets, mainly $Si(O, OH)_4$ units. In both sheets isomorphic substitution by lower charged cations is possible and results in negatively charged layers. This charge is compensated by cations located in the interlamellar space. Characteristic properties of clays are the swelling of interlamellar space (Stepkowska et al., 2004) and interlayer cationic exchange (Bergaya and Vayer, 1997; Czímerová et al., 2006). Clays also present Brønsted acidity, related to –OH groups, and Lewis acidity related to interlayer cations and lamellar cations deficiently coordinated. Hectorite is a clay mineral with formula $(Si_{8.0})$ $[Mg_{6.0-x}Li_x]$ $(OH.F)_4O_{20}M^{n+}_{x/n}\cdot mH_2O$. Hectorite can be used as catalyst, in ionic adsorption and ionic exchange processes, in nanoparticles synthesis, and in nanocomposites preparation. Hectorite can be found in nature, however, in order to work with a reproducible material it must be synthesised. Preparation methods usually involve long time hydrothermal treatments, and other natural clays are still used for main applications (Kloprogge et al., 1999). The introduction of microwave technology for clay synthesis can not only dramatically reduce the synthesis times, but also confer interesting properties to the prepared materials (Vicente et al., 2009, 2010a).

Microwaves belong to waves with frequency between 30000 MHz and 300 MHz. The Magnetron, device that produces fixed frequency microwaves, was designed during the Second World War as part of RADAR development (Mingos and Baghurst, 1997). In a previous work, we managed to synthesise reproducible hectorite clay in a short time using microwaves, obtaining purities

up to 60% (Vicente et al., 2009). However, some silica remained in sample. Our objective in this work is to study different ways to obtain pure hectorite, and to check the influence of these procedures on the properties of purified samples.

### *3.3.2. Experimental*

Hectorite was prepared according to the procedure reported in a previous work (Vicente et al., 2009) in which brucite sheets were proposed to act as crystallisation nuclei of hectorite. Preparation was carried out as follows: A slurry (3 wt. % solids) containing $SiO_2$, fresh brucite $Mg(OH)_2$ (synthesised by precipitation of a 10 M ammonia solution onto $MgCl_{2(aq)}$), and LiF, in a molar ratio 7.5 $SiO_2$:3 $Mg(OH)_2$:1 LiF was vigorously stirred for 1 h. Then, the sample was aged by autoclaving in laboratory microwave equipment (Milestone Ethos Touch Control), at 393 K for 8 h obtaining H1. In order to obtain pure hectorite several procedures were performed:

- Separation by decantation, collecting the supernatant liquid from a H1 suspension that was stirred for 24 h and laid settling down for 2 days (H1-S).

- Treatment of H1 with a solution of $Na_2CO_3$ 0.05 M at 393 K for 5 minutes. (H1-C).

- Decrease of $SiO_2$ amount in the starting slurry using as molar ratio of reactants 4 $SiO_2$:3 $Mg(OH)_2$:1 LiF. After aging this slurry by autoclaving under microwaves at 393 K for 8 h, we obtained H2.

Samples were characterised by X-ray diffraction (XRD), $N_2$ adsorption, transmission Electron Microscopy (TEM), transmission infrared spectroscopy (FTIR) and determination of cation exchange capacity (CEC). The experimental

conditions are indicated in the Experimental Section (2.2).

### *3.3.3. Results and discussion*

TEM images of all samples (H1, H1-S, H1-C and H2) exhibited the lamellar structure typical of smectite clays. TEM images of H1 and H2 are shown in Figure 3.3.3-1 as representative samples. The existence of smectite structure was confirmed by the XRD patterns of samples (Figure 3.3.3-2), where we observed only one crystalline phase corresponding to hectorite. A very broad peak with a maximum at 2θ = 22.8° was assigned to amorphous silica by comparison with the $SiO_2$ diffraction pattern included in the figure. The silica band was more appreciable in sample H1 than in samples H1-C and H2, resulting in a worse definition of (004) reflection (Figure 3.3.3-2). Therefore, we can conclude that there was a decrease of remaining silica in these samples. In contrast, not important differences were observed in the difraction pattern of sample H1-S when comparing it to that obtained for sample H1 suggesting that the remaining amount of silica in samples H1-S and H1 was similar

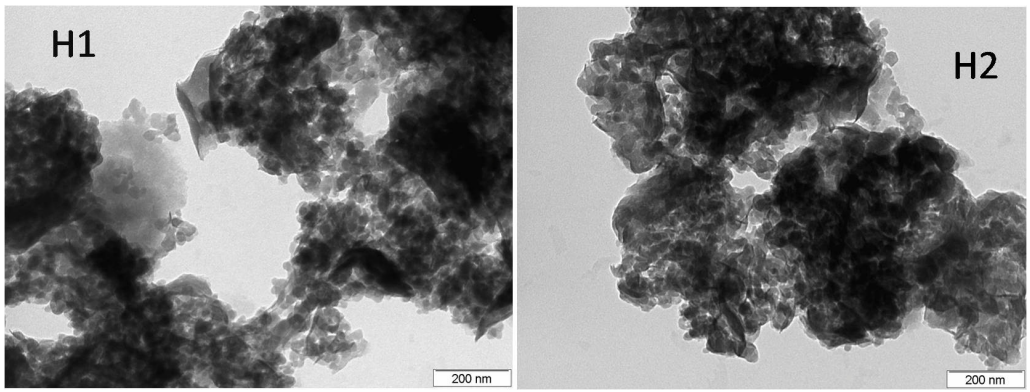


**Figure 3.3.3-1.**TEM images of samples H1 and H2 (x100K).

H1, H1-C and H2 had similar crystallinity, as deduced from their similar crystallite size, calculated from (060) reflection of XRD patterns (Table 3.3.3-1). The lowest crystallite size value obtained for sample H1-S may be explained by the fact that not only the amorphous silica particles but also the biggest clay ones, settled down at the bottom and just the smaller clay particles remained in suspension.

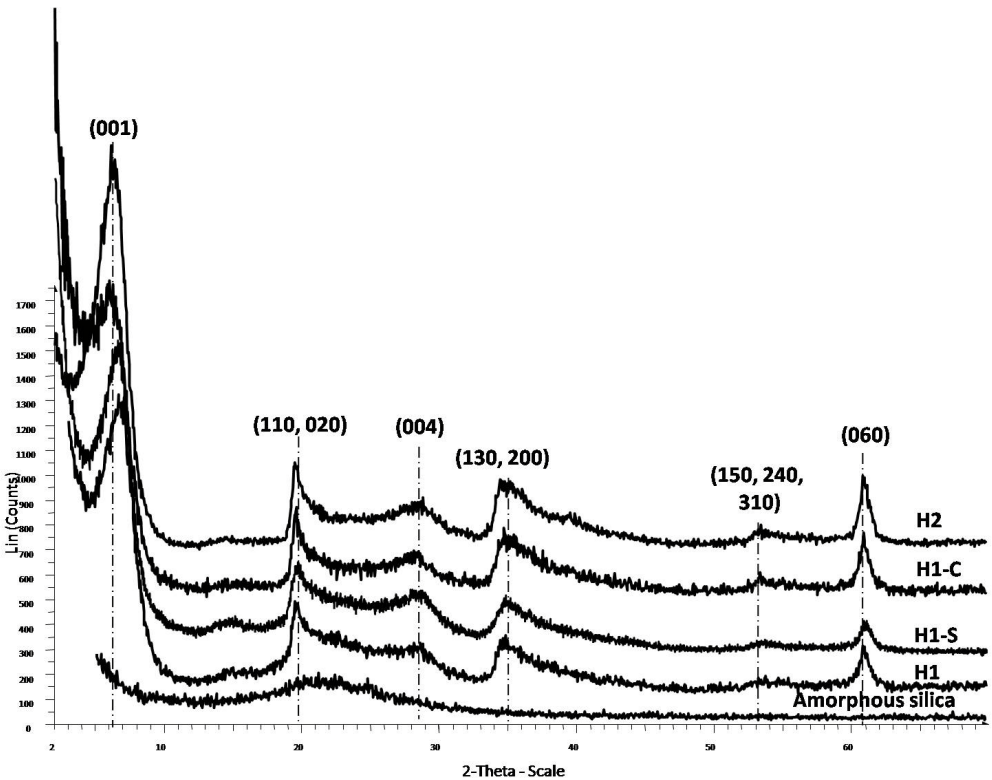


**Figure 3.3.3-2.** XRD patterns of silica, and studied samples.

The basal spacing was higher for samples H1-C and H2 (14.4 and 14.2 Å, respectively) than for H1 (13.2 Å) (Table 3.3.3-1). For conventional prepared hectorites, a higher basal spacing has been attributed to the presence of some residual brucite, ($Mg(OH)_2$), in the interlayer space (Srodon, 2006). However, we

think that the higher basal spacing observed for H1-C and H2 could also be related to the presence of higher amounts of interlamellar cations, which may mean a higher CEC value (Table 3.3.3-1). Nevertheless, the presence of $Mg(OH)_2$ layers cannot be completely discarded although this phase cannot be detected by XRD. Again, not differences were observed when comparing basal spacing of sample H1-S and H1.

**Table 3.3.3-1.** Characterisation data from XRD, and $N_2$ physisorption techniques and CEC determination.

| Sample | Basal spacing (Å) | Crystallite size (0 6 0) (nm) | BET surface area ($m^2/g$) | Hysteresis type | CEC (meq/100g) |
|---|---|---|---|---|---|
| **H1** | 13.2 | 9.3 | 162 | D, B | 64 |
| **H1-S** | 13.4 | 7.9 | 222 | B | 70 |
| **H1-C** | 14.4 | 9.4 | 238 | B | 90 |
| **H2** | 14.2 | 9.9 | 199 | B | 75 |

Figure 3.3.3-3 shows the FTIR spectra taken for samples H1, H1-S, H1-C and H2 and also for $SiO_2$ for comparison. Bands were assigned taking into account the characterisation data reported for clay samples (Rusell and Fraser, 1994; Kloprogge et al., 1999; Kloprogge and Frost, 2000). The band around 1027 $cm^{-1}$ corresponds to the Si–O–Si ordered in the clay mineral layer and can be observed in all samples especially for H1-C and H2, confirming the XRD results. The appearance of one intense band around 1105 $cm^{-1}$ together with a shoulder at 1200 $cm^{-1}$ was related to the presence of the amorphous silica phase, being more intense for H1 and H1-S, in agreement with the XRD results. This agrees the enhancement of CEC values observed for the samples with less content of amorphous silica (H1-C and H2, Table 3.3.3-1) since CEC in silica is $\sim$0. The other IR band observed for samples at 666 $cm^{-1}$ is associated to vibrations related to Mg–OH librations.

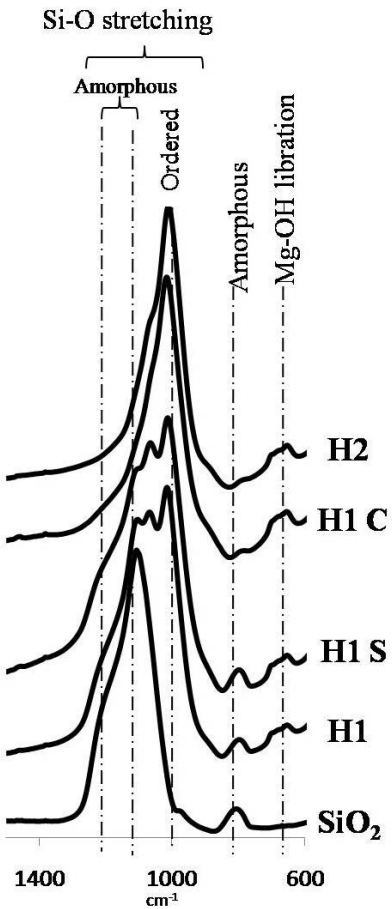


**Figure 3.3.3-3.** FTIR spectra of silica, and studied samples.

From $N_2$ adsorption-desorption isotherms, we observed interesting differences in the hysteresis shape of samples (Figure 3.3.3-4, Table 3.3.3-1). Thus, in sample H1, hysteresis is a mixture of shapes B and D which corresponds to porosity of clay minerals with some contribution of non-parallel platelets separated by small particles. In contrast, the other samples showed a B hysteresis type, related to pores formed by the superposition of crystalline parallel platelets. We also observed higher values of BET area for samples H1-S, H1-C and H2 than H1 (Table 3.3.3-1). This fact together with

the differences observed in the hysteresis shape, is in agreement with the elimination of small silica particles that block the pores and change their shape. The highest increase in BET area when compared to H1 was observed in sample H1-C. This could be related to some disorder in stacking due to $Na_2CO_3$ treatment resulting in a loss of definition of (001) reflection (Figure 3.3.3-2). In sample H2 the higher BET area value could be due to the higher crystallinity of this sample in spite of the absence of silica which blocks the pores.

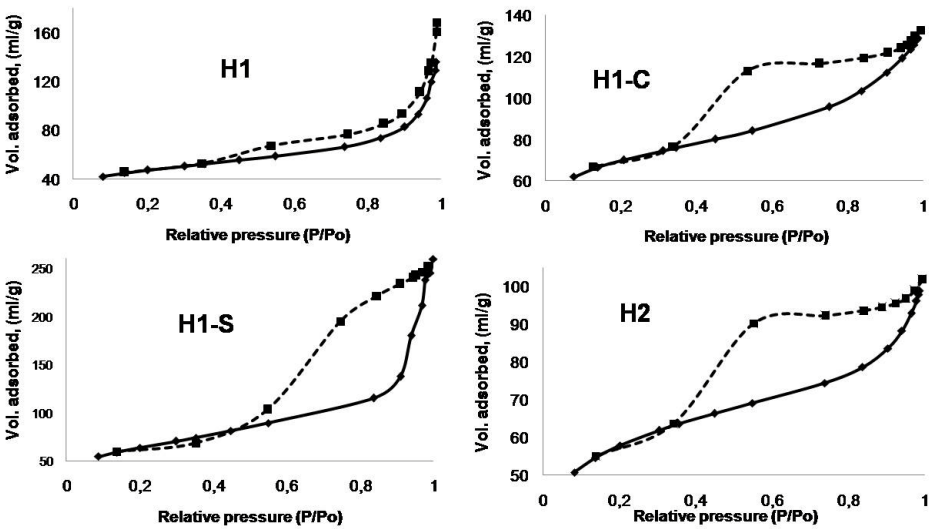


**Figure 3.3.3-4.** $N_2$ adsorption-desorption isotherms of H1, H1-S, H1-C and H2.

### *3.3.4. Conclusions*

Purer hectorite samples with different features were obtained by different procedures. Treating the hectorite with a $Na_2CO_3$ solution or decreasing the silica content in the starting slurry allowed us to obtain the purest hectorites.

### *3.3.5. Acknowledgements*

Authors are grateful for financial support of Ministerio de Ciencia e Innovación and FEDER funds (CTQ2008-04433/PPQ). I. Vicente acknowledges FPU grant from Ministerio de Educación y Ciencia (AP2006-00835).

## 3.4. Microwave-assisted synthesis of saponite

### Abstract

Saponites have been successfully synthesised by using the microwave hydrothermal method at 393 K for 6 h. Al(IV)(Td)/Al(VI)(Oh) ratio and CEC values of the microwaves samples were higher than those obtained for the saponites prepared by conventional hydrothermal method at the same temperature for 72 h. Characteristics of the saponites synthesised under microwaves depended on the initial slurry pH, the presence of fluorides in the reaction medium, and the aging time. When the initial slurry pH was 8, the highest Al(IV)(Td)/Al(VI)(Oh) ratio, and high CEC values were obtained. Moreover, by synthesising saponite with an initial slurry pH of 7 in the presence of fluoride, the highest CEC value was achieved.

### *3.4.1. Introduction*

Saponite $M_x[Mg_6Al_xSi_{8-x}O_{20}(OH)_4]$ (M= Na, Li, $NH_4$) is a trioctahedral 2:1 layered phyllosilicate. The layer consists of an octahedral sheet composed by $Mg(O,OH)_6$ units sandwiched between two $Si(O,OH)_4$ tetrahedral sheets. Some isomorphous substitution of Si(IV) by Al(III) in the tetrahedral sheet causes the layer to be negatively charged, and provides Lewis acidity. This charge is compensated by interlayer exchangeable cations such as $Na^+$, $K^+$, $Ca^{2+}$, or even $H^+$, obtaining, in this case, a Brønsted acidic material. Aluminium can also substitute magnesium in octahedral positions, in a ratio of 3 $Mg^{2+}$=2 $Al^{3+}$ without creation of a positive charge or as suggested by Suquet et al. (1981) in a ratio 1 $Mg^{2+}$=1 $Al^{3+}$, creating positive charge, which compensates the negative one of the layer. Additionally, $Al^{3+}$ and$Mg^{2+}$ can be present as interlayer cations.

Nowadays, interest in natural smectites is increasing due to their important technological applications such as for nanocomposites preparation, (Liu and Breen, 2005; Xue and Pinnavaia, 2008) or heterogeneous catalysts due to their acidity and thermal stability (Varma, 2002; Casagrande et al., 2005). Large availability and low price are major advantages when natural saponite is used. However, non-uniformity in chemical composition, and an important amount of several impurities mixed in this natural clay mineral limit their technological application, especially in catalysis. To obtain an impurity-free reproducible solid, saponite must be synthesised. Saponite synthesising procedures often involve hydrothermal treatments in autoclaves at water autogenous pressure (5–17 MPa), and at 423–723 K for long times, from hours to days (Kloprogge et al., 1994a; Jaber and Miéhé-Brendlé, 2005). Moreover, non-hydrothermal synthetic methods working at 373 K and atmospheric conditions have been also proposed

(Prikhod'ko et al., 2003). The use of hydrothermal conditions has been defended by Kloprogge et al. (1999) due to the high hydrolysis rate of octahedral cations at high temperature that favours nucleation, and growth of saponites. In non-hydrothermal conditions, hydrolysis of cations is obtained using urea. However, preference of $Al^{3+}$ cations for tetrahedral positions is only possible at high Si/Al ratios (Prikhod'ko et al., 2003). Then, the control of physical and chemical properties of saponites, when used for specific applications, is very important (Vogels et al., 2005).

Kloprogge and co-workers studied the influence of many factors, such as slurry pH and chemical composition, influence of $F^-$, aging time, and aging temperature, on the synthesis of ammonium saponite by conventional hydrothermal method (Kloprogge et al., 1994a, 1999; Vogels et al., 1997). The effect of initial dilution in slurry was also studied by Bisio et al. (2008). It is important to remark on the role of aging temperature in the hydrothermal synthesis of saponites. Even after 72 h of thermal treatment, crystallisation was not good at temperatures lower than 473 K (Kloprogge and Frost, 2000). Two key factors to have in mind for the synthesis of saponites, that considerably affect their physicochemical properties, are the incorporation of $Al^{3+}$ in octahedral positions, instead of $Mg^{2+}$, and the nature of the interlayer cation. Besides, other parameters, such as the crystallinity and the layer stacking degree, can also have importance for several applications.

Microwave technology has been used from 80's in different research fields, such as solid dehydration, and promotion of both organic and inorganic reactions (Komarneni et al., 1992; Kingston and Haswell, 1997). In the last years, there is an increasing interest in using microwaves to synthesise mesoporous materials

(Bergadà et al., 2007a, 2007b; Newalkar et al., 2001), not only due to the particular characteristics that the obtained solids can achieve, but also to decreased temperature and synthesis time with the subsequent energy saving. Therefore, microwave reactions constitute valuable processes in Green Chemistry. Recently, hectorite was successfully synthesised by aging the gel precursor by microwave-hydrothermal treatment at 393 K for 16 h (Vicente et al., 2009). This hectorite was purer and more crystalline than the hectorite aged for 8 days by conventional heating. Some preliminary studies about the use of microwaves for saponite preparation have been recently published (Yao et al., 2005, Rico et al., 2008).

The aim of this study was to decrease the temperature and time in the synthesis of ammonium saponites by using microwaves. Some preparation parameters, such as the pH of the initial slurry by using different reactants sources, the presence of fluorides, and the heating time, were modified in order to establish their influence on the saponite synthesis under microwaves. Several saponites were also prepared by conventional heating for comparison. Samples were characterised by XRD, XRF, EDX, TEM, FTIR, CEC determination, $N_2$ adsorption, and $^{27}$Al-MAS-NMR techniques.

### *3.4.2. Experimental*

Saponites were prepared following the method reported by Vogels et al. (1997), but modifying several parameters, and using microwaves for the hydrothermal aging. First, 50 ml of slurry (≈9 wt. % solids),with a $Si^{4+}$:$Al^{3+}$:$Mg^{2+}$:$NH_4^+$ composition ratio of 14.3:2.5:12.5:8, was vigorously stirred for 2 h. Excepting for $NH_4^+$, which was added in excess, this composition ratio

ISBN:/DL:T. 1033-2011

would result in the obtaining of a saponite with the theoretical formula $NH_{4(1.2)}[Mg_6Al_{1.2}Si_{6.8}O_{20}(OH)_4]$. Fumed $SiO_2$ (227$m^2$/g) was used as silica source for all samples. However, different Mg and Al sources were used in order to achieve different pH values in the initial slurry (4.5, 7, and 8) obtaining samples S1, S2 and S3, respectively (Table 3.4.2-1). Then, they were aged by autoclaving using a laboratory microwave equipment (Milestone Ethos Touch Control) at 453 K for 6 h (Table 3.4.2-1). Two more samples were prepared under microwaves: the one at the same preparation conditions than sample S2 but adding $F^-$ into the slurry (Al/F ratio of 1.25) (sample S2F), and the other by increasing the aging time of sample S3 to 12 h (S3-12 h) (Table 3.4.2-1). In order to compare microwaves and conventional heating, two samples were synthesised at the same preparation conditions than samples S2 and S3 but aging the slurry by conventional heating in an autoclave at 453 K for 72 h (samples S2c and S3c) (Table 3.4.2-1). After aging, all samples were washed by centrifugation up to neutrality, and dried overnight in an oven at 353 K.

Samples were characterised by X-ray diffraction (XRD), transmission infrared spectroscopy (FTIR), X-ray fluorescence (XRF), energy dispersive X-ray (EDX), $N_2$ adsorption, $^{27}$Al–MAS–NMR, transmission Electron Microscopy (TEM), and determination of cation exchange capacity (CEC). The experimental conditions are indicated in the Experimental Section (2.2).

**Table 3.4.2-1.** Preparation conditions of the samples.

| Sample | Initial slurry pH | Reactants used $Si^{4+}$:$Al^{3+}$: $Mg^{2+}$:$NH_4^+$ ratio= 14.3:2.5:12.5:8 | $F^-$ addition | Use of microwaves | Aging time.(h) |
|---|---|---|---|---|---|
| S1 | 4.5 | $Mg(NO_3)_2{\cdot}6H_2O$, $Al(NO_3)_3 9{\cdot}H_2O$, $NH_4CH_3COO$ | --- | Yes | 6 |
| S2 | 7 | $Mg(CH_3COO)_2{\cdot}4H_2O$, $C_9H_{21}O_3Al$, $NH_3$ (aq). | --- | Yes | 6 |
| S2F | 7 | $Mg(CH_3COO)_2{\cdot}4H_2O$, $C_9H_{21}O_3Al$, $NH_3$ (aq) | $NH_4F$ | Yes | 6 |
| S2c | 7 | $Mg(CH_3COO)_2{\cdot}4H_2O$, $C_9H_{21}O_3Al$, $NH_3$ (aq) | --- | No | 72 |
| S3 | 8 | $Mg(CH_3COO)_2{\cdot}4H_2O$, $Al(OH)(CH_3COO)_2$, $NH_3$ (aq) | --- | Yes | 6 |
| S3-12 h | 8 | $Mg(CH_3COO)_2{\cdot}4H_2O$, $Al(OH)(CH_3COO)_2$, $NH_3$ (aq) | --- | Yes | 12 |
| S3c | 8 | $Mg(CH_3COO)_2{\cdot}4H_2O$, $Al(OH)(CH_3COO)_2$, $NH_3$ (aq) | --- | No | 72 |

### *3.4.3. Results and discussion*

*Use of microwaves for the synthesis of saponites*

Samples S1, S2 and S3 were synthesised with the same Si source (fumed SiO2), the same interlayer cation ($NH_4^+$), but with different Al and Mg sources (Table 3.4.2-1) following the reactants ratio reported by Vogels et al. (1997) (Table 3.4.2-1). From these reactants, we achieved three different pH values of the initial slurry (4.5, 7, and 8 for samples S1, S2 and S3, respectively). After 6 h of hydrothermal aging, the solution pH was similar for all samples (around 4.5).

UNIVERSITAT ROVIRA I VIRGILI
SYNTHESIS OF HECTORITES AND SAPONITES WITH MICROWAVES AND THEIR APPLICATION IN CATALYSIS AND COMPOSI
Isabel Vicente Valverde
ISBN:/DL:T. 1033-2011

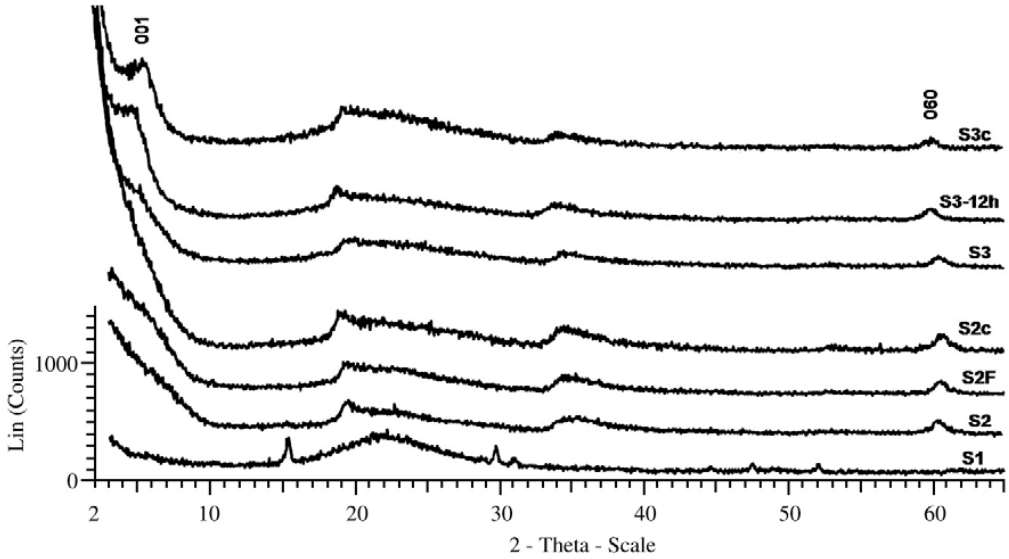


**Figure 3.4.3-1.** XRD patterns of the synthesised samples.

Figure 3.4.3-1 shows the XRD patterns obtained for these three samples. Several data obtained from XRD are also summarised in Table 3.4.3-1. The XRD pattern of S1 corresponds to a very amorphous solid with a wide band characteristic of amorphous silica around 22.8° whereas samples S2 and S3 showed the presence of several reflections characteristic of clays minerals, and a less intense band corresponding to the amorphous silica. No other crystalline phases were detected for S2 and S3 by XRD, such as bayerite ($Al(OH)_3$), which was found by other authors in the preparation of saponites when pH reached values between 6.4 and 5.4 (Vogels et al., 1997). In fact, when pH dropped down these values, these authors reported that bayerite disappeared. Although 001 reflection, related to the layer stacking, was not observed for any of these samples, 060 reflection, which is characteristic of trioctahedral clay minerals (Srodon, 2006), appeared clearly for S2 and S3 with a d060 of 0.153 nm (Table 3.4.3-1). This involves the occupation of the octahedral positions by $Mg^{2+}$.

Regarding the crystallinity of the saponite phase for S2 and S3, we observed that S3 was slight more crystalline than S2 since its crystallite size, determined from 060 reflection, was higher (Table 3.4.3-1). As commented before, the stacking degree of the layers for saponites S2 and S3 were very low. This indicates a very limited ordering in the c-axis for these samples. However, a reflection corresponding to a basal distance around 16 Å (2Θ≈5°) started to be defined for sample S3 (Figure 3.4.3-1). In the literature, this high value has been related to the presence of two water layers, which are typical when $Mg^{2+}$ is present in the interlayer space (Kloprogge et al., 1994b; Suquet et al., 1975).

**Table 3.4.3-1.** Characterisation of the samples prepared under microwaves.

| Sample | Si/Mg ratio ‡ (1.1) | | Si/Al Ratio ‡ (5.7) | | Mg/Al Ratio ‡ (5) | | d(060) nm | 060 Crystallite size (nm) | CEC (meq/ 100g) | BET Area ($m^2/g$) |
|---|---|---|---|---|---|---|---|---|---|---|
| | XRF | EDX | XRF | EDX | XRF | EDX | | | | |
| S1 | 125.3 | --- | 4.1 | 3.8 | 0 | 0 | --- | --- | --- | --- |
| S2 | 1.8 | 1.2 | 4.1 | 7.6 | 2.3 | 6.5 | 0.153 | 6.0 | 52 | 226 |
| S2F | 1.5 | 1.3 | 4.8 | 5.8 | 3.2 | 4.5 | 0.153 | 6.2 | 65 | 279 |
| S3 | 2.4 | 2.2 | 5.2 | 6 | 2.2 | 2.7 | 0.153 | 6.2 | 55 | 270 |
| S3-12h | 1.7 | 1.6 | 5.1 | 5.2 | 2.8 | 3.3 | 0.153 | 8.0 | 21 | 241 |

‡ Values between parentheses correspond to the initial reactants ratio.

Figure 3.4.3-2 shows the FTIR spectra taken for S1, S2, and S3. Bands were assigned taking into account the characterisation data reported for saponite samples (Kloprogge et al., 1999; Kloprogge and Frost, 2000; Rusell and Fraser, 1994). The appearance of one intense band around 1105 $cm^{-1}$ together with a shoulder at 1200 $cm^{-1}$ confirmed the presence of the amorphous silica phase, as observed by XRD, which was higher in the order S1>S3>S2. It is important to note the observation of one band around 1027 $cm^{-1}$, which corresponds to the Si–O–Si ordered in the clay mineral layer, for S2 and S3. This is again in

agreement with the XRD results. Three other IR bands were observed for S2 and S3 at 1401 $cm^{-1}$, 3675 $cm^{-1}$, and 666 $cm^{-1}$, which are associated to $NH_4^+$ bending, vibrations related to the Mg–OH stretch, and Mg–OH librations, respectively.

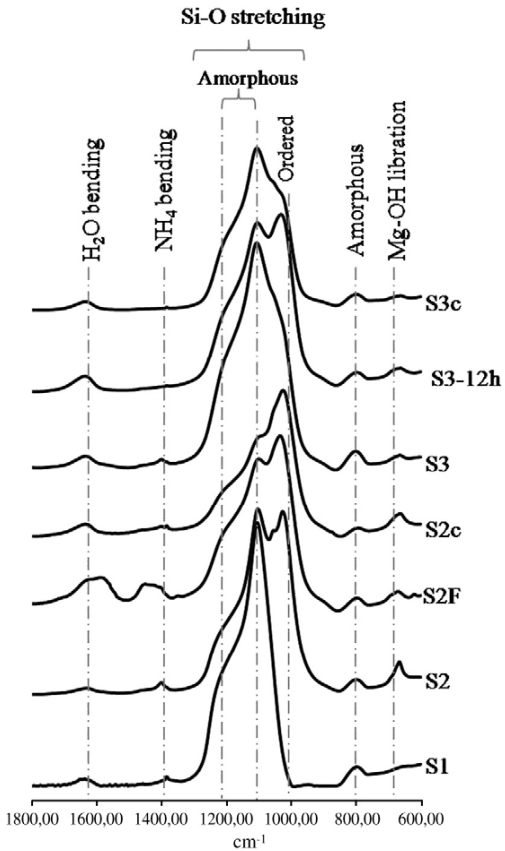


**Figure 3.4.3-2.** FTIR spectra for all samples.

XRF results revealed the presence of silicon and aluminium whereas magnesium was not practically detected for the amorphous sample S1 (Table 3.4.3-1). This can be explained by the high solubility of magnesium species in the acidic medium. With respect to the samples S2 and S3, XRF data indicated that magnesium started to be incorporated in the structure, in higher amounts for

S2, although both samples presented higher bulk Si/Mg ratios, and lower bulk Mg/Al ratios than the stoichiometric ratios (Table 3.4.3-1). For S3, the Si/Al ratio was 5.2, near the theoretical value of 5.7. By comparing these results with those obtained from EDX (Table 3.4.3-1), which correspond to surface composition, we can see that there was more Si and Mg in the external surface, especially for the sample prepared at pH 7 (S2), which showed surface Si/Al and surface Mg/Al ratios much higher (7.6 and 6.5, respectively) than the theoretical values (5.7 and 5, respectively). This means that these samples initially have nuclei richer in Al with a later progressive incorporation of Si and Mg.

Figure 3.4.3-3 shows the $^{27}$Al–MAS-NMR spectra obtained for several samples whereas Figure 3.4.3-4 depicts the Al(IV)(Td)/Al(VI)(Oh) ratio calculated for all of them. By increasing the initial slurry pH, tetrahedral aluminium increased. Thus, while S1 had Al mainly in octahedral (Oh) positions, S3 presented important amounts of Al in tetrahedral (Td) coordination. This is coherent with the formation of octahedral aluminium species at acid pH (S1). However, at basic pH (S3), the formation of $[Al(OH)_4]^-$ species with tetrahedral coordination could favour their incorporation into the tetrahedral sheets. The low Al(IV)(Td)/ Al(VI)(Oh) ratio observed for S2 (0.5) (Figure 3.4.3-4) could be related to the possible formation of octahedral aluminium species like amorphous bayerite from pH 6.5, not detected by XRD. These species can be incorporated in the octahedral sheets. As we can see, the peak due to tetrahedral Al appeared unfolded with one peak between 60 and 64 ppm, characteristic of the ordered tetrahedral aluminium, and another around 56 ppm, which has been assigned to more amorphous tetrahedral aluminium (Kloprogge et al., 1994a). S2 had less content of tetrahedral Al than S3, but its ordered tetrahedral aluminium was

higher (Figure 3.4.3-3).

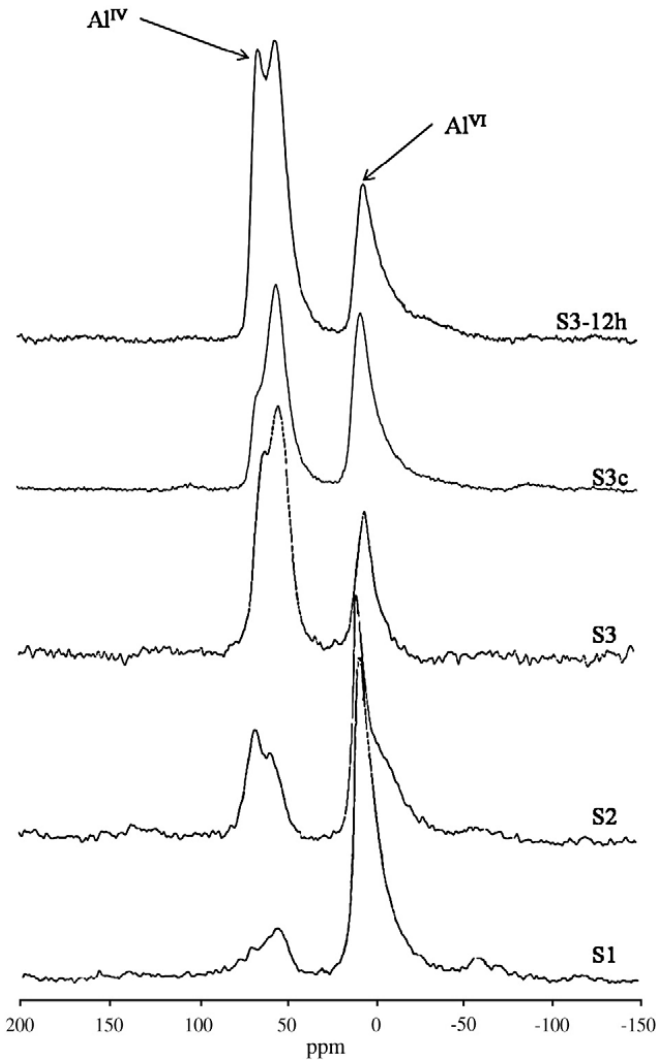


**Figure 3.4.3-3.** $^{27}$Al-MAS-NMR spectra for samples S1, S2, S3, S3c, and S3-12 h.

UNIVERSITAT ROVIRA I VIRGILI
SYNTHESIS OF HECTORITES AND SAPONITES WITH MICROWAVES AND THEIR APPLICATION IN CATALYSIS AND COMPOSI
Isabel Vicente Valverde
ISBN:/DL:T. 1033-2011

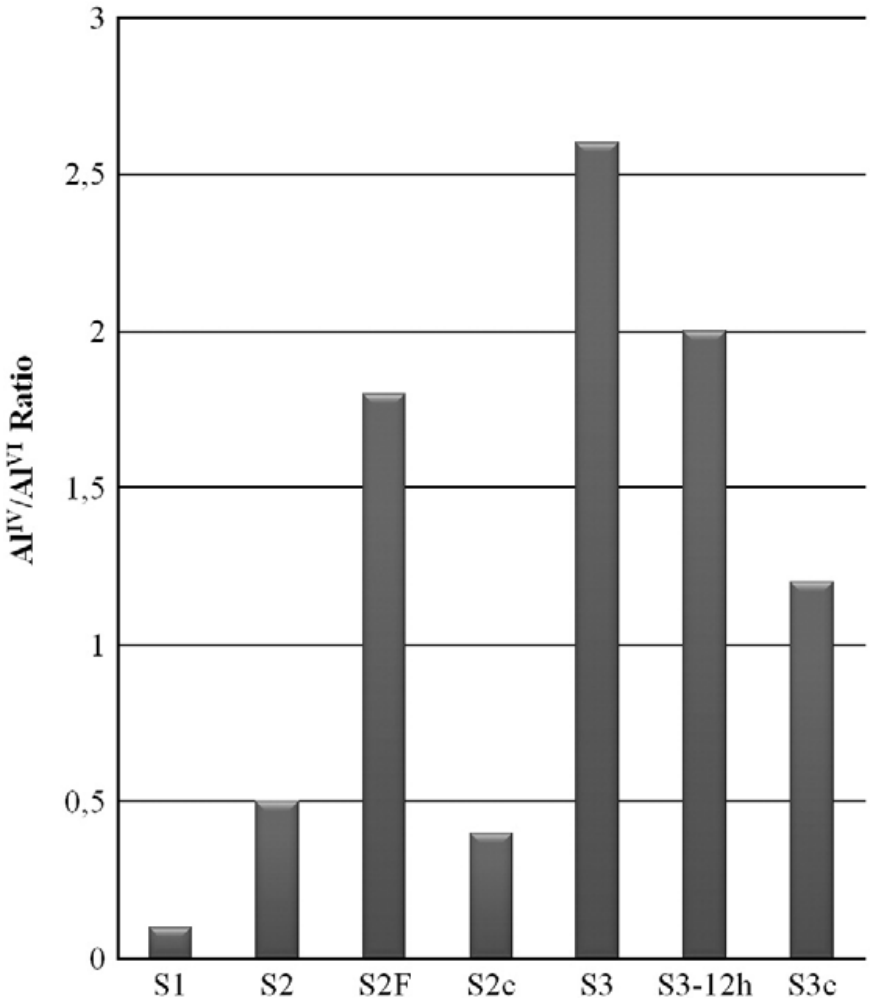


**Figure 3.4.3-4.** Al(IV)(Td)/Al(VI)(Oh) ratio obtained from $^{27}$Al-MAS-NMR spectra for all samples.

Regarding $N_2$ adsorption data, S3 exhibited higher BET specific surface area than S2 although S3 showed a slight more crystalline saponite phase (Table 3.4.3-1). This can be explained by the presence of higher amounts of amorphous silica in sample S3, as observed by FTIR (Figure 3.4.3-2).

With respect to the CEC values, determined for S2 and S3, they were very similar (Table 3.4.3-1) contrarily to the expected having in mind the higher amount of tetrahedral Al observed for S3 (Figure 3.4.3-3). Anyway, the higher percentage of ordered tetrahedral Al, and the lower amorphous silica content, which has no contribution to CEC, obtained for S2 could explain these values.

In order to have more information about the preparation of saponites, several modifications in the preparation procedure were made. Thus, one sample was synthesised at the same reaction conditions than S2 but adding $NH_4F$ (Al/F=1.25) to the reaction medium (sample S2F), and another sample was prepared by increasing the preparation time of S3 until 12 h (sample S3-12 h).

XRD pattern of S2F was very similar to that of S2 (Figure 3.4.3-1) confirming the formation of the clay mineral phase. The fluorinated saponite had slight higher crystallinity than S2 since its crystallite size value was higher (Table 3.4.3-1). Interestingly, the addition of $F^-$ allowed us to obtain Si/Mg, Si/Al and Mg/Al ratios more similar to those of the theoretical clay mineral (Table 3.4.3-1). FTIR spectrum of S2F showed an important improvement in the arranging of the O–Si–O in the layer (Figure 3.4.3-2). Besides, S2F had higher Al(Td)/Al(Oh) ratio (1.8) than S2 (0.5) (Figure 3.4.3-4) whereas the relative amount of ordered tetrahedral Al with respect to the total tetrahedral Al was similar for both samples. The high total content of ordered tetrahedral Al together with the lower amorphous silica amount (Figure 3.4.3-2) observed for S2F, justifies its higher CEC (65 meq/100 g) when compared to that of S2 (Table 3.4.3-1). From the $N_2$ adsorption results, S2F presented higher BET area than S2 (Table 3.4.3-1). This could be related to the appearance of additional porosity probably associated to the emptying of the pores occupied by the amorphous silica because of its

incorporation in the structure.

By increasing the preparation time of saponite S3 from 6 to 12 h (S3-12 h), there was an increasing of the clay mineral crystallinity (crystallite size of 8 Å, Table 3.4.3-1), as expected, accompanied by a best definition of the reflection (001) (Figure 3.4.3-1), associated to the stacking, with a basal distance of 16.3 Å, similar to that of S3. FTIR spectrum of S3-12 h also showed an improvement in the arrangement of the O–Si–O in the layer, as well as, a decrease in the $NH_4^+$ content (Figure 3.4.3-2). This sample had a composition closer to that of the stoichiometric clay mineral than sample S3, showing mainly an increase of Mg content (Table 3.4.3-1). At longer preparation time, the octahedral aluminium increased (Figure 3.4.3-3), and consequently the Al(Td)/Al(Oh) ratio decreased (Figure 3.4.3-4). This higher content of octahedral aluminium could be explained by the substitution of $Mg^{2+}$ by $Al^{3+}$ in the octahedral sheets, and also by the occupation of the interlayer space by some $Al^{3+}$ and/or $Mg^{2+}$, as deduced from the disappearance of the $NH_4^+$ band observed by FTIR for S3-12 h (Figure 3.4.3-2). Both effects contribute to the important decrease of measurable CEC obtained for this sample (from 44 meq/100 g in S3 to 21 meq/100 g in S3-12 h) (Table 3.4.3-1), since the layer has less negative charge, and also the interlayer $Al^{3+}$ and/or $Mg^{2+}$ cations are hardly exchangeable.

TEM images of saponites S2, S3, and S3-12 h (Figure 3.4.3-5a, b and c) showed the layer morphology characteristic of clay minerals. In agreement with other techniques, S2 presented a higher disorder of its layers whereas for S3-12 h, obtained at longer preparation time, we observed a higher ordering of the layers, which also had higher length than the other samples.

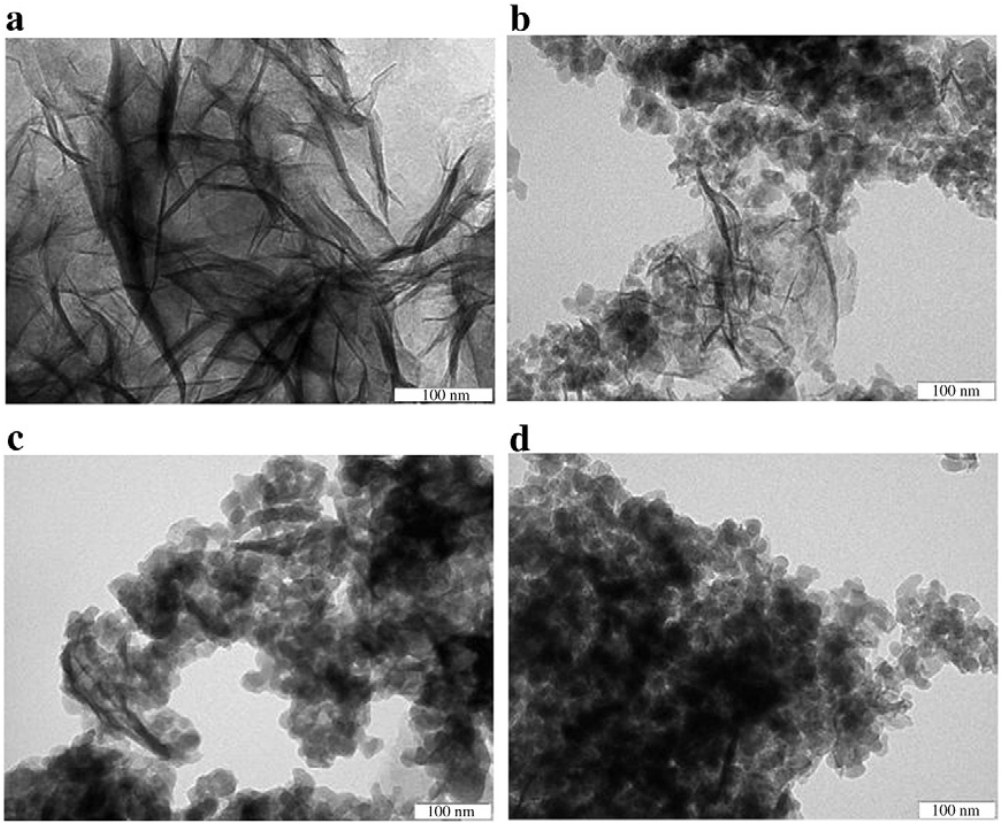


**Figure 3.4.3-5.** TEM image of samples a) S2 (×250 k), b) S3 (×200 k), c) S3-12 h (×200 k), and d) S3c (×200 k).

*Comparison with the saponites prepared by conventional heating*

Two samples were prepared by conventional method, S2c and S3c, at the same preparation conditions than those used to synthesise samples S2 and S3, respectively, but aging the slurry by conventional heating in an autoclave at 453 K for 72 h (Table 3.4.2-1). XRD patterns of S2c and S3c (Figure 3.4.3-1) allowed us to identify them as trioctahedral clay minerals, with d060 values of 0.153 nm (Table 3.4.3-2). The crystallinity of these saponites was higher than those prepared by microwaves. S3c was the most crystalline with a length of 7.8 nm

(Table 3.4.3-2). Another point to note is that the samples prepared by conventional heating presented similar layer ordering than the microwaved ones. Also in this case, XRD reflection (001) started to be defined for sample S3c, with a basal distance value of 16.3 Å. This involves the presence of magnesium in the interlayer space with two water layers (Kloprogge et al., 1994b). FTIR spectra variation between S2c and S3c (Figure 3.4.3-2) was similar to that observed between the samples prepared under microwaves (S2 and S3) since S3c had higher content of amorphous silica than S2c. However, S3 and S3c exhibited an ordered/amorphous Si-O stretching ratio very similar whereas when comparing S2 and S2c, we observed that S2c had a major contribution of ordered Si-O-Si. It is important to comment the decrease in the intensity of the NH4+ bending band, and the decrease in the intensity of the IR bands related to the presence of Mg for the samples prepared by conventional heating, especially for S3c (Figure 3.4.3-2).

**Table 3.4.3-2.** Characterisation of samples prepared by conventional heating

| Sample | Si/Mg ratio ‡ (1.1) EDX | Si/Al Ratio ‡ (5.7) EDX | Mg/Al ratio ‡ (5) EDX | d(060) nm. | 060 Crystallite size (nm) | CEC (meq/100g) | BET Area ($m^2/g$) |
|---|---|---|---|---|---|---|---|
| S2c | 1.5 | 5.9 | 3.9 | 0.153 | 6.3 | 50 | 346 |
| S3c | 3.4 | 5.2 | 1.5 | 0.153 | 7.8 | 34 | 215 |

‡ Values between parentheses correspond to the initial reactants ratio

With respect to the composition, the samples prepared by conventional heating showed by EDX, a lower magnesium content in the external surface than the samples synthesised under microwaves. The pH of the reaction medium become more acidic with time. Thus, the longer time used to prepare the conventional samples favours a substitution in the octahedral sheets of $Mg^{2+}$

by $Al^{3+}$, especially for S3c, as confirmed by comparing the IR bands assigned to Mg-OH (Figure 3.4.3-2). By comparing the Al (Td)/Al(Oh) ratio for S3 (2.6) with respect to S3c (1.2), and S2 (0.5) with respect to S2c (0.4) (Figure 3.4.3-4), we can confirm the incorporation of aluminium in the octahedral positions for the samples prepared by conventional heating, especially for S3c.

S3c had lower specific surface area than S3. This is in agreement with the higher crystallinity (higher crystallite size) observed for saponite S3c from XRD (Figure 3.4.3-1) since the amount of amorphous silica was very similar for both samples. On the other hand, S2c showed higher specific surface area than S2. This can be explained by some partial occupation of the clay mineral porosity by amorphous silica in S2 taking into account that in this sample, the amorphous silica content was higher.

By comparing CEC values, we observed that S3c had lower CEC (34 meq/100 g, Table 3.4.3-2) than S3 (55 meq/100 g, Table 3.4.3-1). The substitution of magnesium by aluminium in the octahedral sheets (coherent with the composition, Al(Td)/Al(Oh) ratio, and IR results) could involve some compensation of the layer charge generated by the substitution of silicon by aluminium in the tetrahedral sheets. Therefore, the total charge should be lower, explaining the lower CEC value of S3c. Besides, the presence of $Al^{3+}$ in the interlayer space, which is difficult to exchange, could contribute to this measurable CEC decrease. In the case of S2 and S2c, the difference in their CEC values was very small. In fact, the Al(Td)/Al(Oh) ratio variation was minor and, as observed by FTIR, the content of magnesium in the structure was slightly lower for S2c (Figure 3.4.3-2). Consequently, the lower charge compensation in the layer together with the decrease of the amorphous silica

ISBN:/DL:T. 1033-2011

observed for this sample, could explain this minor variation.

Figure 3.4.3-5d shows the TEM image taken for S3c where we can observe the high ordering of the saponite layers, with similar length to those of S3-12 h (Figure 3.4.3-5c), prepared under microwaves at much shorter time.

### *3.4.4. Conclusions*

Hydrothermal microwave treatment provides faster synthesis of saponites, whose characteristics depend on the initial slurry pH or the presence of fluoride in the reaction medium. At initial slurry pH of 7 in the presence of fluoride, we obtained in 6 h a saponite with the same crystallinity, higher Al(Td)/Al(Oh) ratio, and higher CEC (65 meq/ 100 g) than the saponite prepared by conventional heating method for a much longer time (72 h). When the initial slurry pH was 8, after 6 h of microwave treatment, saponite had very high Al (Td)/Al(Oh) ratio (around 2.6), and CEC of 55 meq/100 g, both higher than those of its corresponding conventional prepared sample. When the preparation time under microwaves was increased from 6 to 12 h, the crystallinity of saponite was higher, the amount of amorphous silica was lower, although measurable CEC and $NH_4^+$ decreased.

### *3.4.5. Acknowledgments*

The authors are grateful for the financial support of the Ministerio de Educación y Ciencia of Spain and FEDER funds (CTQ2005-02384/ PPQ and CTQ2008-04433/PPQ) and for the FPU grant (AP2006-00835) also financed by the Ministerio de Educación y Ciencia of Spain. The authors acknowledge Dr. Teresa Blasco Lanzuela from the Instituto de Tecnología Química (Valencia, Spain), for the performance of $^{27}$Al-MAS-NMR spectra.

# Chapter 4

## Saponites and hectorites as catalytic supports for the hydrogenation of styrene oxide

## 4.1. Introduction

### *4.1.1. 2-phenylethanol (2-PEA)*

2-phenylethanol (2-PEA) is a colourless transparent liquid and the main component of rose scent. It is used as a fragrance material in alimentary and perfume industry, and cosmetic production. 2-PEA is also present in foods like cocoa, cheese, coffee or cider, which had a fermentation step in their production. This alcohol is stable to alkali and, therefore, ideally suited for use in soap perfumes. (Bauer et al., 2001; Mookherjee et al., 1996). 2-phenylethanol is also used in pharmaceutical industry as local anaesthetic, antiseptic and solvent since it has propellant and fungicide properties (Zhu et al., 2011). When used in food chemistry, it is necessary for 2-PEA to be toxic compound free. 2-phenylethanol is obtained by low yielded procedures from natural sources like essential oils from flowers and plants (Bauer et al., 2001; Mookherjee et al., 1996). In order to obtain 2-PEA in higher amounts, many chemical methods have been developed. However, all of them reported environmental problems or are expensive.

### *4.1.2. Industrial methods for 2-phenylethanol (2-PEA) production*

Two of the main industrial processes for 2-PEA production are the Friedel-Craft alkylation (Bauer et al., 2001; Wilson, 1991, Scheme 4.1.2-1a) and the synthesis using Grignard reactants (Mookherjee et al., 1996, Scheme 4.1.2-1b).

Both processes have as principal disadvantages the high amount of wastes generated and the low purity of the obtained 2-PEA because of separation problems.

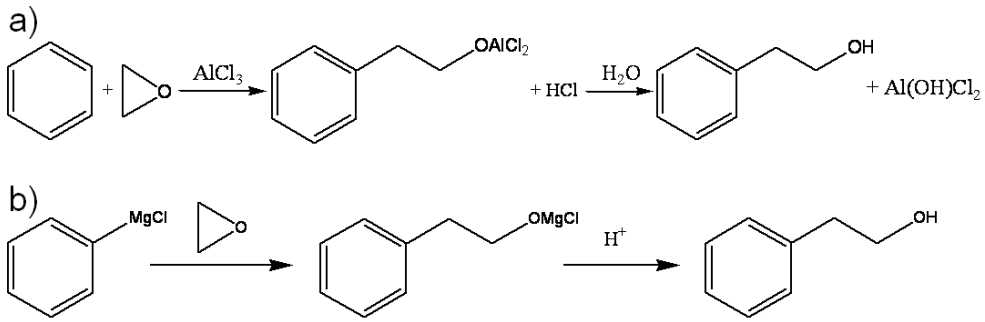


**Scheme 4.1.2-1.** Synthesis of 2-PEA by a) Friedel-Craft alkylation and b) using Grignard reactants.

Another widely described method is the styrene epoxide ring-opening reaction using as reductants hydrides or alkaline metals (Sreekumar et al., 1998, Scheme 4.1.2-2). However, the obtention of the most substituted alcohol, 1-phenylethanol (1) was more favoured than 2-phenylethanol (2).

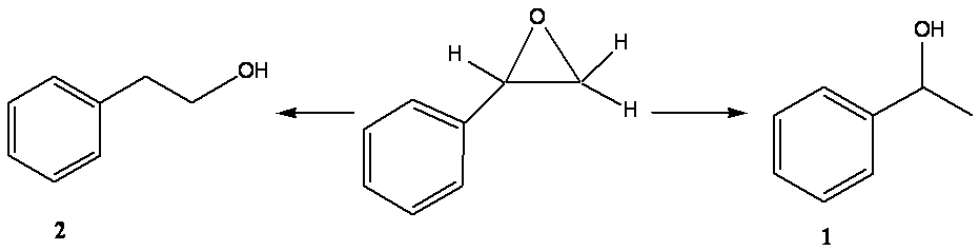


**Scheme 4.1.2-2.** Reaction products of styrene oxide reduction. (1) 1-phenylethanol; (2) 2-phenylethanol.

Afterwards, the reduction of styrene oxide was reported using as reductant zinc borohydride supported on silica and aluminium phosphate (Campelo and Chekraborty, 1996; Ranu and Das, 1990). Interestingly, 2-phenylethanol (90%) was obtained as main product since the use of an inorganic solid could control the selectivity towards the primary alcohol (2-PEA). However, many separation steps were necessary to obtain 2-PEA.

### *4.1.3. Catalysis as an alternative to industrial methods*

That is why in last decades the use of homogeneous and heterogeneous catalysts in the hydrogenation of styrene oxide has been studied as an alternative to the industrial methods.

Next, the most relevant studies are detailed.

*Homogeneous catalysts*

In order to obtain 2-phenylethanol, anion and cation metal catalysts have been used (Fujitsu et al., 1981; Grey et al., 1981).

The first studies about the use of homogeneous catalysts for the hydrogenation of styrene oxide were published in 1977. While Wilkison catalyst showed low activity for the hydrogenation of 2-PEA (Mochida et al., 1977), rhodium catalysts were used and yielded 2-PEA with 70% of selectivity. In 1981, ruthenium catalysts were also tested (Grey et al., 1981). In all the above mentioned studies, even after long reaction times, low conversion and low selectivity to 2-PEA (30 %) were obtained. It was not until 2001, when higher conversion and selectivity to 2-PEA were achieved (90% yield to 2-PEA) starting from methyl phenylacetate (Nomura et al., 2001., Scheme 4.1.3-1).

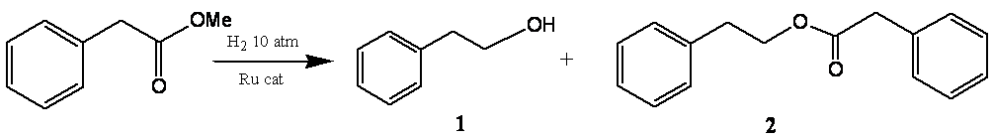


**Scheme 4.1.3-1.** Methyl phenylacetate hydrogenation using a Ru-phosphine catalyst, (1) 2-phenylethanol; (2) phenylethyl phenylacetate.

The use of homogeneous catalysts involved problems in the separation of 2-PEA and in the catalyst recuperation. One alternative could be to anchorage these homogeneous catalysts in solid supports (Islam et al., 2010), or the use of biphasic systems that can prevent catalysts deactivation (Sendovski et al., 2010).

*Heterogeneous catalysts*

Another interesting alternative to avoid the problems mentioned above, is the use of heterogeneous catalysts for the hydrogenation of styrene oxide to obtain selectively 2-phenylethanol (Bellefon et al., 1998, Scheme 4.1.3-2 ) resulting in lower cost and lower environmental problems.

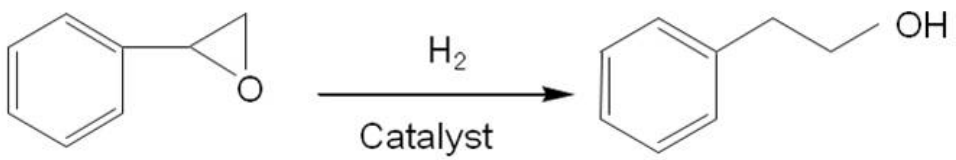


**Scheme 4.1.3-2.** Catalytic hydrogenation of styrene oxide.

There is one patent from 1950 (Wood, 1950) in which styrene oxide was hydrogenated to 2-phenylethanol at low temperature (0- 50 ºC) and low pressure (6-15 atm). However, selectivity to 2-PEA was also low and ethylbenzene and polymerisation products were also obtained.

In 1958 Hopff et al. observed that the presence of water and the addition of small amounts of alkaline substances (NaOH, $Na_2CO_3$, KOH, $K_2CO_3$, $Ca(OH)_2$, CaO, $Ba(OH)_2$) to the reaction medium, improved the selectivity to 2-PEA by controlling the appearance of another subproducts. It did not seem that reaction products were related to the alkaline used but to the pH, obtaining the best results for pH between 7 and 8.

Mitsui et al. tried to explain the positive effect of the alkaline substances by studying the influence of different metal catalysts when $NaOH_{(aq)}$ was added to the reaction medium (Mitsui et al., 1973).

The use of Ni-Raney resulted in the obtention of ethylbenzene and 2-phenylethanol as main products. Scheme 4.1.3-3, illustrates the proposed mechanism.

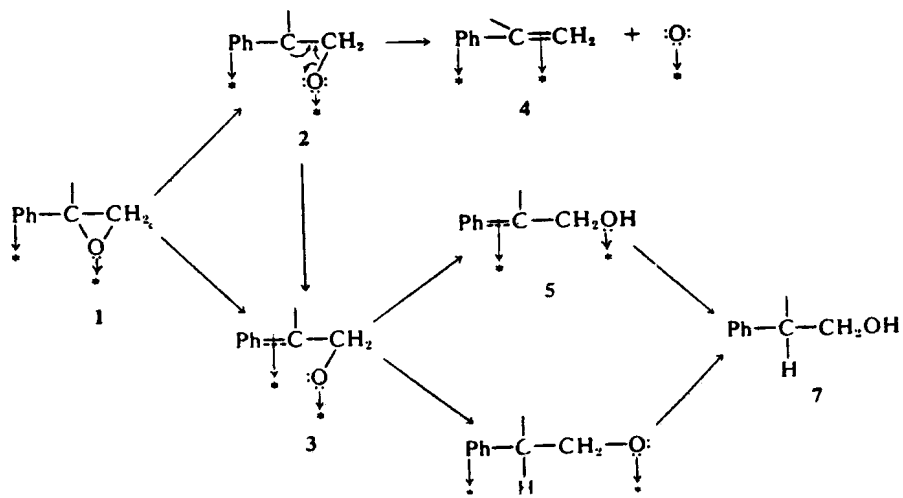


**Scheme 4.1.3-3.** Proposed mechanism by Mitsui et al for the hydrogenation of styrene oxide when using Ni-Raney catalysts.

The strong adsorption of the epoxide oxygen or the phenyl group increases the tension of the epoxide ring that results in the formation of the radical (2) or the π-benzyl complex (3). The radical formation is less favoured as time passed because of the aging of the catalyst, as it was confirmed by observing an increase of deoxygenated products (4) when more fresh catalyst was added to the reaction. The fact that the addition of NaOH to the reaction medium decreased the ethylbenzene formation was explained because of the presence of the hydroxyl group, which decreased the adsorption of the epoxide oxygen and favoured the π-benzyl complex formation (3).

Moreover, when palladium catalysts were used, 2-phenylethanol was obtained and no deoxygenated products were detected, indicating that the styrene oxide hydrogenolysis occurred through a $SN_2$ mechanism (Scheme 4.1.3-4).

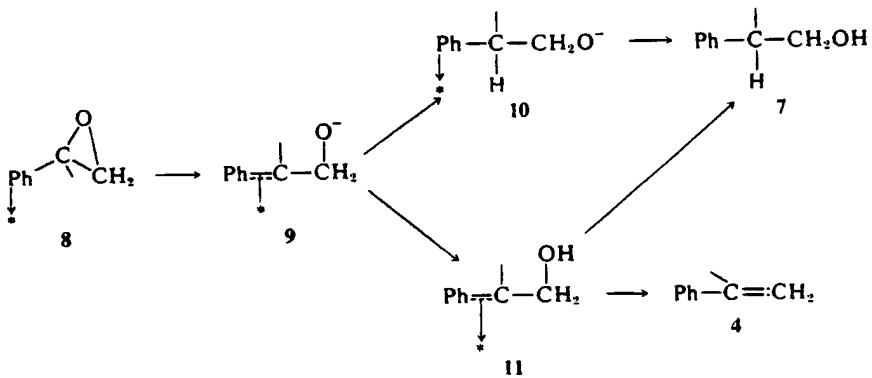


**Scheme 4.1.3-4.** Proposed mechanism by Mitsui et al. for the hydrogenation of styrene oxide when using palladium catalysts.

In 1998 Yadav and Chandalia studied the influence of several parameters (type and amount of catalyst, the stirring speed, the reaction temperature and the reagents concentration) for the hydrogenation of styrene oxide using Pd/C and Ni/Raney catalysts.

More recently, one patent describes the formation of 2-phenylethanol using metal-supported catalysts of nickel, palladium and platinum in the presence of organic as well as inorganic alkalis that promote the hydrogenation obtaining almost total conversion and total selectivity (99%) to 2-PEA at mild reaction conditions (313-393 K and 2-5 atm.).

Almost all the reported studies about the hydrogenation of styrene oxide have been performed in the liquid phase. However, there are few studies where styrene oxide hydrogenation was studied in the gas phase using supported palladium and supported platinum catalysts. (Kirm et al., 2005, 2007). At these conditions, when using an acid support, 1-phenylethanol and phenylacetaldehyde were the main products. Besides, when using a basic support, 2-phenylethanol was the main product.

In a previous work of our research work, in our research group the use of metal catalysts supported on solids with controlled basicity resulted in total conversion and total selectivity to 2-PEA (Bergadà et al., 2007b; 2008). Besides, long catalytic lives were observed. Nonetheless, there are no studies about the behaviour of metal catalysts supported on acid solids. The acid properties of clay minerals together with their specific surface areas could became these solids in interesting supports.

### *4.1.4. Other transformation reactions of styrene oxide*

Other transformation reactions of styrene oxide, can take place in the presence of acid sites (Bergadà et al. 2009, González et al. 2009, Salla et al. 2005, Scheme 4.1.4-1):

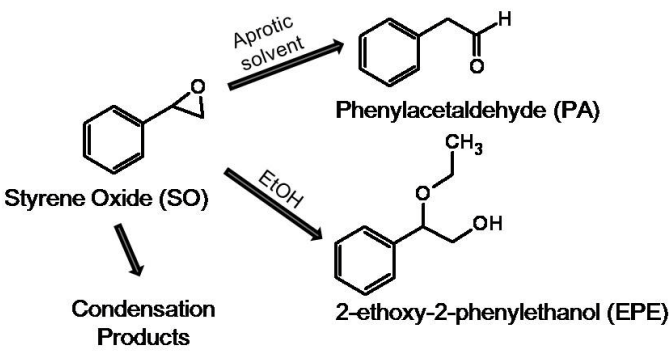


**Scheme 4.1.4-1.** Main products of other transformation reactions of styrene oxide isomerisation.

- Isomerisation of styrene oxide to phenylacetaldehyde (PA), which is catalysed by Brønsted acid sites. PA is an interesting product since it is used at industrial scale in fine chemistry to produce fragrances (this aldehyde gives a narcissus-like smell in floral perfumes), pharmaceuticals, insecticides, fungicides and herbicides (Hölderich and Barsnick, 2001; Kochkar et al., 2002). This reaction is favoured in aprotic solvents.

- Ring-opening reaction of styrene oxide to 2-ethoxy-2-phenylethanol occurs when ethanol is used as solvent. This reaction is catalysed by Lewis and Brønsted acid sites with medium strength.

- Condensation reactions that cause catalyst deactivation. They are catalysed by strong Brønsted acid sites in the presence of Lewis acid sites.

## 4.2. Ni nanoparticles supported on microwave-synthesised saponite for the hydrogenation of styrene oxide

### Abstract

Several saponites were synthesised under microwaves, at different preparation conditions, to be used as supports of nickel nanoparticles for the catalytic hydrogenation of styrene oxide to 2-phenylethanol. Ni/saponites obtained by impregnation with the highest nickel content (20 wt %) or by using saponites synthesised at lower pH (pH=7) resulted in high activity, high selectivity to 2-phenylethanol, and high resistance to deactivation catalysts. Catalytic results were related to the different NiO-saponite interactions observed by TPR.

### *4.2.1. Introduction*

Saponite $M_x[Mg_6Al_xSi_{8-x}O_{20}(OH)_4]$ (M=Na, Li, $NH_4$) is a trioctahedral 2:1 smectite where some substitution of Si(IV) by Al(III) in the tetrahedral (Td) sheet causes the negative charge of layers. This charge is compensated by interlayer exchangeable cations. When these cations are exchanged by transition metal cations ($Ni^{2+}$, $Pd^{2+}$, $Cu^{2+}$), metallic nanoparticles can be obtained, after reduction, in the interlayer space. Aluminium can also substitute magnesium in octahedral (Oh) positions, in a ratio $3Mg^{2+} = 2\ Al^{3+}$ without creation of positive charge, or as suggested by Suquet et al. (1981), in a ratio $1\ Mg^{2+} = 1\ Al^{3+}$, creating positive charge, which compensates the negative charge of the tetrahedral sheet. Additionally, $Al^{3+}$ and $Mg^{2+}$ can be also present as interlayer cations.

Nowadays, interest in smectites is increasing due to their important technological applications such as for nanocomposites preparation (Liu and Breen, 2005; Xue and Pinnavaia, 2008) or as heterogeneous catalysts due to their acidity and thermal stability (Varma, 2002; Casagrande et al., 2005). Large availability and low price are major advantages for using raw saponite. However, to obtain a reproducible composition, saponite must be synthesised.

Saponite synthesising procedures often involve hydrothermal treatments in autoclaves at water autogenous pressure (5-17 MPa), and at 423-723 K for long times, from hours to days (Kloprogge et al., 1994a; Jaber and Miéhe-Brendlé, 2005, 2008; Vogels et al., 1997; Vogels et al., 2005; Zhang et al., 2010; Zhou, 2010). There is an increasing interest in using microwaves to synthesise and to modify microporous and mesoporous materials (Newalkar et al., 2001; Bergadà et al., 2007a; Vicente et al., 2009; González et al., 2009). Some studies on the use of microwaves for saponite preparation have been published (Yao et al.,

2005; Rico et al., 2008; Trujillano et al.; 2010; Vicente et al., 2010; Zhang et al., 2010). However, residual amounts of amorphous silica were observed for all samples when using softer preparation conditions.

2-phenylethanol (2-PEA), the main component of rose oils, is widely used as a component in all chemical perfumes and as an additive in foods. Catalytic hydrogenation of styrene oxide to selectively obtain 2-phenylethanol is a cleaner alternative to the economical, environmental and purification problems shown by classical industrial production methods (Bauer et al., 2001; Wilson, 1991). Bulk nickel, palladium, and platinum catalysts have shown to be good catalysts for this reaction (Mitsui et al., 1973; Gibson and Theiling, 1977). The use of basic solids as catalytic supports considerably improved conversion and selectivity to 2-phenylethanol, as well as catalyst life (Bergadà et al., 2007b; 2008). Nevertheless, there is no information about the behaviour of metal catalysts in the presence of acid sites for this reaction.

Other transformation reactions of styrene oxide can take place in the presence of acid sites: isomerisation to phenylacetaldehyde (PA) catalysed by Brønsted acid sites, ring-opening reaction to 2-ethoxy- 2-phenylethanol (2-EPE), catalysed by Lewis and Brønsted acid sites with medium strength, and condensation reactions, which are responsible for catalyst deactivation and are catalysed by strong Brønsted acid sites in the presence of Lewis acid sites (Bergadà et al. 2009, González et al. 2009, Salla et al. 2005).

The aim of this work was to study the catalytic behaviour of several saponite-supported nickel catalysts for the hydrogenation of styrene oxide to 2-phenylethanol. The influence of residual amorphous silica in saponites on the

catalytic activity was also evaluated. Ni/saponite catalysts were obtained by impregnation with different nickel contents or by cation exchange. Saponites were synthesised under microwaves at different preparation conditions. Samples were characterised by XRD, XRF, TPR, TEM, FTIR, C.E.C. determination, $N_2$ adsorption, and $^{27}Al$ NMR techniques. The experimental conditions are indicated in the Experimental Section (2.2).

### *4.2.2. Experimental*

#### *Synthesis of saponites*

Magnesium acetate (Aldrich 98 % min. pur.), lithium hydroxide (Scharlau, 99 % min. pur.), and fumed $SiO_2$ (Aldrich, 99.8 % pur., BET area 227 $m^2/g$, particle size 11 nm) were used as reagents for all samples. Nevertheless, different Al reagents were employed to achieve different pH values in the initial slurry: aluminium basic acetate (Sigma-Aldrich, 14.8 % min. Al content) to obtain pH 8, and aluminium isopropoxide (Aldrich, 98 % min. pur.) to obtain pH 7.

Three samples were prepared at initial slurry pH of 8 with different $Si^{4+}/Al^{3+}/Mg^{2+}/Li^{+}$ molar ratios: 11.4/2.5/12.5/8 (20 % lower $SiO_2$ content than the stoichiometric amount), 14.3/2.5/12.5/8 (stoichiometric amount), and 26.8/2.5/12.5/8 (190 % higher $SiO_2$ content than the stoichiometric amount). Then, they were aged by autoclaving under microwaves (Milestone Ethos Touch Control) at 453 K for 6 h (S8a, S8b and S8c, respectively). Two more samples were synthesised at the same preparation conditions than S8a and S8b but at initial slurry pH of 7 (S7a and S7b, respectively). After aging, pH was similar (around 4.5) for all samples, which were washed by centrifugation up to neutrality, and dried overnight in an oven at 353 K.

*Preparation of saponites-supported nickel catalysts.*

Table 4.2.2-1 presents the preparation conditions of saponite-supported nickel catalysts. Nickel was introduced by two procedures: impregnation and cation exchange. All saponites were impregnated with nickel nitrate in the appropriate amounts to obtain 15 wt % of Ni in the final catalysts. Samples were calcined in air at 623 K (NiOs15-S8a, NiOs15-S8b, NiOs15-S8c, NiOs15-S7a, NiOs15-S7b), and reduced under pure hydrogen at 623 K for 6 h (Nis15-S8a, Nis15-S8b, Nis15-S8c, Nis15-S7a, Nis15-S7b). Two more catalysts were obtained by impregnation of S8a with nickel nitrate to result in 10 wt %, and 20 wt % of Ni in the final catalysts, which were obtained after calcination-reduction at the same conditions than the above samples (Nis10-S8a and Nis20-S8a, respectively).

**Table 4.2.2-1.** Preparation conditions of the catalysts.

| Catalyst | %Ni | Nickel introduction by | Reduction T (K) |
|---|---|---|---|
| Nis10-S8a | 10 | Impregnation | 623 |
| Nis15-S8a | 15 | Impregnation | 623 |
| Nis20-S8a | 20 | Impregnation | 623 |
| Nis15-S8b | 15 | Impregnation | 623 |
| Nis15-S8c | 15 | Impregnation | 623 |
| Nie/1-S8a | 1.2 | Cation exchange | 623 |
| Nie/1-S8b | 1.4 | Cation exchange | 623 |
| Nie/1-S8c | 1.6 | Cation exchange | 623 |
| Nie/2-S8c | 1.6 | Cation exchange | 673 |
| Nis15-S7a | 15 | Impregnation | 623 |
| Nis15-S7b | 15 | Impregnation | 623 |

ISBN:/DL:T. 1033-2011

$Ni^{2+}$-exchanged saponites were prepared by stirring 35 ml of $Ni(NO_3)_2 \cdot 6H_2O$ 0.25 M with 1 g of S8a, S8b and S8c at 338 K for 2 h. Samples were calcined in air at 623 K, and reduced under pure hydrogen at 623 K for 6 h (Nie1-S8a, Nie1-S8b, Nie1-S8c) (Table 4.2.2-1). $Ni^{2+}$-exchanged S8c was also reduced under pure hydrogen but at 673 K for 6 h (Nie2-S8c).

*Characterisation of samples*

Samples were characterised by X-ray diffraction (XRD), transmission infrared spectroscopy (FTIR), X-ray fluorescence (XRF), N2 adsorption, transmission electron microscopy (TEM), aluminium magic angle spinning nuclear magnetic resonance 27Al-MAS-NMR, temperature-programmed reduction (TPR), and determination of cation exchange capacity (CEC). The experimental conditions are indicated in the Experimental Section (2.2).

*Catalytic Activity Determination*

Catalytic hydrogenation of styrene oxide was performed in the liquid phase, using for all tests 1 g of catalyst, 150 mL of absolute ethanol (Panreac, 96 %) and 2 mmol of styrene oxide (Aldrich, 97 %) with a hydrogen flow of 2 mL/s and mechanical stirring at 500 rpm. The reaction was performed at room temperature. Sample was taken at 1, and 2 h of reaction. The reaction products were analysed by gas chromatography, using a chromatograph model Shimadzu GC-2010 equipped with a 30 m capillary column DB-1 coated with phenylmethylsilicon and a FID detector. They were quantified by adding an internal standard and by using calibrated lines.

UNIVERSITAT ROVIRA I VIRGILI
SYNTHESIS OF HECTORITES AND SAPONITES WITH MICROWAVES AND THEIR APPLICATION IN CATALYSIS AND COMPOSI
Isabel Vicente Valverde
ISBN:/DL:T. 1033-2011

## *4.2.3.Results and discussion*

### *Characterisation of saponites*

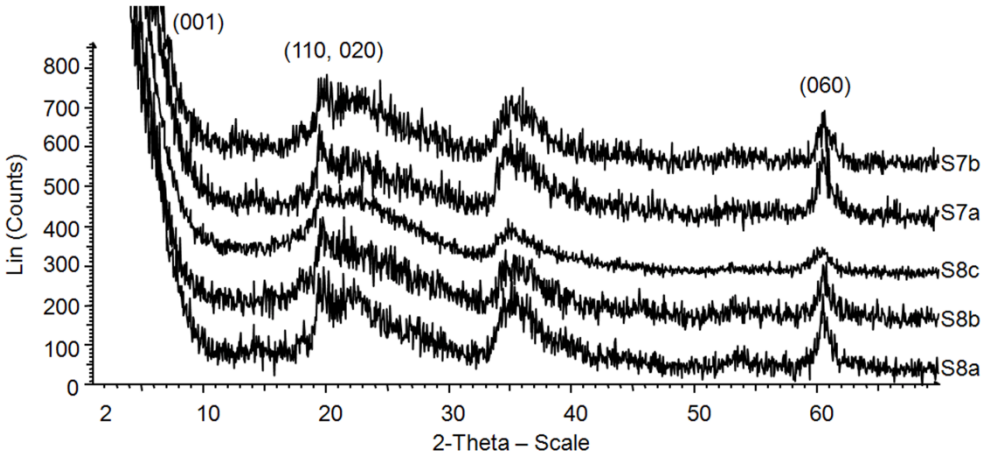


**Figure 4.2.3-1.** XRD patterns of samples S8a, S8b, S8c, S7a and S7b.

XRD patterns of S8a, S8b and S8c (Figure 4.2.3-1) showed the presence of reflections characteristic of clays minerals, and a broad band around 22.8º corresponding to amorphous silica, which decreased from S8c to S8a, making it possible to better distinguish the 020 reflection. Although the 001 reflection, related to layer stacking, was not observed for any of these samples, the 060 reflection, which is characteristic of trioctahedral clay minerals (Srodon, 2006), appeared clearly for all of them with a $d_{060}$ of 0.153 nm (Table 4.2.3-1). This involves the occupation of octahedral positions by $Mg^{2+}$. S8c was slightly less crystalline than S8a and S8b since its crystallite size, determined from the 060 reflection, was lower (Table 4.2.3-1). The lower stacking degree of the layers observed for the three saponites indicated a very limited ordering in the c axis.

**Table 4.2.3-1.** Characterisation data of saponite samples.

| Sample | d(060) nm | Crystallite size (060) (nm) | Si/Mg ratio[a] | Si/Al ratio[a] | Mg/Al ratio[a] | Al (Td)/ Al(Oh) ratio | C.E.C. (meq/ 100g) | BET Area ($m^2/g$) |
|---|---|---|---|---|---|---|---|---|
| S8a | 0.1528 | 6.6 | 1.6 (0.9) | 3.8 (4.6) | 2.3 (5) | 1.0 | 40 | 344 |
| S8b | 0.1528 | 6.7 | 2.4 (1.1) | 5.0 (5.7) | 2.0 (5) | 1.1 | 49 | 386 |
| S8c | 0.1530 | 6.2 | 4.5 (2.1) | 9.7 (10.7) | 2.2 (5) | 2.5 | 55 | 290 |
| S7a | 0.1528 | 5.7 | 1.7 (0.9) | 3.1 (4.6) | 1.9 (5) | 1.0 | 45 | 314 |
| S7b | 0.1528 | 5.9 | 1.9 (1.1) | 3.6 (5.7) | 1.8 (5) | 1.1 | 35 | 339 |

[a]Values in parentheses correspond to the initial reagent ratio

FTIR spectra for S8a, S8b, and S8c are illustrated in Figure 4.2.3-2. Bands were assigned taking into account the characterisation data reported for saponite samples (Kloprogge et al., 1999; Kloprogge and Frost, 2000; Russel and Fraser, 1994). The appearance of one intense band around 1105 $cm^{-1}$ together with a shoulder at 1200 $cm^{-1}$ confirmed the presence of amorphous silica in S8c, as detected by XRD. The intensity of this band decreased in the order S8c > S8b > S8a, as expected. For S8a and S8b, the band mainly observed was that due to the Si-O stretching in a ordered structure, which appeared around 1027 $cm^{-1}$.

XRF results revealed the presence of silicon, magnesium and aluminium in the three samples (Table 4.2.3-1). The Si content increased from S8a to S8c, and consequently the Si/Mg and Si/Al ratios also increased, according to the molar ratios of the reagents used. The amount of Mg was similar in the three samples, and was always lower than the expected value. This can be explained by the magnesium solubilisation at the pH of the work (from 8 to 4.5). The content of Al was also similar in the three samples, and was always higher than the expected value. This means that, in addition to tetrahedral aluminium, aluminium can be

also in octahedral positions in the layers as well as in the interlamellar space. These contributions should be more important when the content of Si is lower, as deduced from the important decrease of Al (Td)/Al(Oh) ratio observed by $^{27}$Al-NMR (Table 4.2.3-1) when the amount of $SiO_2$ used in the synthesis decreased, specially for S8a.

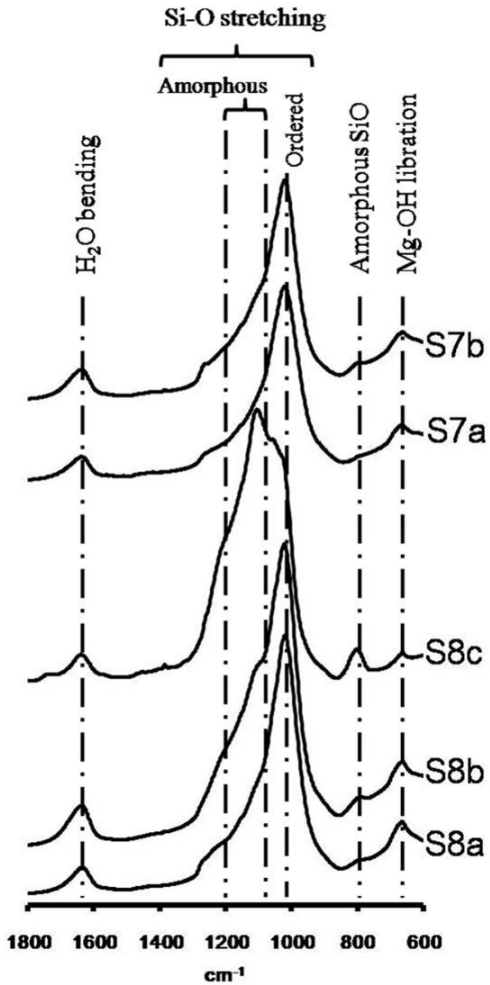


**Figure 4.2.3-2.** FTIR spectra of samples S8a, S8b, S8c, S7a and S7b.

Regarding $N_2$ adsorption data (Table 4.2.3-1), S8c exhibited a lower BET surface area than S8b and S8a, despite its lower crystallite size. This can be explained by the higher amount of amorphous silica, which may block saponite pores, that was observed by FTIR for S8c (Figure 4.2.3-2), which may block saponite pores.

With respect to C.E.C. values, they increased in the order S8a < S8b < S8c. The higher percentage of tetrahedral aluminium (higher substitution of Si by Al in the tetrahedral sheet) observed in S8c can explain its higher C.E.C. since amorphous silica had no contribution. The lower C.E.C. values of S8a and S8b can be justified because some amount of Oh aluminium, that may be located in the interlamellar space as $Al^{3+}$ or as hydrolysed aluminium species, cannot be exchanged by the copper complex used in the determination of C.E.C. Besides, some aluminium can be in the octahedral sheet, instead of magnesium, counteracting the positive charge generated in the tetrahedral sheet.

XRD patterns of samples S7 showed the typical reflections of trioctahedral smectites with a low order in the stacking (Figure 4.2.3-1). The main difference between S7 and S8 samples was the lower crystallite size, calculated from the 060 reflection, of S7 samples (5.7 and 5.9 nm) with respect to the S8 ones (6.6 and 6.7 nm) (Table 4.2.3-1).

FTIR spectra for S7a and S7b were similar to the FTIR spectrum of S8a (Figure 4.2.3-2). This means that the amount of amorphous silica in these samples was very low, according to XRF results.

Si, Mg and Al contents were similar in S7 samples despite the ratio of reagents used (Table 4.2.3-1). It is important to remark on the higher amount of aluminium

of these samples. Consequently, part of this aluminium would be occupying octahedral positions, either layer or interlamellar, as in samples S8a and S8b. This was in agreement with the Al(Td)/Al(Oh) ratios, calculated from $^{27}$Al-NMR spectra, which showed a similar tendency as for S8a and S8b, respectively (Table 4.2.3-1).

Specific surface areas of samples S7 were similar but lower than those observed for corresponding S8 samples (Table 4.2.3-1). The presence of hydrolysed $Al(OH)^{2+}$ species in the interlamellar space could partially block the pores resulting in lower BET areas. This agrees with the low C.E.C. values calculated for these samples (Table 4.2.3-1) since these hydrolysed $Al(OH)^{2+}$ species may be difficult to be exchanged by the copper complex used in the C.E.C. determination procedure. Additionally, some $Al^{3+}$ occupying octahedral positions in the saponite layer could also contribute to these lower C.E.C values.

In conclusion, the amount of amorphous $SiO_2$ present in the synthesised saponites depended on the molar ratio of reagents and the initial slurry pH, and determined the properties of the saponites.

*Catalytic activity of nickel/saponite catalysts in the hydrogenation of styrene oxide.*

Saponites (S7, S8), and the silica source used as reagent, showed negligible conversion values for the styrene oxide hydrogenation, styrene oxide isomerisation, and styrene oxide ring-opening reactions.

Nis15-S8a, Nis15-S8b and Nis15-S8c, prepared from saponites with different silica contents (S8a, S8b and S8c) impregnated with the same percentage of nickel (15 wt %), resulted in almost total selectivity to 2-PEA for different

conversion values after 1 h of reaction. (Figure 4.2.3-3). Conversion was higher (55 %) for the sample with higher silica content (Nis15-S8c). Nevertheless, the order of conversion (Nis15-S8c> Nis15-S8a> Nis15-S8b), did not follow the order of silica content. Therefore, some contribution of silica to the catalysts activity cannot be discarded especially taking into account that Ni/fumed $SiO_2$ (15 wt % of nickel) also yielded high conversion and high selectivity to 2-PEA after 1 h of reaction.

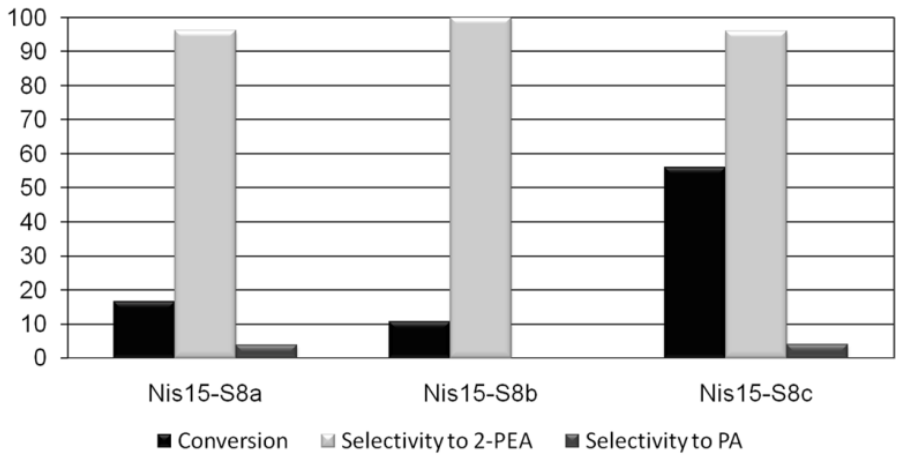


**Figure 4.2.3-3.** Catalytic results after 1 h of reaction of samples Nis15-S8a, Nis15-S8b and Nis15-S8c.

In order to understand the differences observed in the catalytic behaviour of these catalysts, the reducibility of their precursors was studied by TPR. Thermograms of the three samples showed mainly three peaks (Figure 4.2.3-4) the maxima of which are presented in Table 4.2.3-2. The first peak appeared around 523 K with low intensity for all samples. The second peak, around 703 K, exhibited a different intensity in the order NiOs15-S8a> NiOs15-S8c> NiOs15-S8b (Figure 4.2.3-4).

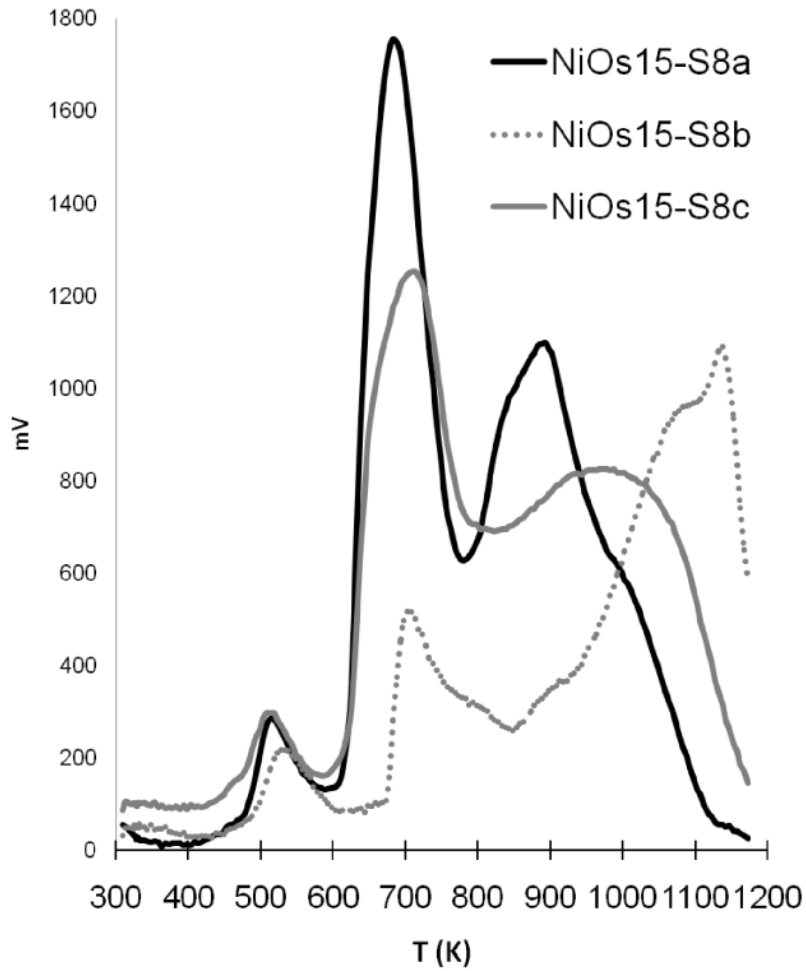


**Figure 4.2.3-4.** TPR curves of samples NiOs15-S8a, NiOs15-S8b and NiOs15-S8c.

Finally, the third peak presented significant differences in the maximum reduction temperature, which was at 888 K, 978 K and 1083 K for NiOs15-S8a, NiOs15-S8c and NiOs15-S8b, respectively (Table 4.2.3-2).

**Table 4.2.3-2.** Characterisation data from TPR curves of catalytic precursors.

| Catalyst | T Peak 1 (K) | T Peak 2 (K) | T Peak 3 (K) |
|---|---|---|---|
| NiOs15-S8a | 513 | 688 | 888, 998 |
| NiOs15-S8b | 566 | 708 | 1083, 1138 |
| NiOs15-S8c | 518 | 718 | 978 |
| NiOs15-S7a | 523 | 698 | 883, 993 |
| NiOs15-S7b | 518 | 693 | 873, 983 |

[a]Temperature corresponding to the maximum of the peak.

Since different NiO-support interactions were observed for each precursor, their corresponding catalysts may have nickel sites with different characteristics, and consequently different activity should be expected. The lowest conversion of catalyst Nis15-S8b could be related to the presence of metal nickel sites with a higher influence of support. Actually, the TEM image of Nis15-S8b (Figure 4.2.3-5a) showed the presence of smaller and more dispersed nanoparticles than Nis15-S8a and Nis15-S8c (Figure 4.2.3-8b, Figure 4.2.3-5b). The sizes of nickel particles for Nis15-S8b ranged from 5 to 10 nm. This agrees with the crystallite size (7 nm) calculated from its XRD pattern that only showed the presence of the nickel phase. Moreover, maximum reduction temperatures of peaks 2 and 3 of NiOs15-S8c were higher than those of NiOs15-S8a (Table 4.2.3-2). This should be related to slightly higher NiO-support interaction, which after reduction, resulted in more active nickel nanoparticles for this reaction. This explained the higher conversion observed for Nis15-S8c.

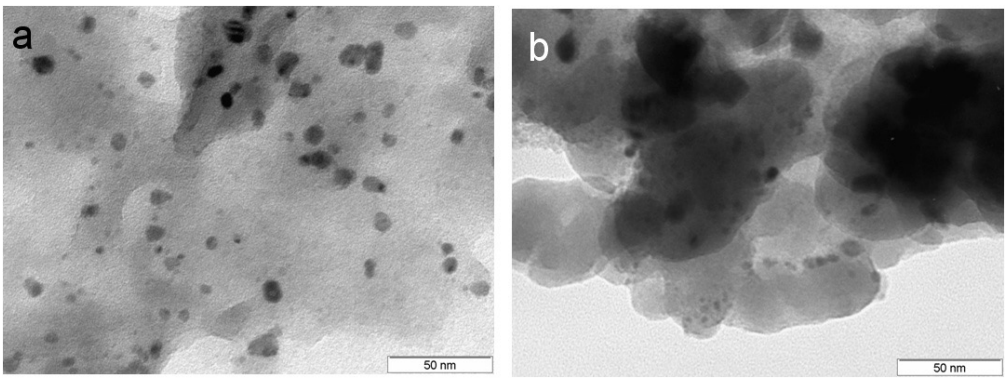


**Figure 4.2.3-5.** TEM images of samples: a)Nis15-S8b x500k and b)Nis15-S8c x500k.

High selectivity to 2-PEA was explained in nickel catalysts promoted by basic solutions through the formation of the π benzyl complex from the adsorbed styrene oxide, that yielded a primary alkoxide ion, which was stabilised by NaOH, and finally hydrogenated to the primary alcohol (Mitsui et al., 1973). Another possible pathway in a basic medium was the formation of the secondary alkoxide ion, which through hydride attack gave 2-PEA (Mitsui et al., 1973, Rode et al., 2000, 2003).

The high selectivity to 2-PEA in these Ni/saponite catalysts without basic promotion could be explained by the formation of a primary alkoxide ion, stabilised by acid sites, which yielded the primary alcohol by hydrogenation. Actually, the presence of Brønsted acid sites was confirmed since phenylacetaldehyde was detected at short reaction times for these catalysts. Fortunately, this compound was hydrogenated to 2-PEA, and after 6 h and 10 h for Nis15-S8a and Nis15-S8b, respectively, total conversion and total selectivity to 2-PEA was obtained. The catalytic behaviour of these catalysts remained constant after five runs.

Conversion and selectivity results of the Ni/saponite catalysts obtained by

cation exchange and later calcination-reduction (NieS8a/1, NieS8b/1, NieS8c/1, NieS8c/2) were calculated (Table 4.2.3-3). Activity of fumed silica reagent subjected to the same preparation procedure than the exchanged catalysts was also tested. No adsorption of nickel by silica was observed and conversion was negligible.

**Table 4.2.3-3.** Catalytic results after 2 h of reaction of samplesNie/1-S8a, Nie/1-S8b, Nie/1-S8c and Nie/2-S8c.

| Catalyst | Conversion (%) | Selectivity to PA (%)[a] | Selectivity to 2-PEA (%)[b] | Selectivity to 2-EPE (%)[c] |
|---|---|---|---|---|
| Nie/1-S8a | 22 | 72 | 0 | 28 |
| Nie/1-S8b | 15 | 60 | 0 | 40 |
| Nie/1-S8c | 25 | 60 | 40 | 0 |
| Nie/2-S8c | 100 | 0 | 0 | 100 |

[a]PA: phenylacetaldehyde, [b]2-PEA: 2-phenylethanol.

[c]2-EPE: 2-ethoxy-2-phenylethanol.

NieS8a/1, NieS8b/1, and NieS8c/1 prepared from saponites synthesised with different silica content, showed low conversion (15-25 %), high selectivity to phenylacetaldehyde (60-72 %), and fast deactivation (after 2 h of reaction conversion was almost constant). The low conversion values may be related to the low percentage of nickel in these samples (< 2 %) together with the presence of some acid sites that deactivated catalysts by the formation of condensation products (Salla et al., 2005). The high selectivity to phenylacetaldehyde (PA) can be associated with Brønsted acid sites generated during NiO formation. The appearance of 2-ethoxy-2-phenylethanol (2-EPE) in catalysts NieS8a/1 and NieS8b/1 could be related to the formation of some Lewis acid sites during thermal treatments. Interestingly, NieS8c/1 also gave 2-phenylethanol (40 %) whereas 2-EPE did not appear. This could be explained by two facts: one was

its slightly higher Ni content (Table 4.2.2-1), since it was prepared from the saponite with higher C.E.C. (Table 4.2.3-1), having in mind that metal sites are responsible for hydrogenation of styrene oxide to 2-phenylethanol; the other one was the absence of Lewis acid sites competing with metal ones for the styrene oxide transformation, since with NieS8c/1 the ring-opening reaction to 2-PEA did not take place (Table 4.2.3-3). On the other hand, the absence of 2-phenylethanol for NieS8a/1 and NieS8b/1 could be attributed to the competition of hydrogenation and ring-opening reactions since, in these catalysts, 2-EPE was obtained.

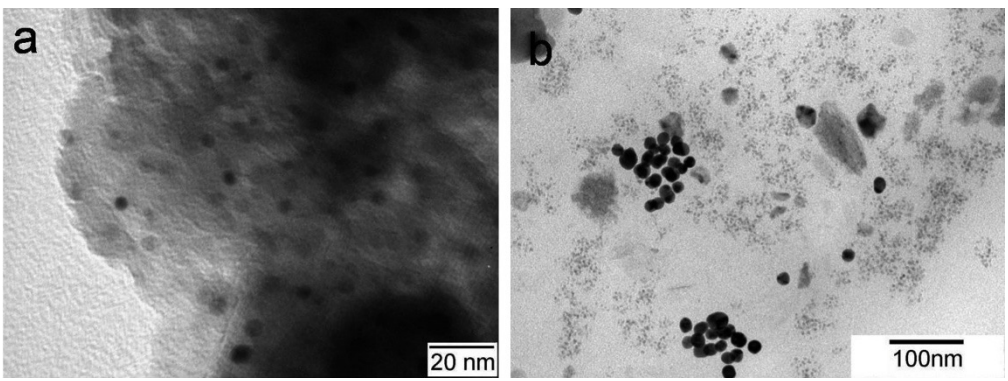


**Figure 4.2.3-6.** TEM images of samples: a) Nie1-S8b x800k and b) Nie1-S8c x200k.

Regarding TEM images of catalysts NieS8b/1 and NieS8c/1 (Figure 4.2.3-6), dark nanoparticles with sizes around 15 nm, probably of nickel, were observed in catalyst NieS8c/1. In contrast, catalyst NieS8b/1 showed lighter nanoparticles around 2 nm supposed to contein NiO phase. This could mean that degree of reduction was lower for this catalyst, and consequently lower water formation during $Ni^{2+}$ reduction could be expected, favouring the saponite dehydroxylation, and therefore the appearance of higher amounts of Lewis acid sites that justify the higher selectivity to 2-EPE observed (40 %). Catalyst NieS8c/2 improved

conversion (100 %) with respect to NieS8c/1 but total selectivity to the non desired 2-ethoxy-2-phenylethanol (2-EPE) was obtained. The higher reduction temperature used to prepare this catalyst should favour a higher dehydroxylation of saponite resulting in a loss of Brønsted acid sites together with the generation of higher amounts of Lewis acid sites. The loss of Brønsted acidity explained the lack of detection of phenylacetaldehyde whereas the higher amounts of Lewis acid sites catalysed the formation of 2-EPE (Table 4.2.3-3). This reaction seems to be faster than hydrogenation. The presence of amorphous silica should not contribute to the activity since free $SiO_2$ and adsorbed nickel-$SiO_2$ were not active, as commented above.

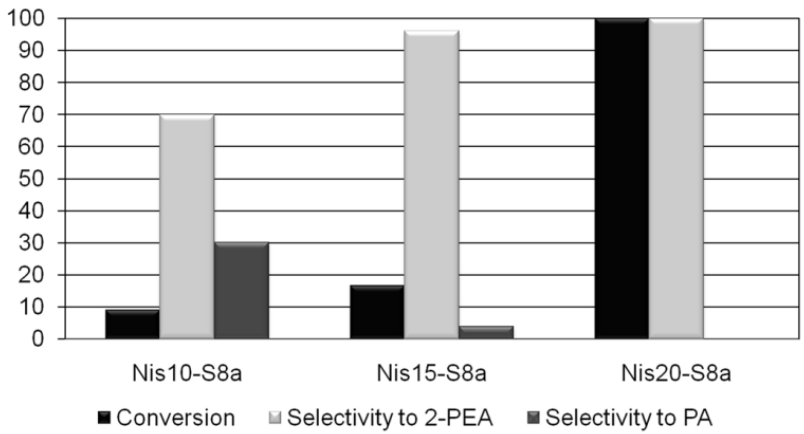


**Figure 4.2.3-7.** Catalytic results after 1 h of reaction of samples Nis10-S8a, Nis15-S8a and Nis20-S8a.

The activity results of the catalysts obtained from the impregnation of saponite S8a with different Ni contents (Nis10-S8a, Nis15-S8a, Nis20-S8a) are illustrated in Figure 4.2.3-7. When nickel percentage in the catalyst was lower, conversion and selectivity values to 2-PEA decreased, at the expense of phenylacetaldehyde formation. The most active catalyst was that prepared with

the highest nickel content (Nis20-S8a) with total conversion and total selectivity to 2-PEA at 1 h of reaction whereas conversion of Nis10-S8a and Nis15-S8a were quite low (10 % and 18 %, respectively). Moreover, while Nis15-S8a reached total conversion and total selectivity to 2-PEA at 6 h of reaction, it was not possible to obtain total conversion, even after a long time of reaction, for Nis10S8a, confirming its deactivation.

The increase of selectivity to PA and the deactivation observed for Nis10-S8a, can be explained by the higher accessibility of the reactants to the acid sites because of the lower coverage of nickel. These acid sites catalysed the styrene oxide isomerisation to PA and the formation of condensation products (Bergadà et al. 2009, González et al. 2009; Salla et al., 2005).

TEM was used to monitor the size of nickel nanoparticles on catalysts Nis10-S8a, Nis15-S8a and Nis20-S8a (Figure 4.2.3-8). An increase of nickel coverage on the saponite surface was observed at higher nickel content, together with an increase in the average nanoparticle size, from 10 nm for the catalyst with the lowest Ni content (Nis10-S8a) to 25 nm for the catalyst with higher Ni content (Nis20-S8a).

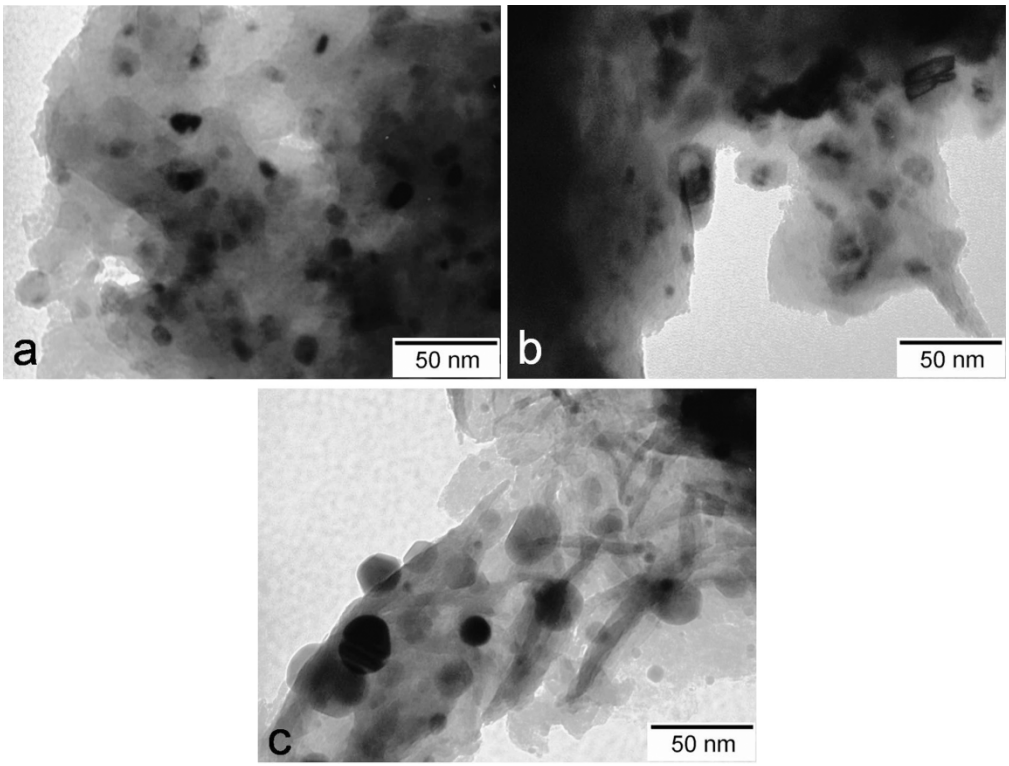


**Figure 4.2.3-8.** TEM images of samples: a)Nis10-S8a, b) Nis15-S8a, and c) Nis20-S8a x500k.

Catalytic results of Nis15-S7a and Nis15-S7b, prepared by impregnating the saponites synthesised at pH=7 with 15 wt % of nickel the saponites synthesised at pH=7, are presented in Figure 4.2.3-9. To compare these results with those obtained with Nis15-S8a and Nis15-S8b (Figure 4.2.3-3), it is important to remember that no residual amounts of $SiO_2$ were observed for saponites S7 by FTIR (Figure 4.2.3-2).

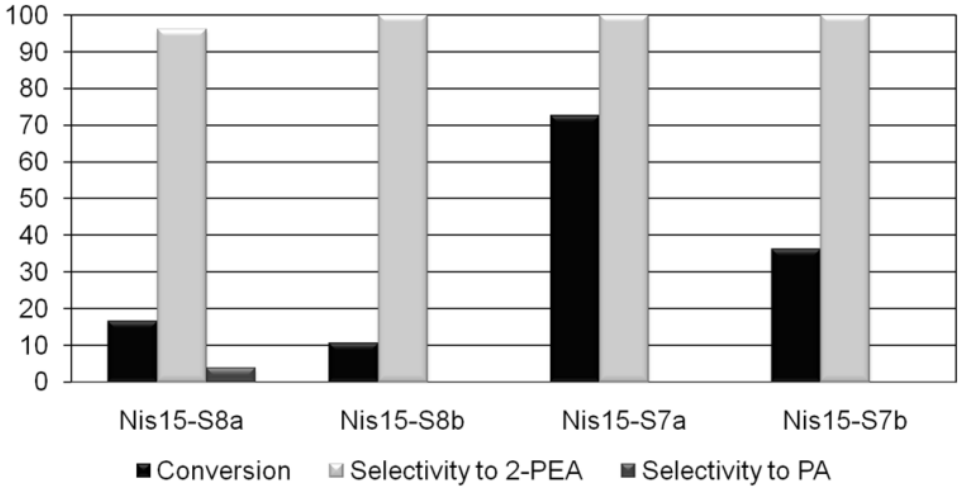


**Figure 4.2.3-9.** Catalytic results after 1 h of reaction of samples Nis15-S8a, Nis15-S8b, Nis15-S7a and Nis15-S7b.

Selectivity to 2-phenylethanol was almost 100 % for all catalysts after 1 h of reaction but important differences arose with respect to conversion (Nis15-S7a > Nis15-S7b > Nis15-S8a > Nis15-S8b). The higher conversion of the catalysts prepared with S7 can be explained by the presence of metal nickel sites, the interaction of which with the support conferred them higher activity. Interestingly, the intensity of peak 3 around 983 K observed in the TPR of their catalytic precursors (Figure 4.2.3-4, Figure 4.2.3-10 and Table 4.2.3-2) was higher for the catalysts which showed higher conversion (Nis15-S7a > Nis15-S7b > Nis15-S8a) according to the higher intensity also observed in the TPR for the catalytic precursor of Nis15-S8c (Figure 4.2.3-4), which also exhibited higher conversion than Nis15-S8a and Nis15-S8b. Therefore, the presence of high amounts of metallic nickel with medium support interaction may be responsible for the electronic characteristics of these metal sites favouring conversion. The higher conversion of Nis15-S7a and Nis15-S7b, the saponites of which did not show

residual amorphous silica, confirmed that the presence of silica did not have an important contribution to the activity of Ni/saponite catalysts.

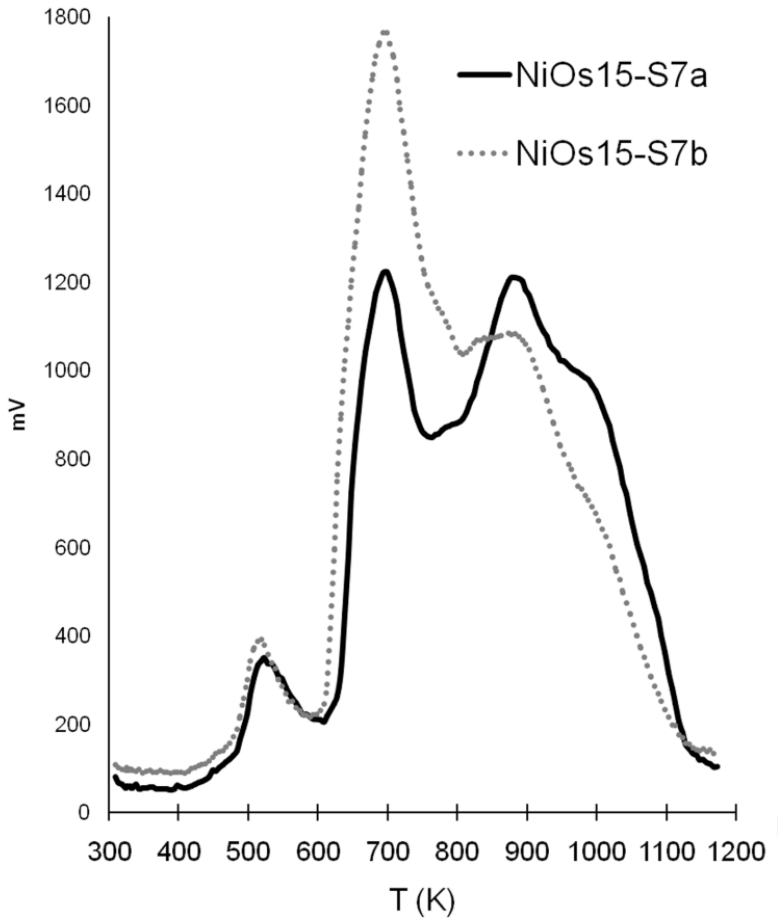


**Figure 4.2.3-10.** TPR curves of samples NiOs15-S7a and NiOs15-S7b.

### *4.2.4. Conclusions*

The use of microwaved-synthesised saponites as supports of nickel nanoparticles for the catalytic hydrogenation of styrene oxide resulted in high activity, high selectivity to 2-phenylethanol and high resistance to deactivation catalytic systems. Saponites with different properties were obtained by modifying the ratio of reagents and the synthesis pH.

The activity of Ni/saponites, obtained from impregnation of saponites with nickel nitrate and later calcination-reduction, mainly depended on the nickel content and the initial slurry pH used for the synthesis of saponite. These results were related to the presence of metal nickel sites with different activity since different NiO-saponite interactions were observed by TPR for their precursors. The presence of amorphous silica in higher or lower amounts in the synthesised saponites cannot explain the different behaviour of these catalysts.

Ni/saponites, prepared from $Ni^{2+}$ cation exchange of saponites synthesised with different silica content and later calcination-reduction, showed lower conversion and lower selectivity to 2-phenylethanol than impregnated catalysts, and higher selectivity to phenylacetaldehyde.

### *4.2.5. Acknowledgements*

The authors are grateful for the financial support of the Ministerio de Educación y Ciencia of Spain and FEDER funds (CTQ2008-04433/PPQ) and for the FPU grant (AP2006-00835) also financed by the Ministerio de Educación y Ciencia of Spain.

## 4.3.Ni nanoparticles supported on microwave-synthesised hectorite for the hydrogenation of styrene oxide.

### Abstract

Several hectorites were synthesised with microwaves, and treated by different procedures, to be used as supports of nickel nanoparticles for the catalytic hydrogenation of styrene oxide to 2-phenylethanol. One more hectorite sample was synthesised by the conventional aging method, for comparison. The impregnation of a microwaved-synthesised hectorite with 10 wt % of nickel content, resulted in high activity, high selectivity to 2-phenylethanol, and high resistance to deactivation hectorite-supported nickel catalyst. Catalytic results have been related to the different NiO-hectorite interactions observed by TPR and also to the presence of acid sites. Both facts are consequence of hectorite purity and the use of microwaves for hectorite synthesis.

### *4.3.1. Introduction*

2-Phenylethanol (2-PEA), the main component of rose oils, is widely used as component in chemical perfumes, and as additive in foods, due to its pleasant smell (Mookherjee et al., 1996). Catalytic hydrogenation of styrene oxide to obtain selectively 2-phenylethanol is a cleaner alternative to the economical, environmental and purification problems shown by classical industrial production methods, such as the Friedel–Crafts alkylation of benzene with ethylene oxide (Bauer et al., 2001), the reaction of chlorobenzene with Grignard-type reactants followed by several reaction steps (Rode et al., 2000), or the ring opening of the epoxide with reduction agents such as hydrides or alkaline metals (Eliel and Delmonte; 1956, Krishnamurthy et al., 1973; Sreekumar et al., 1998).

Catalytic hydrogenation of styrene oxide to obtain 2-phenylethanol has been studied from 50's to solve the important problems mentioned above (Wood and Clifton, 1950). Bulk nickel, palladium and platinum catalysts have shown to be good catalysts for this reaction ( Gibson and Theiling, 1977; Mitsui, 1973) . Their activity and selectivity were considerably improved with the addition of basic solutions to the reaction medium (Mitsui, 1973). However, the basic medium could also favour condensation reactions that may deactivate the catalyst (Yadav and Chandalia, 1998). In previous studies in our research group, high selective and high resistant to deactivation catalysts were prepared using basic solids as supports of nickel catalysts (Bergadà et al., 2007b, 2008)

Other transformation reactions of styrene oxide can take place in the presence of acid sites: isomerisation to phenylacetaldehyde (PA) catalysed by Brønsted acid sites; ring-opening reaction to 2-ethoxy- 2-phenylethanol (2-EPE), catalysed by Lewis and Brønsted acid sites with medium strength, and condensation

reactions, which are responsible for catalyst deactivation and are catalysed by strong Brønsted acid sites in the presence of Lewis acid sites. (Bergada et al., 2009, Gonzalez et al., 2009; Salla et al., 2005). Indeed, it is possible to characterise the acidity of samples by studying the products obtained when using 2-phenylethanol as substrate.

Hectorite is a trioctahedral 2:1 mineral clay with formula $(Si_{8.0})$ $[Mg_{6.0-x}Li_x]$ $(OH.F)_4O_{20}M^{n+}_{x/n}\cdot mH_2O$, where some substitution of Mg(II) by Li(I) in the Octahedral (Oh) sheet, causes the negative charge of layers. This charge is compensated by interlayer exchangeable cations. When these cations are exchanged by transition metal cations ($Ni^{2+}$, $Pd^{2+}$, $Cu^{2+}$), metallic nanoparticles can be obtained, after reduction, in the interlayer space. Hectorite can be used for nanocomposites preparation, (Liu and Breen 2005, Xue and Pinnavaia, 2008), as heterogeneous catalysts due to their acidity and thermal stability (Casagrande et al., 2005; Varma, 2002), in ionic adsorption, ionic exchange processes and in nanoparticles synthesis. Although clays can be found in nature, in order to work with a reproducible material they must be synthesised. However, preparation methods usually involve long time hydrothermal treatments (Kloprogge et al., 1999).

In a previous study, we achieved to synthesise hectorite clays using microwaves, obtaining a reproducible material up to 24 times faster than by conventional ways. However, residual amounts of amorphous silica were observed for all samples.

The aim of this study was to evaluate the catalytic behaviour of several hectorite-supported nickel catalysts for the hydrogenation of styrene oxide to 2-phenylethanol. The influence of using microwave or conventional heating during hectorite aging, the effect of residual silica in synthesised hectorites and the presence of acid sites in competition with metal sites, were also studied. Ni/hectorite catalysts were obtained by impregnation with different nickel contents or by cation exchange.

### *4.3.2. Experimental*

#### *Synthesis of hectorites*

Hectorites were prepared following the method reported by Vicente et al. (2009; 2010b) in which brucite sheets were proposed to act as crystallisation nuclei of hectorite. Preparation was carried out as follows: 50 ml of a slurry composed by $SiO_2$, freshly prepared brucite $Mg(OH)_2$ and LiF was vigorously stirred for 1 h. Fresh brucite was previously synthesised by precipitation from an aqueous solution of $MgCl_2$ with ammonia. The slurry contained 3 wt. % solids and the molar ratio of the reagents was $SiO_2$: $Mg(OH)_2$: LiF=7.5:3:1. The sample was aged by autoclaving in laboratory microwave equipment (Milestone Ethos Touch Control), at 393 K for 8 h (sample H1). With the aim of comparing conventional aging with microwave hydrothermal treatment, one hectorite sample was obtained by aging in an autoclave heated at 393 K in a conventional oven for 8 days (sample H1conv). H1 was exchanged with $NH_4NO_3$ and calcined at 623 K for 6 h to obtain an acid hectorite (H1ac). Lastly, in order to obtain pure hectorite, the $SiO_2$ reagent amount was decreased in the starting slurry, using as reagents molar ratio 4 $SiO_2$: 3 $Mg(OH)_2$: 1 LiF (Vicente et al., 2010b). After aging

this slurry by autoclaving with microwaves at 393 K for 8 h, sample H2, was obtained. All samples were washed by dialysis and dried overnight in an oven at 353 K.

*Preparation of hectorite-supported nickel catalysts.*

Table 4.3.2-1 shows the preparation conditions of hectorite-supported nickel catalysts. Nickel was introduced by two procedures: impregnation and cation exchange. All hectorites were impregnated with nickel nitrate in the appropriate amounts to obtain 5 wt % of Ni in the final catalysts. Samples were calcined in air at 623 K (NiOs5-H1, NiOs5-H1ac, NiOs5-H1conv, NiOs5-H2), and reduced under pure hydrogen at 623 K for 6 h (Nis5-H1, Nis5-H1ac, Nis5-H1conv, Nis5-H2). Parallel procedure was carried out with the silica source reagent (Nis5-$SiO_2$) to provide a benchmark for comparison. One more catalyst was obtained by impregnating H1 with nickel nitrate to result in 10 wt % of Ni in the final catalyst, which was obtained after calcination-reduction at the same conditions than the above samples (Nis10-H1).

$Ni^{2+}$-exchanged hectorites were prepared by stirring 35 ml of $Ni(NO_3)_2 \cdot 6H_2O$ 0.25 M with 1 g of H1 at 338 K for 2 h (NiOe-H1). Sample was reduced using two procedures: (a) Reduction with ethyleneglycol and later elimination of reductant excess at 453 K for 5 h under vacuum (Nie/1-H1), following the method reported by de Lima et al. (2003), and (b) reduction with hydrazine (Li et al., 2006) and later elimination of the hydrazine excess at 473 K for 1 h under pure nitrogen until the pH of released vapours was 8 (Nie/2pH8-H1). In order to improve the activity of the catalysts, Nie1-H1 was treated with a 0.01 m NaOH solution for 10 minutes (Nie/1NaOH-H1) and Nie/2pH8-H1 was dried 1 more

hour until the pH of released vapours was 7 (Nie/2pH7-H1).

**Table 4.3.2-1.** Preparation conditions of the catalysts.

| Catalyst | wt. %Ni | Nickel introduction by | Reduction parameters |
|---|---|---|---|
| Nis5-$SiO_2$ | 5 | Impregnation | Calcination at 623 K + Reduction with $H_2$ at 623 K |
| Nis5-H1 | 5 | Impregnation | Calcination at 623 K + Reduction with $H_2$ at 623 K |
| Nis10-H1 | 10 | Impregnation | Calcination at 623 K + Reduction with $H_2$ at 623 K |
| Nis5-H1c | 5 | Impregnation | Calcination at 623 K + Reduction with $H_2$ at 623 K |
| Nis5-H1ac | 5 | Impregnation | Calcination at 623 K + Reduction with $H_2$ at 623 K |
| Nis5-H1conv | 5 | Impregnation | Calcination at 623 K + Reduction with $H_2$ at 623 K |
| Nis5-H2 | 5 | Impregnation | Calcination at 623 K + Reduction with $H_2$ at 623 K |
| Nie/1-H1 | 2 | Exchange | Reduction with ethylene glycol; elimination at 453 K |
| Nie/1NaOH-H1 | 2 | Exchange | Reduction with ethylene glycol; elimination at 453 K. Treatment with NaOH |
| Nie/2pH8-H1c | 2 | Exchange | Reduction with hydrazine; elimination at 473 K until pH 8 |
| Nie/2pH7-H1c | 2 | Exchange | Reduction with hydrazine; elimination at 473 K until pH 7 |

*Characterisation of samples*

Samples were characterised by X-ray diffraction (XRD), transmission infrared spectroscopy (FTIR), X-ray fluorescence (XRF), $N_2$ adsorption, transmission electron microscopy (TEM), temperature-programmed reduction (TPR), and determination of cation exchange capacity (CEC). The experimental conditions are indicated in the Experimental Section (2.2).

*Catalytic Activity Determination*

Catalytic hydrogenation of styrene oxide was performed in the liquid phase, using, for all tests, 1 g of catalyst, 150 mL of absolute ethanol (Panreac, 96 %) and 2 mmol of styrene oxide (Aldrich, 97 %) with a hydrogen flow of 2 mL/s and mechanic stirring of 500 rpm. The reaction was performed at room temperature. Sample was taken at 5 min, 1, 2, and 6 h of reaction. Impregnated catalysts were reused at least for 3 times. The reaction products were analysed by gas chromatography, using a chromatograph model Shimadzu GC-2010 equipped with a 30 m capillary column DB-1 coated with phenylmethylsilicon and a FID detector. They were quantified by adding an internal standard and by using calibration lines.

### *4.3.3. Results and Discussion*

*Characterisation of hectorites*

The existence of smectite structure was confirmed from the XRD patterns of samples (Figure 4.3.3-1), where we observed only one crystalline phase corresponding to hectorite. A very broad band with a maximum at $2\theta = 22.8°$ was assigned to amorphous silica by comparison with the $SiO_2$ diffraction pattern included in the figure. The silica band was more appreciable in samples H1, H1conv and H1ac than in sample H2, resulting in a worse definition of 004 reflection (Figure 4.3.3-1). Therefore, we can conclude that residual silica was lower in H2.

UNIVERSITAT ROVIRA I VIRGILI
SYNTHESIS OF HECTORITES AND SAPONITES WITH MICROWAVES AND THEIR APPLICATION IN CATALYSIS AND COMPOSI
Isabel Vicente Valverde
ISBN:/DL:T. 1033-2011

**Figure 4.3.3-1.** XRD patterns oh samples H1, H1conv, H1ac and H2.

**Table 4.3.3-1.** Characterisation data of hectorite samples

| Sample | Si/Mg Ratio | Mg/Li Ratio | d (0 0 1) (nm) | Crystallite size (0 6 0) (nm) | CEC (meq/100g) | BET area ($m^2$/g) |
|---|---|---|---|---|---|---|
| H1 | 2.7 | 6.1 | 13.3 | 9.3 | 64 | 162 |
| H1ac | --- | --- | 13.2 | 7.4 | --- | 219 |
| H1conv | 2.3 | 3.6 | 12.6 | 7.9 | 53 | 165 |
| H2 | 1.9 | 5.5 | 14.2 | 9.9 | 75 | 199 |

H1 and H2 had similar crystallinity, as deduced from their similar crystallite size, calculated from the 060 reflection of XRD patterns (Table 4.3.3-1). In contrast, crystallite sizes of H1ac and H1conv were smaller. In the case of H1ac, this may be due to some layer disaggregation produced in the exchange step during its synthesis. For H1conv, the lower crystallite size could be associated with the use of conventional heating during aging, which seems to be less effective than the use of microwaves.

The basal spacing was higher for sample H2 (14.2 Å) than for the other samples (12.6-13.3 Å) (Table 4.3.3-1). This may be related to the presence of higher amounts of interlamellar cations, in agreement with its higher CEC value (Table 4.3.2-1).

Figure 4.3.3-2 shows the FTIR spectra taken for samples H1, H1-conv and H1-ac. Bands were assigned taking into account the characterisation data reported for clay samples (Kloprogge et al., 1999; Kloprogge and Frost, 2000; Russel and Fraser, 1994). The band around 1027 $cm^{-1}$ corresponds to the Si–O–Si ordered in the clay mineral layer and can be observed in all samples, especially for H2, confirming the XRD results. The appearance of one intense band around 1105 $cm^{-1}$ together with a shoulder at 1200 $cm^{-1}$ was related to the presence of the amorphous silica phase, being more intense for H1, according to XRD results. This agrees the enhancement of CEC value observed for the sample with less amorphous silica content (H2, Table 4.3.2-1) since CEC in silica was $\sim$0. The other IR band observed for samples at 666 $cm^{-1}$ was associated to vibrations related to Mg–OH librations.

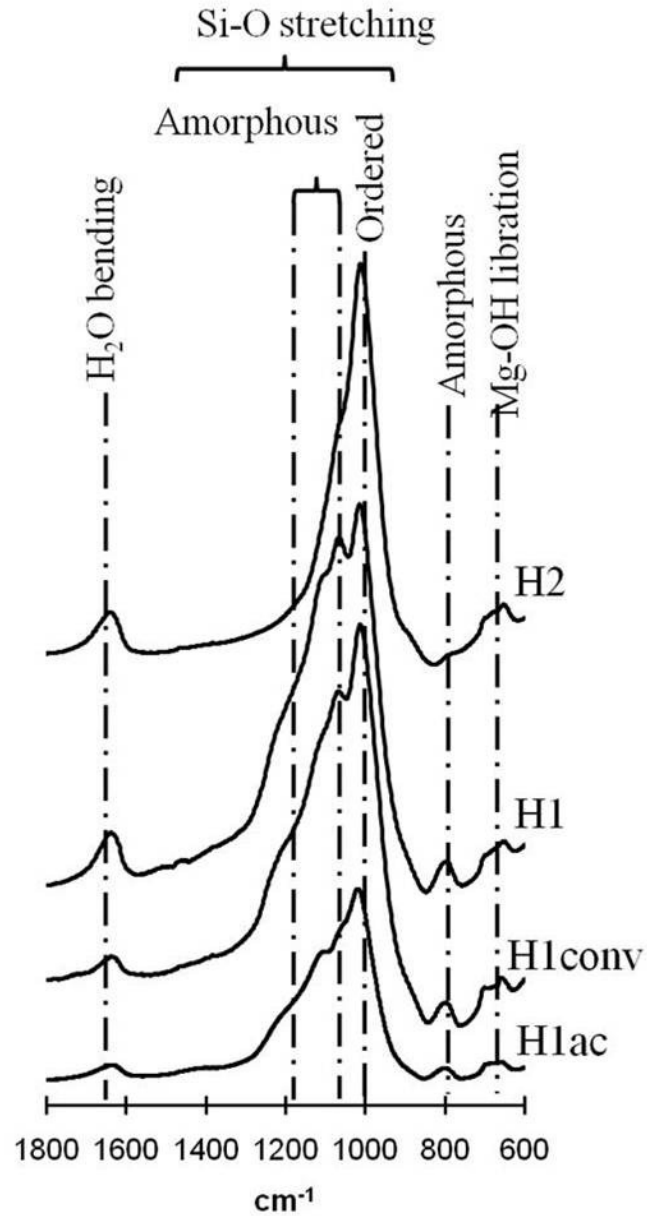


**Figure 4.3.3-2.** FTIR spectra of samples

From XRF results, Si/Mg and Mg/Li ratios were determined (Table 4.3.3-1). The Si/Mg ratios of samples H1 and H1conv were higher than that expected for a theoretical pure hectorite (Si/Mg=1.7, when x=1.2) due to the presence of the amorphous silica. H1 had much higher Mg/Li ratio (6.1) than sample H1conv (3.6) (Table 4.3.3-1). Assuming that magnesium and lithium are in the hectorite structure (in the layers or in the interlamellar space), the higher Mg/Li ratio of H1 could be attributed to the presence of higher amounts of magnesium ions in the interlamellar space. Higher BET areas were observed for H1ac and H2 than H1 and H1conv (Table 4.3.3-1). In the case of H1ac, this fact could be related to some disorder in stacking due to the performed treatments performed during its preparation, resulting in a loss of definition of the 001 reflection. The higher BET area of sample H2 could be explained by the almost totally absence of silica, which may block the pores of the other samples.

*Catalytic Activity*

Hectorites (H1, H1c, H1ac, H1conv, and H2) and the silica used as reagent showed negligible conversion values for the styrene oxide hydrogenation, styrene oxide isomerisation, and styrene oxide ring-opening reactions after 6 h of reaction. The presence of weak acid sites may explain these results. Nis5-$SiO_2$ catalyst gave 25% of conversion and 100% of selectivity to 2-PEA for the hydrogenation of styrene oxide at 1 h of reaction but it deactivates from the first reuse.

Catalysts prepared from hectorite synthesised with microwaves or by conventional aging impregnated with 5 wt % content of nickel (Nis5-H1 and Nis5-H1conv, respectively), resulted in total selectivity to 2-PEA (Table 4.3.3-2). Catalyst Nis5-H1conv showed higher conversion (88 %) than catalyst Nis5-H1 (40%). However, the catalyst prepared from the hectorite synthesised by conventional aging suffered higher deactivation since after 3 runs at 1 h of reaction conversion decreased to 60 %. On the other hand, for Nis5-H1 no deactivation after 3 runs was observed (Table 4.3.3-2). Both catalysts maintained total selectivity to 2-PEA after 3 runs.

**Table 4.3.3-2.** Catalytic results at 1 h of reaction of samples Nis5-H1, Nis10-H1, Nis5-H1ac, Nis5-H1conv and Nis5-H2 at 1 h of reaction after 1 and 3 runs.

| Catalyst | 1 run | | 3 runs | | |
|---|---|---|---|---|---|
| | Conversion | Sel. to 2-PEA (%) | Conversion | Sel. to PA (%) | Sel. to 2-PEA (%) |
| Nis5-H1 | 40 | 100 | 40 | n. d. | 100 |
| Nis10-H1 | 100 | 100 | 100 | n. d. | 100 |
| Nis5-H1ac | 66 | 100 | 54 | 4 | 96 |
| Nis5-H1conv | 88 | 100 | 58 | 1 | 99 |
| Nis5-H2 | 78 | 100 | 58 | 2 | 98 |

Sel.: Selectivity; PA: phenylacetaldehyde; 2-PEA: 2-phenylethanol; n.d. Non detected.

TEM images of both catalysts (Figure 4.3.3-3) showed the presence of dispersed nanoparticles sized around 8-15 nm (Figure 4.3.3-3a).

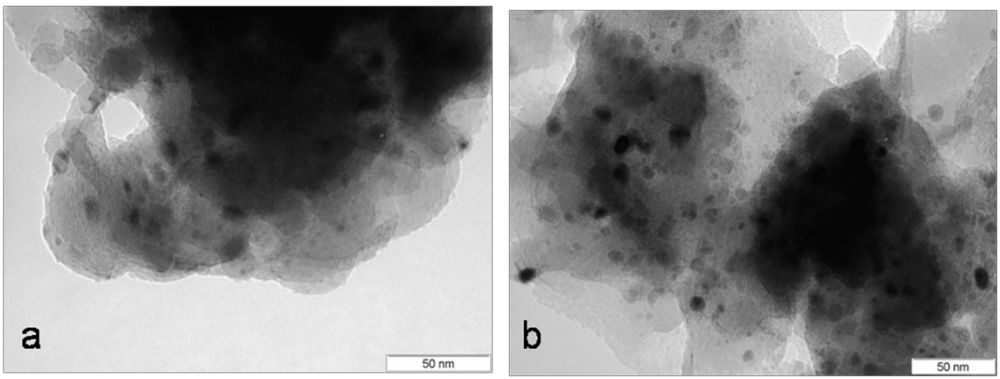


**Figure 4.3.3-3.** TEM images of samples Nis5-H1 and Nis5-H1conv.

In order to understand the differences observed in the catalytic behaviour of these catalysts, the reducibility of their precursors was studied by TPR. Thermograms of both samples showed mainly three peaks (Figure 4.3.3-4). The first peak had low intensity for both samples. Since different NiO-support interactions were observed for each precursor, their corresponding catalysts may have nickel sites with different characteristics, and consequently different activity should be expected. In a previous study, Ni/saponite catalysts were tested for this reaction (Vicente et al., In press). TPR curves with similar shape were obtained for their precursors. In general, it was observed that, the more active the catalyst, the higher the intensity of the third reduction peak, which was related to NiO sites with high interaction with the support. Therefore, the higher conversion of catalyst Nis5-H1conv could be attributed to a higher content of metal nickel sites with higher influence of support that results in a higher intensity of the third peak of its precursor (NiOs5-H1conv) when compared to that of NiO5s-H1.

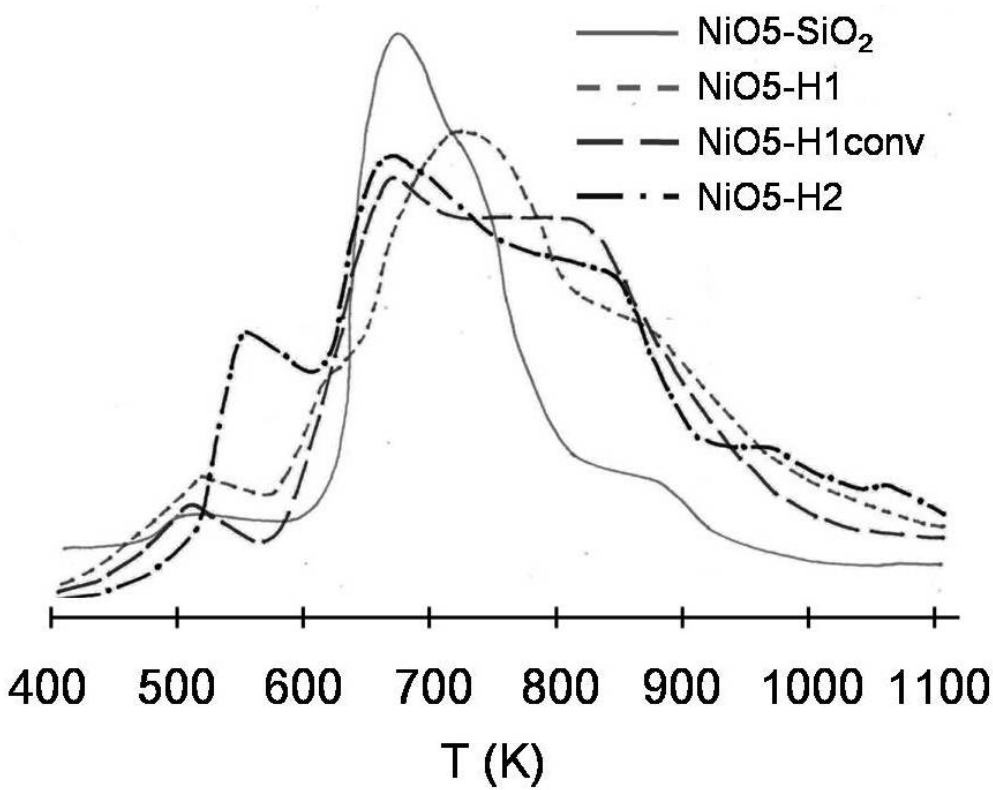


**Figure 4.3.3-4.** TPR of samples NiO5-$SiO_2$, NiOs5-H1, NiOs5-H1conv and NiOs5-H2.

High selectivity to 2-PEA was explained in nickel catalysts promoted by basic solutions through the formation of $\pi$ benzyl complex from the adsorbed styrene oxide, that yielded a primary alkoxide ion, which was stabilised by NaOH, and finally hydrogenated to the primary alcohol (Mitsui et al., 1973). Another possible pathway in basic medium was the formation of the secondary alkoxide ion, which through hydride attack gave 2-PEA (Mitsui et al., 1973, Rode et al., 2000, 2003).

The high selectivity to 2-PEA in these Ni/hectorite catalysts without basic promotion could be explained by the formation of a primary alkoxide ion,

stabilised by acid sites, which yielded the primary alcohol by hydrogenation. Even though conversion was negligible when H1, H1c, H1ac, H1conv and H2 were tested, the later calcination-reduction steps performed to obtain the catalysts may result in some modifications such as their acidic properties. Actually, the presence of Brønsted acid sites in Nis5-H1conv was confirmed since phenylacetaldehyde (PA) was detected at shorter reaction times. This compound was quickly hydrogenated to 2-PEA in the first two reuses. However, PA remained longer during the third run although after 2 h the only product observed was 2-PEA. For catalyst Nis5-H1conv, the higher accessibility to the acid sites, because of the lower crystallinity of initial hectorite, could be also responsible for the deactivation of the catalyst, through the formation of condensation products from PA (Bergadà et al. 2009, González et al. 2009; Salla et al., 2005).

Catalyst Nis5-H2, prepared from hectorite with lower silica content than H1, and impregnated with the same content of nickel (5 wt %), showed total selectivity to 2-PEA and higher activity (78 % conversion) than Nis5-H1 (Table 4.3.3-2). The third run, its conversion dropped to 58 % and 2 % of PA was observed. The appearance of PA as by-product after one hour of reaction on the third reuse (Table 4.3.3-2), and the deactivation observed for Nis5-H2 can be explained by the higher accessibility of the reactants to the acid sites because of the high surface area of this support (H2, Table 4.3.3-1).

When TPR curve of its precursor (NiOs5-H2, Figure 4.3.3-4) was analysed, similar shape to that of NiOs5-H1conv, was observed. This explains the similar catalytic behaviour obtained for both catalysts (Table 4.3.3-2). Moreover, TPR of NiOs5-H2 showed higher intensity of the first reduction peak than NiOs5-

H1conv. The intensity of this peak can be related to NiO that can be easily reduced to Ni particles that afterwards became agglomerated because of their low interaction with the support. This resulted in the formation of bigger Ni nanoparticles in Nis5-H2 (around 20-25 nm) than in Nis5-H1, as observed by TEM (Figure 4.3.3-5). Apart from these Ni particles, other Ni particles around 5-10 nm were obtained for this catalyst (Figure 4.3.3-5).

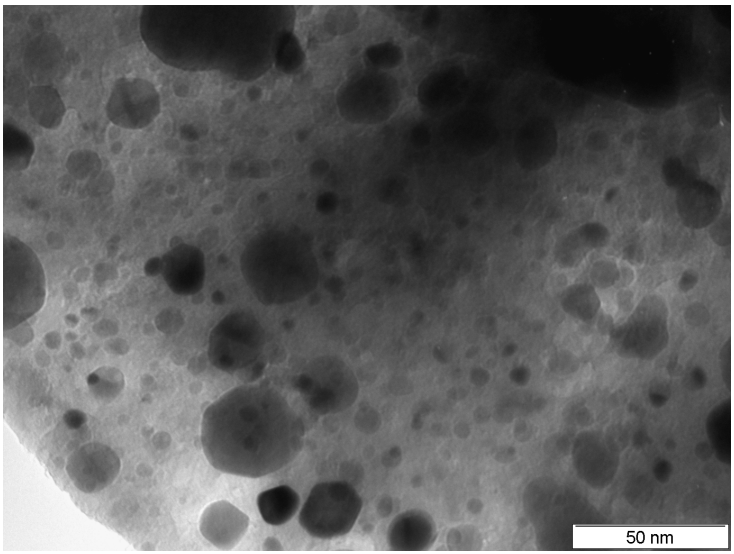


**Figure 4.3.3-5.** TEM image of sample Nis5-H2 x500k.

One more catalytic test was performed using as catalyst Nis5-H1ac. This catalyst, which was prepared using an acidified hectorite impregnated with 5 wt % Ni, had total selectivity to 2-PEA and higher conversion (66 %) than Nis-H1 (Table 4.3.3-2). TEM image of Nis5-H1ac (Figure 4.3.3-6) showed the presence of Ni nanoparticles with sizes around 8-15 nm, had similar to those observed for Nis5-H1 (Figure 4.3.3-3).

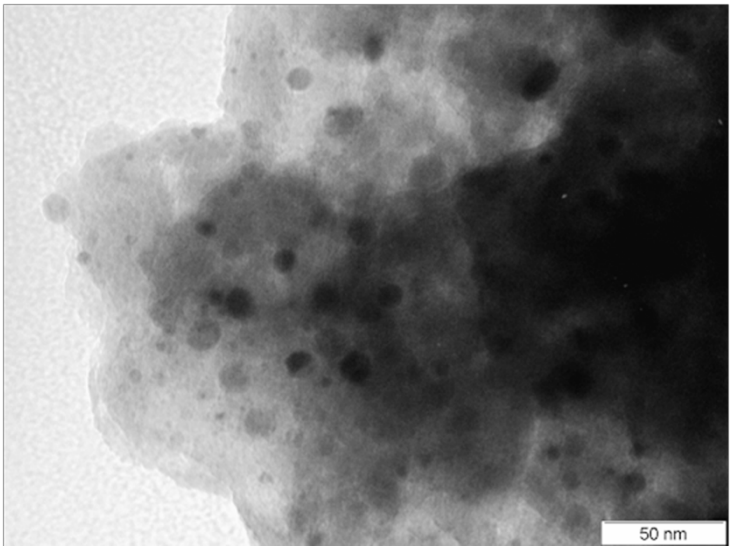


**Figure 4.3.3-6** TEM image of sample Nis5-H1ac x500k.

In order to explain the catalytic behaviour of Nis5-H1ac, TPR of its catalytic precursor was performed.

TPR curve of NiOs5-H1ac (Figure 4.3.3-7) showed again three peaks: the first one with low intensity, and the second and third peaks the intensities of which were higher than those of NiOs5-H1 (Figure 4.3.3-7). This is in agreement with the higher activity observed for Nis5-H1ac when compared with Nis5-H1. However, 4% of phenylacetaldehyde was obtained after one hour of the third reuse for catalyst Nis5-H1ac (Table 4.3.3-1). The appearance of PA, together with the decrease of activity observed, may be related to the formation of condensation products catalysed by the acid sites of support that deactivated the catalyst.

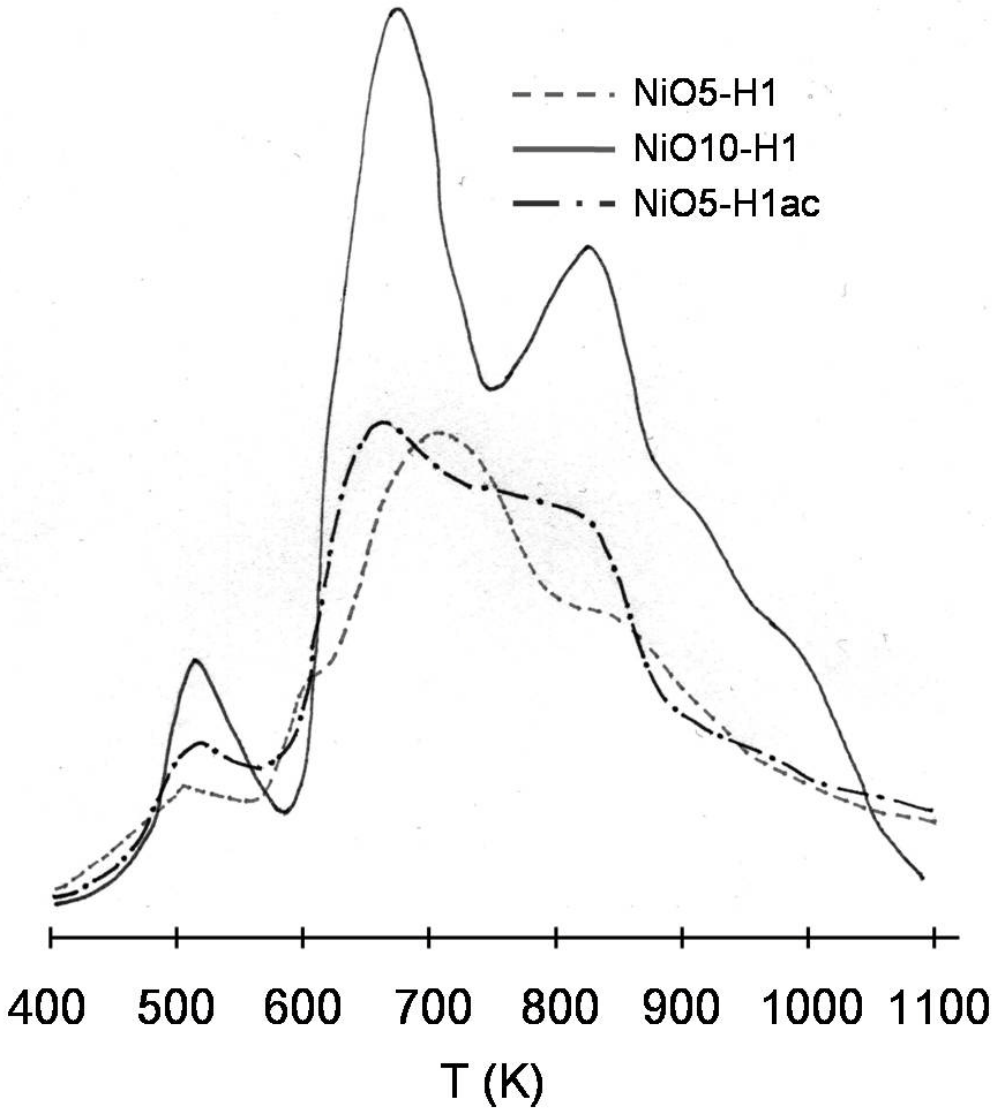


**Figure 4.3.3-7.** TPR curves of catalytic precursors.

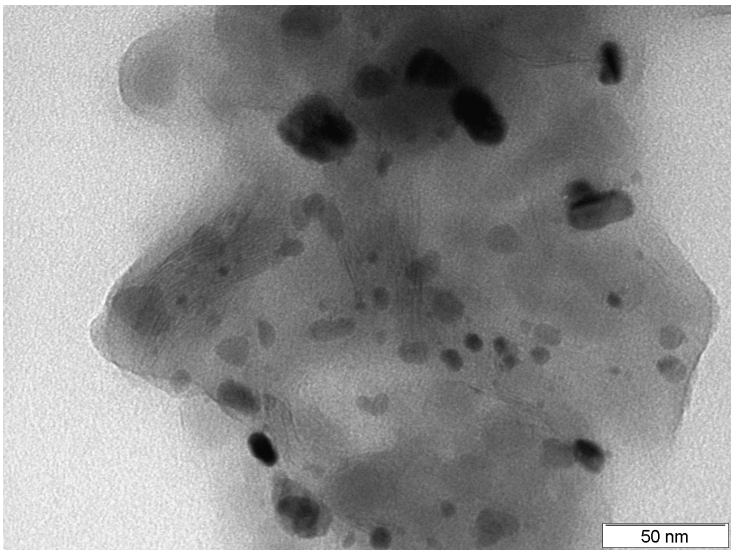


**Figure 4.3.3-8.** TEM image of simple Nis10-H1 x400k.

Figure 4.3.3-8 corresponds to TEM image of catalyst Nis10-H1, where Ni-nanoparticles with two main average diameters (20 and 10 nm) were observed. This catalyst was prepared using as support H1 but increasing the Ni content to 10 wt %. When it was tested, total conversion and total selectivity to 2-PEA were yielded after one hour of reaction. This catalytic result maintained after 3 runs.

When comparing the TPR curve of NiOs10-H1 to that of NiOs5-H1, higher intensity for the three peaks was observed (Figure 4.3.3-7). The nickel nanoparticles of 20 nm observed could be related to the higher intensity of the first reduction peak since there was a higher amount of NiO particles that could be more easily reduced. This favoured the existence of more agglomerated Ni particles. The high selectivity to 2-PEA and high conversion of this catalyst may be related to the higher amount of Ni metal interacting strongly with the support as confirmed by the higher intensity of the third peak from the TPR curve of its precursor, NiOs10-H1. Besides, the better coverage of acid sites because of the

higher amount of Ni introduced should minimise Nis10-H1 deactivation without decreasing its activity.

Figure 4.3.3-9 illustrates conversion and selectivity results of Ni/hectorite catalysts obtained by cation exchange (Nie-H1/1, Ni-H1/NaOH, Nie-H1/2pH8 and Nie-H1/2pH7).

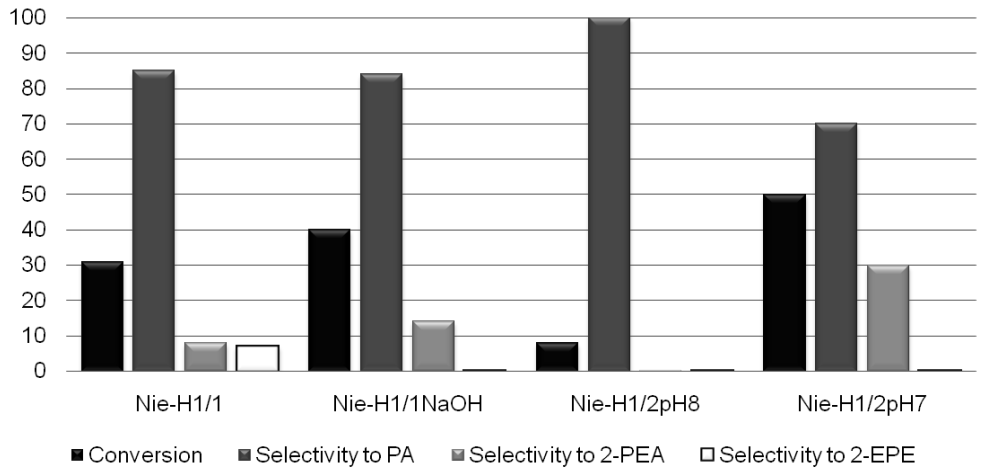


**Figure 4.3.3-9.** Catalytic results of samples Nie-H1/1, Nie-H1/1NaOH, Nie-H1/2pH8 and Nie-H1/2pH7.

Activity of the silica reagent submitted to the same preparation procedure than the exchanged catalysts was also tested. No adsorption of nickel by silica was observed and conversion was negligible.

The use of ethylene glycol to reduce $Ni^{2+}$ in the exchanged hectorite H1 Nie-H1/1 gave well dispersed Ni nanoparticles, with sizes around 2-5 nm, as observed by TEM (Figure 4.3.3-10a). The low conversion (30 % Figure 4.3.3-9) , low selectivity to 2-PEA (8%, Figure 4.3.3-9) and high selectivity to PA (85%, Figure 4.3.3-9) obtained after 2 h of reaction, may be related to the low

percentage of nickel in these samples (2 %) together with the presence of some active acid sites, which initially catalysed the formation of PA and afterwards deactivated catalysts by the formation of condensation products (Salla et al., 2005). In order to neutralise these acid sites, this catalyst was treated with a NaOH 0.05 M solution after reduction and followed by a drying step prior to the catalytic test (Ni-H1/NaOH). Conversion and selectivity to 2-PEA slightly increased to 40% and 15%, respectively, at two hours of reaction. However, catalyst deactivation was also observed.

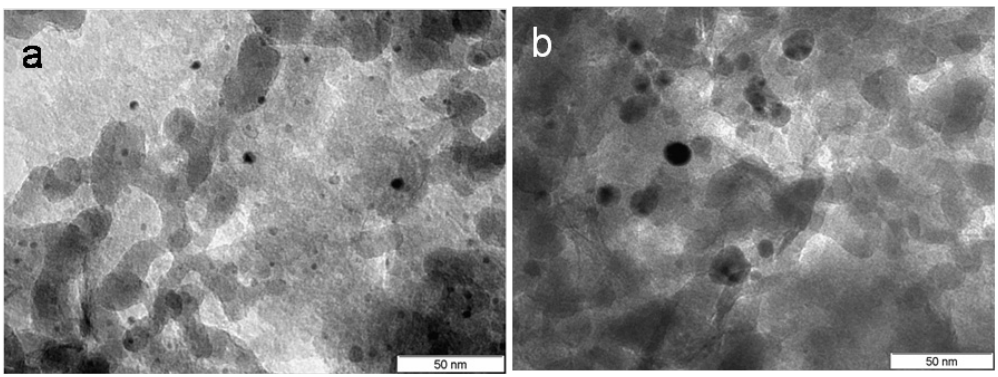


**Figure 4.3.3-10.** TEM images of samples a) Nie/1-H1 x 500k and b) Nie/2pH7-H1 x 500k.

With the aim to control these acid sites, and given its basicity, hydrazine was used to reduce $Ni^{2+}$ exchanged hectorite. Then hydrazine was used to reduce $Ni^{2+}$ exchanged hectorite H1 with the aim to control the hectorite acid sites taking advantage of the hydrazine basicity. The hydrazine excess was eliminated by heating at 473 K for 1 h under pure nitrogen until the pH of released vapours was 8 (Nie/2pH8-H1). When this catalyst was tested, extremely low conversion after 2 h of reaction (8% Figure 4.3.3-9), was observed. This could be related to an important blockage of metal and acid sites by remaining hydrazine. In order

to improve the behaviour of catalyst, hydrazine was eliminated after the reduction step at 473 K for 3 h until the pH of released vapours was 7 (Nie/2pH7-H1). The resulting catalyst showed Ni particles with sizes around 10-15 nm (Figure 4.3.3-10b). A significant improvement of conversion (50% Figure 4.3.3-9) at 2 h of reaction was observed when using this catalyst although only 30% of selectivity to 2-PEA was obtained (Figure 4.3.3-9). The high selectivity to PA (70%, Figure 4.3.3-9) and the catalyst deactivation could suppose that not only the hydrazine that blocked the metal sites was eliminated, but also the one that blocked the acid ones.

### *4.3.4. Conclusions*

The use of microwaved-synthesised hectorites as supports of nickel nanoparticles for the catalytic hydrogenation of styrene oxide resulted in high active, high selective to 2-phenylethanol and high resistant to deactivation catalytic systems.

The activity of Ni/hectorite, obtained from impregnation of hectorites with nickel nitrate and later calcination-reduction, mainly depended on the use of microwave during hectorite synthesis, the nickel content and the hectorite purity. These results were related to the presence of different amounts and different accessibility of acid sites, and also to metal nickel sites with different activity since different NiO-saponite interactions were observed by TPR for their precursors. Ni/hectorites, prepared from $Ni^{2+}$ cation exchange of hectorite synthesised under microwave and later calcination-reduction, showed lower conversion and lower selectivity to 2-phenylethanol than impregnated catalysts, and higher selectivity to phenylacetaldehyde. The conversion and selectivity to 2-PEA increased when higher amount of hydrazine was eliminated. However the

hydrazine elimination was not selective for the metal sites. The phenylacetaldehyde formation and the catalyst deactivation could be explained by the accessibility to acid sites.

### *4.3.5. Acknowledgments*

The authors are grateful for the financial support of the Ministerio de Educación y Ciencia of Spain and FEDER funds (CTQ2008-04433/PPQ) and for the FPU grant (AP2006-00835) also financed by the Ministerio de Educación y Ciencia of Spain.

# Chapter 5

## Hectorite in Polyurethane Composites

# Characterisation of composites prepared by dispersion of hectorite, synthesised with microwaves, in polyurethane.

## Abstract

A selection of nanocomposite samples were prepared by dispersion of one hectorite (H2SB), synthesised with microwaves, in a commercial polyurethane (PU) with clay contents of 1, 2, 5 and 20 wt% (related to the total composite). Another set of composites were prepared under the same conditions but using a commercial hectorite (Laponite) as clay for comparison. The samples were studied by XRD, DRIFTS, TGA, and dynamic thermal analysis. Dispersion of 1 and 2 wt% H2SB in PU was achieved since because no diffraction peaks were observed in the XRD patterns. Thermomechanical results of H2SB nanocomposites were similar to those of laponite dispersed in polyurethane found in the bibliography.

## *5.1. Introduction*

The study of nanocomposites formed by polymers and clays (usually montmorillonite, saponite or hectorite) is a field in expansion due to the obtention of materials which showed improved stiffness and toughness, enhanced barrier properties and fire and ignition resistance together with their cost-effectiveness (Alexandre and Dubois, 2000; Bujdák and Iyi, 2006; Chen at al., 2008; Moncada et al., 2007; Urbanzyk et al., 2006; Wang et al., 2002)

*Nanocomposite structures*

Three main types of composites may be obtained when a clay is dispersed within a polymer matrix, which type depends on the nature of the reagents (clay, polymeric matrix) and the method of preparation. (Figure 5.1-1, Alexandre and Dubois, 2000, Chen et al., 2008):

- Phase separated composites, when the polymer is unable to intercalate between the clay layers. (Figure 5.1-1a).
- Intercalated composites, in which one or more extended polymer chains are intercalated between the silicate layers resulting in a well ordered multilayer morphology built up with alternating polymeric and silicate layers. (Figure 5.1-1b)
- Exfoliated composites, when each clay layer is completely and uniformly dispersed in a continuous polymer matrix. (Figure 5.1-1c).

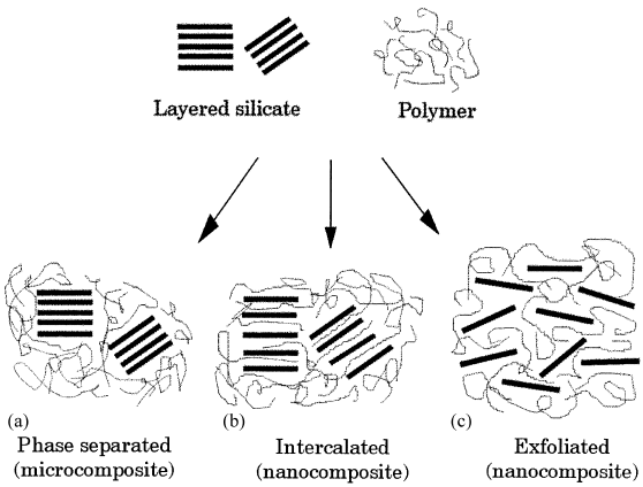


**Figure 5.1-1.** Diferent types of composites (Alexandre and Dubois, 2000).

In the case of phase-separated composites, their properties remain in the same range as traditional composites. Intercalated and exfoliated composites can be classified as nanocomposites. Polymer nanocomposites represent a new class of composite materials (Dimitry et al., 2010) with particle-filled polymers in which at least one dimension of the dispersed particles is in the nanometre range. This can result in the improvement of properties for the related composite materials at much lower filler contents; for instance 3–5 wt% of nano-sized filler gives comparable properties to those obtained for 30 –50 wt% of micron-sized filler.

There are many studies concerning polymer nanocomposites based on various polymer matrices. As a brief sample: nylon 6 (Liu and Breen, 2005), polystyrene (Chen et al., 2008), polypropylene, polyethylene (Shah and Paul, 2006), polyimide, poly(methylmethacrylate) and polyurethane (Chattopadhyay and Raju, 2007).

Two complementary techniques are used in order to characterise these structures. XRD is used to identify intercalated structures. In such nanocomposites, the repetitive multilayer structure is well preserved, allowing the interlayer spacing to be determined. The intercalation of the polymer chains usually increases the interlayer spacing, in comparison with the spacing of the clay used (Figure 5.1-1), leading to a shift of the reflection towards lower angles. As far as an exfoliated structure is concerned, no reflections are visible in the XRD patterns either because of a much too large spacing between the layers (i.e. exceeding 8 nm in the case of ordered structure when using a Cr X-ray tube) or because the clay dispersed in the nanocomposite does not present any ordering. Transmission electron microscopy (TEM) is used to confirm the presence of exfoliated structures in a nanocomposite.

*Polymer-clay nanocomposites synthesis methods*

In order to obtain polymer-clay nanocomposites three methods are typically used:

- "In situ" polymerisation method, in which clay is directly added to a monomer, followed by dispersal mixing. Heating and usually the presence of an initiator starts the polymerisation reaction (Okada and Usuki, 2006).
- Solution method, in which the clay is exfoliated into single layers using a solvent in which the polymer (or a prepolymer in case of insoluble polymers such as polyimide) is soluble. The polymer then adsorbs onto the delaminated clay sheets before, during or after evaporation of the solvent (or the precipitated mixture). The sheets often reassemble sandwiching the polymer although exfoliated

ISBN:/DL:T. 1033-2011

composites can be obtained using this method. This method is often used with water-soluble polymers, such as PEO, poly(vinyl alcohol) and poly(vinyl pyrolidone), although the use of other solvents, such as toluene (Furuichi et al., 1996), chloroform (Shen et al, 2002), dimethylacetamide (Chang et al., 2001) and tetrahydrofuran (Zhang and Wilkie, 2003), have also been reported.

- Melt-processing methods. The use of some solvents, often incurs higher costs. Besides, environmentally benign and easily removed solvents are not always available. Sometimes small solvent molecules rather than the desired macromolecule intercalate into the host clay galleries. For these reasons the clay can be mixed within the polymer matrix in the molten state in the absence of solvents. Under these conditions and if the layer surfaces are sufficiently compatible with the chosen polymer, the polymer can enter the interlayer space and form either an intercalated or an exfoliated nanocomposite.

Besides these three methods, others include co-vulcanization (Pinnavaia and Beall, 2000), solid-state intercalation (Khaorapapong, 2001), sol–gel, emulsion (Xu et al., 2003) and supercritical $CO_2$ fluid (Zhao and Samulski, 2006) methods.

The use of unmodified clays for polymer-clay nanocomposites synthesis, greatly limits the type of polymers that can be intercalated. This limitation is overcome by replacing the original, inorganic interlayer cations with organic cations (often alkylammonium cations but also phosphonium and sulfonium cations).

ISBN:/DL:T. 1033-2011

However, chemical modification of clays may result in thermal degradation of the organoclay, and also the composite, at low temperatures, even during melt processing. Furthermore, the modifying agent may not be compatible with the matrix polymer and the process itself adds to production costs, as does the process of clay modification.

The usefulness of solution methods are limited because of, the limited numbers of solvents that can both dissolve polymers and disperse nanoparticles.

For this reason Kumar et al. (2005) developed a solvent-exchange method to effectively and uniformly disperse laponite nanoparticles in polymers, resulting in an improvement of the mechanical, thermal, optical, and/or electrical properties of composites by more complete exfoliation and dispersion of nanoparticles therein.

Synthetic smectites like hectorite can be dispersed in many organic, polar solvents owing to its hydrophilic character, which promotes the separation of clay platelets via osmotic pressure produced by the hydration of intercalated ions. In non-polar solvents, the large energy barrier created by the reduced wettability and the absence of osmotically driven platelet separation prevents direct dispersion of the clay. With that solvent-exchange method is possible to disperse polar nanoparticles, such as Laponite, in organic solvents.

This procedure can be used to fully disperse polar nanoparticles within different polymer systems with little to no modification. The procedure requires the use of two solvents, A and B that meet four criteria:

- Solvent A must fully disperse and exfoliate the nanoparticles.

- Solvent A and B must be fully miscible,
- Solvent B must have a higher boiling point than solvent A.
- Solvent B must fully dissolve the polymer.

For example for a Polyurethane/Hectorite system the optimal solvent pair could be deionised water (A) and N,N- dimethylacetamide (DMAc) (B).

*Composites: Trying to simulate nature*

Polyurethanes (PUs) are segmented polymers with a microphase-separated morphology, this means the polymer is composed of hard segments (HS) and soft segments (SS) that combine to give the PU moderate stiffness, high rubber-like extensibility and easy processability (Figure 5.1-2).

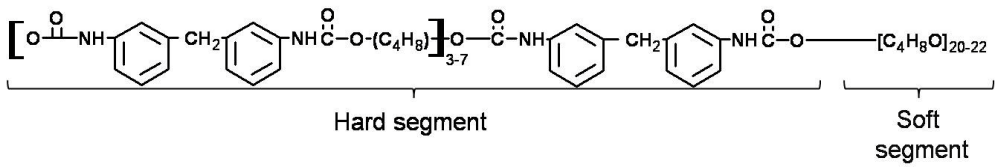


**Figure 5.1-2.** Structure of Polyurethane.

Thermodynamic incompatibility of the HS and SS drives the polymer system into a two- phase morphology in which hydrogen-bonded, crystalline hard microdomains form amid the rubbery soft domains. The stiffness (or elastic modulus, E) and strength (tensile stress at break, $\sigma_{max}$ of the PU increase with HS content, whereas the extensibility (strain at failure, $\varepsilon_{max}$) increases with SS content). The flexibility of urethane chemistry enables the chemical structure of the HS and SS domains to be systematically varied to control the thermal transition temperatures and thermomechanical properties of the polyurethane. Synthetically, it is difficult to increase the elastic modulus of polyurethane and

maintain its high extensibility, or vice-versa: an increase in one often results in a decrease in the other (Liff et al., 2007).

High-performance biomaterials, such as silk (Vollrath and Knight, 2001) and bone (Smith et al., 1999), exhibit unparalleled combinations of stiffness, strength, extensibility and toughness by exploiting hierarchical structures in which stiff nanometre-size crystallites are embedded and dispersed in softer protein matrices (Vollrath and Knight, 2001). Some studies show that araneid spiders modify the stiffness and strength of silk by regulating the ordering of polypeptide chains and/or through formation of nanocrystallites during spinning (Porter et al., 2005).

Successful mechanical enhancement of polymer matrices via reinforcement is expected only when the nanoparticles are fully exfoliated in the polymer matrix. This can prove difficult because the organic, hydrophobic polymer matrices thermodynamically and kinetically inhibit the dispersal of the inorganic, hydrophilic clay. Despite numerous advances, synthetic polymer nanocomposites have yet to show the superior toughness of natural biomaterials such as silk. Like a majority of engineering materials, the nanocomposites are either stiff but not extensible, like steel, or extensible but not stiff, like rubber.

Liff et al., (2007) using the solvent-exchange approach to exfoliate nanoparticles reported by Kumar et al., (2005) observed that, the unmodified Laponite nanoparticles preferentially reinforced the polyurethane hard microdomains, rather than being dispersed throughout the soft and hard segments. Consequently the elastic modulus, E and the tensile failure at break, $\sigma_{max}$ increased whilst maintaining the characteristically high $\varepsilon_{max}$ of a typical

polyurethane. To optimise this microsegregation, it was key that the dimensions of clay platelets were similar in magnitude to the natural dimensions of the HS domains that microphase separate, HS length=3−11nm (Martin et al., 1999, Figure 5.1-3). The stronger affinity of the hydrophilic, non-surface-modified Laponite with the more polar HS rather than with the more organophilic SS allowed the Laponite to segregate into the hard microdomains during the processing of the TPU, decreasing the undesired stiffening of the soft domain without compromising the large $\varepsilon_{max}$ of the polyurethane composite. However, Liff and co-workers pointed out that the size of Laponite platelets (25 x 1 nm.) was larger than the hard domains of the polyurethane. This made possible some undesirable interaction of laponite platelets with the soft domains of the polyurethane.

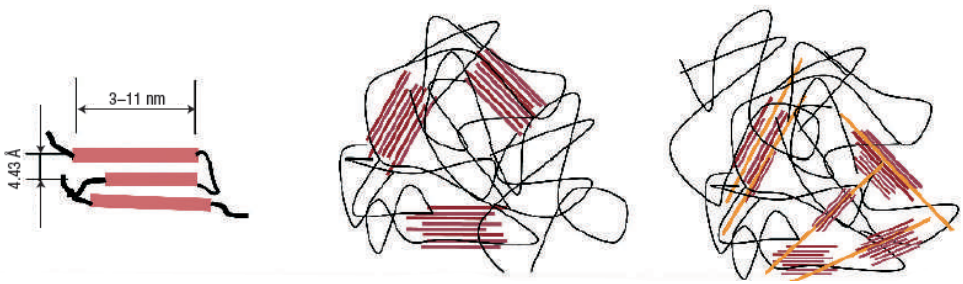


**Figure 5.1-3.** The charged Laponite platelets (in orange) preferentially reinforce the polar hard domains (Liff et al., 2007).

Since we achieved to synthesise a hectorite with small crystallite size (10 nm), calculated from 060 reflection of its XRD pattern, our objective was to study the feasibility of using a microwave synthesised hectorite in the formation of composites with commercial polyurethane following the procedure by Kumar et al (2005).

UNIVERSITAT ROVIRA I VIRGILI
SYNTHESIS OF HECTORITES AND SAPONITES WITH MICROWAVES AND THEIR APPLICATION IN CATALYSIS AND COMPOSI
Isabel Vicente Valverde
ISBN:/DL:T. 1033-2011

## *5.2. Experimental section*

### *Synthesis of hectorite*

$Li^+$-Hectorite (H2) was synthesised according to the procedure previously reported (Vicente et al., 2009, Figure 5.2-1) from a slurry (3 wt. % solids) containing $SiO_2$, fresh brucite $Mg(OH)_2$, and LiF, in a molar ratio of 4:3:1, respectively. The slurry was aged by autoclaving in laboratory microwave equipment (Milestone Ethos Touch Control), at 393 K for 8 h. Afterwards the sample was washed by dialysis and dried at 353 K. In order to obtain the smallest particles of clay, H2 was stirred for 24 h and then allowed to sediment for a further 24 h. The supernatant was collected and dried at 353 K, obtaining H2SB.

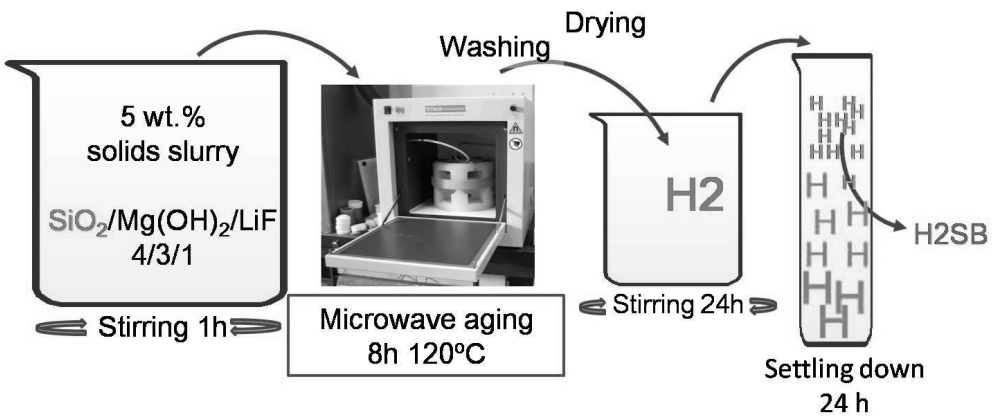


**Figure 5.2-1**. H2SB preparation procedure.

*Preparation of composites*

A set of nanocomposite samples were prepared, using a commercial PU and with clay contents of 1, 2, 5 and 20 wt% (related to the total composite, Figure 5.2-2).

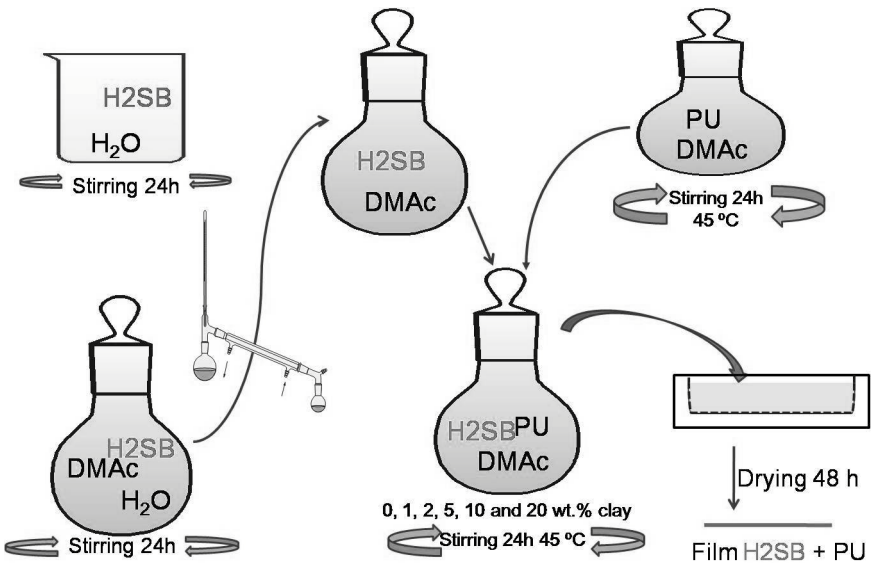


**Figure 5.2-2.** Composites preparation.

Hectorite was dispersed in dimethylacetamide (DMAc) via the solvent-exchange procedure outlined by Kumar et al., 2005. One gram of hectorite was added to 100 g water and stirred for one day. Then, 200 g of DMAc was added to the hectorite/water suspension and stirred for one day. Water was removed by distillation at 438 K until a hectorite/DMAc suspension was formed. 1.5 g polyurethane was dissolved in 400 ml. DMAc. The dissolved polyurethane, hectorite/DMAc suspension and additional DMAc were mixed resulting in hectorite–DMAc dispersion in DMAc to obtain composites with different clay content. The polyurethane concentration in the solution was maintained at 1.4–

1.6 wt%. Polyurethane/hectorite nanocomposite films with 80-120 μm thicknesses were prepared in Teflon containers (6 cm × 4 cm x 2cm) by evaporation of DMAc at 343 K. The final clay concentration in the dry film was controlled by varying the hectorite concentration in the hectorite–polyurethane–DMAc solution (Figure 5.2-2).

Another set of composites was prepared using the same conditions but with commercial hectorite (Laponite) instead of microwaved synthesised hectorite as clay for comparison

*Characterisation of samples*

Clay samples were studied using X-ray diffraction (XRD), diffuse reflectance Fourier transform infrared spectroscopy (DRIFTS) thermogravimetric analysis (TGA) and transmission electron microscope (TEM). Composite samples were characterised by XRD, DRIFTS, TGA and thermo mechanical dynamic analysis, using the experimental conditions indicated in Section 2.2.

## *5.3. Results and discussion*

*Characterisation of hectorites*

No crystalline phases other than hectorite were observed in the powder XRD patterns of H2SB and Laponite (Figure 5.3-1). The d001 spacing of H2SB was 13.4 Å, but it was not possible to determine the corresponding value for the Laponite sample. The 001, 002 and 004 reflections were more prominent in the trace obtained from H2SB than that of Laponite, which is due to a more ordered orientation of the clay layers in the former.

UNIVERSITAT ROVIRA I VIRGILI
SYNTHESIS OF HECTORITES AND SAPONITES WITH MICROWAVES AND THEIR APPLICATION IN CATALYSIS AND COMPOSI
Isabel Vicente Valverde
ISBN:/DL:T. 1033-2011

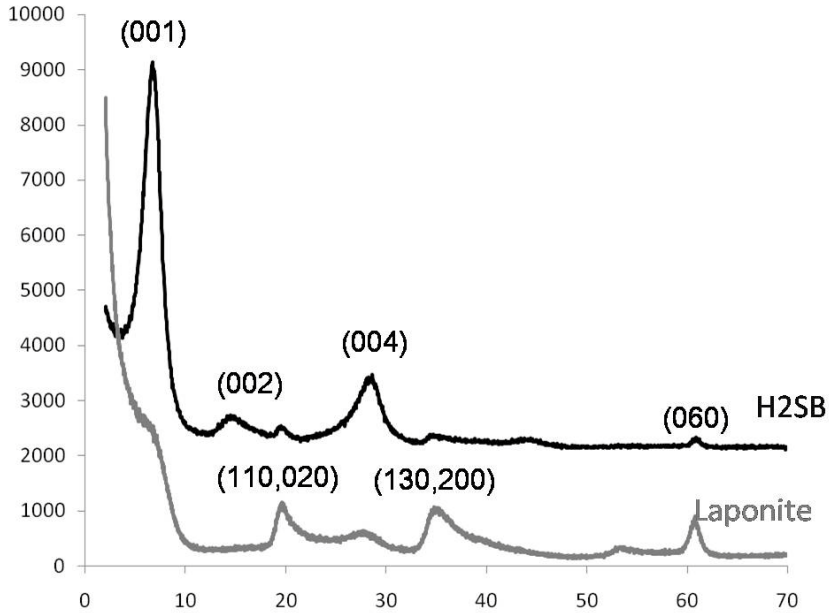


**Figure 5.3-1.** XRD pattern of H2SB and Laponite.

The crystallite size, calculated from 060 reflection, was slightly smaller for Laponite than for H2SB (Table 5.3-1). This contrasted with the data reported by Liff et al., (2007) where the diameter of the Laponite platelets was determined as 25 nm. When comparing sizes with the ones observed in the TEM images (Figure 5.3-2) the latter ones are sensibly larger (≈ 200 nm), and may be due to some layer aggregation when the sampled was manipulated for its TEM observation.

**Table 5.3-1**. Characterisation data of samples from XRD data

| Sample | Basal spacing (Å) | Crystallite size (0 6 0) (nm) |
|---|---|---|
| H2SB | 13.4 | 8 |
| Laponite | ---- | 7 |

UNIVERSITAT ROVIRA I VIRGILI
SYNTHESIS OF HECTORITES AND SAPONITES WITH MICROWAVES AND THEIR APPLICATION IN CATALYSIS AND COMPOSI
Isabel Vicente Valverde
ISBN:/DL:T. 1033-2011

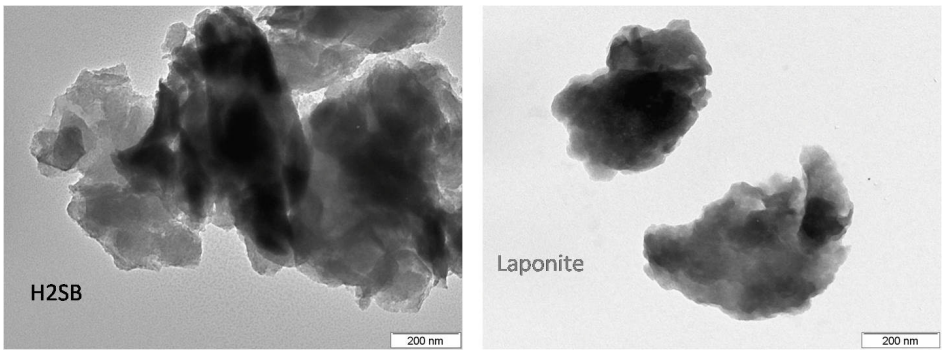


**Figure 5.3-2.** TEM images x 100 k of H2SB (left) and Laponite (right).

Nevertheless, when Laponite was mixed with polyethylene glycol MW=600 (PEG 600), (Figure 5.3-3) it swelled and oriented the clay layers resulting in the presence of 001 reflection together with 002-006 reflections. This indicates a more ordered system than that obtained with H2SB treated in the same manner (Figure 5.3-3). The increase in basal spacing achieved with H2SB was slightly higher than that obtained for the Laponite sample. This may be due to different water contents in the two samples.

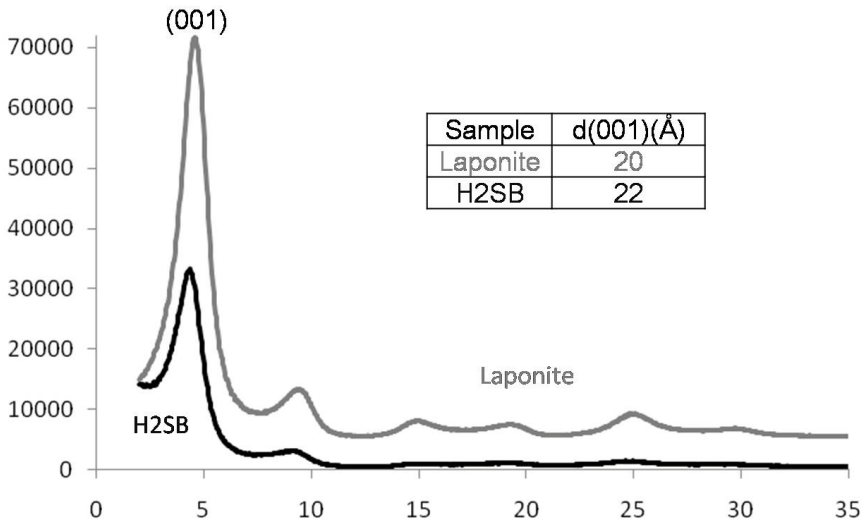


**Figure 5.3-3.** XRD patterns of PEG600 oriented H2SB and Laponite.

Figure 5.3-4, compares the DRIFTS spectra of H2SB and Laponite samples. Bands were assigned taking into account the characterisation data reported for clay samples (Russell and Fraser, 1994; Kloprogge et al., 1999; Kloprogge and Frost, 2000). The band around 1027 $cm^{-1}$ corresponds to ordered Si–O–Si in the clay mineral. The appearance of shoulder bands around 1105 $cm^{-1}$ and 1200 $cm^{-1}$ was related to the presence of the amorphous silica phase. The low intensity of these bands for both samples indicated a low concentration of the amorphous silica starting material and a high conversion to hectorite. Additionally, several broad bands were observed in the Laponite spectrum, between 1200 $cm^{-1}$ and 1400 $cm^{-1}$, that may be due to some remaining reagents or impurities (Figure 5.3-4).

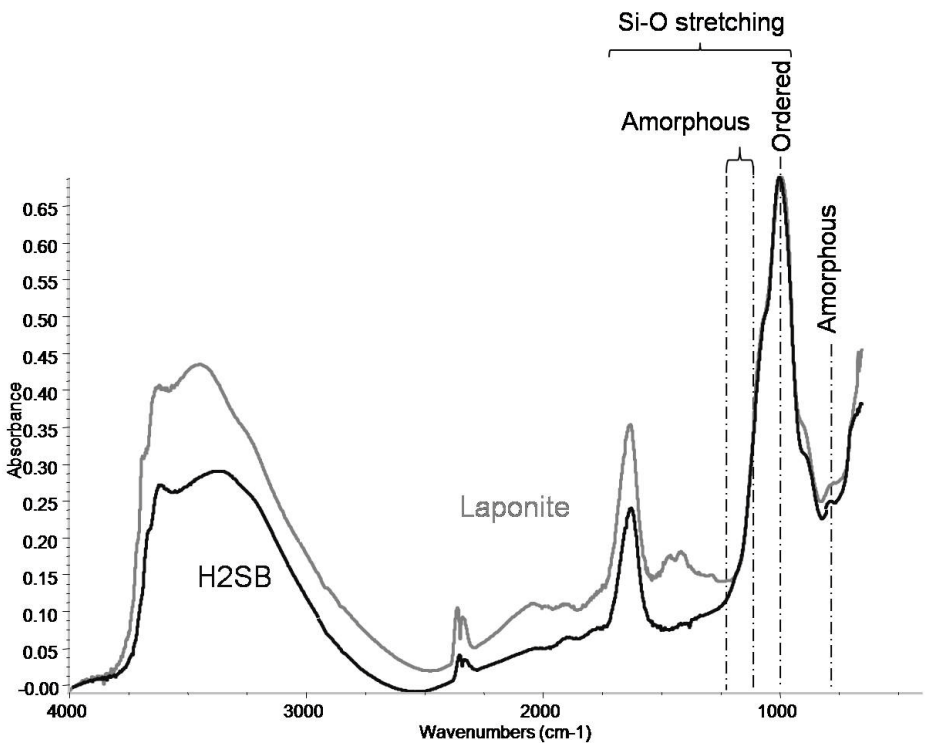


**Figure 5.3-4.** DRIFTS spectra of H2SB and Laponite.

UNIVERSITAT ROVIRA I VIRGILI
SYNTHESIS OF HECTORITES AND SAPONITES WITH MICROWAVES AND THEIR APPLICATION IN CATALYSIS AND COMPOSI
Isabel Vicente Valverde
ISBN:/DL:T. 1033-2011

TGA curves, and their derivatives, of the two hectorites showed two peaks for both samples (Figure 5.3-5). The first peak around 373 K is related to dehydration of samples whereas the second, around 973-1073 K, can be associated with their dehydroxilation. H2SB contained much more water of hydration.

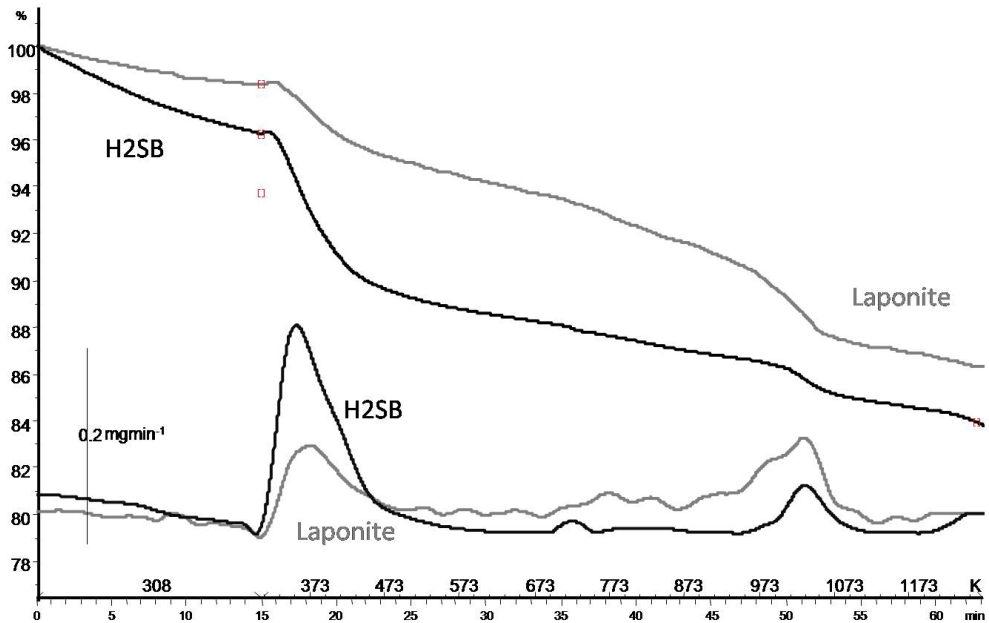


**Figure 5.3-5.** TGA curves of H2SB and Laponite (upper-two) and their negative derivatives (bottom-two).

The curves presented slight differences. Dehydroxylation in H2SB occurred over a narrower temperature than in Laponite, perhaps relating to the higher homogeneity of the former sample.

*Characterisation of composites*

Figure 5.3-6 illustrates some composite films prepared with 1 and 20 wt.% of H2SB and Laponite.

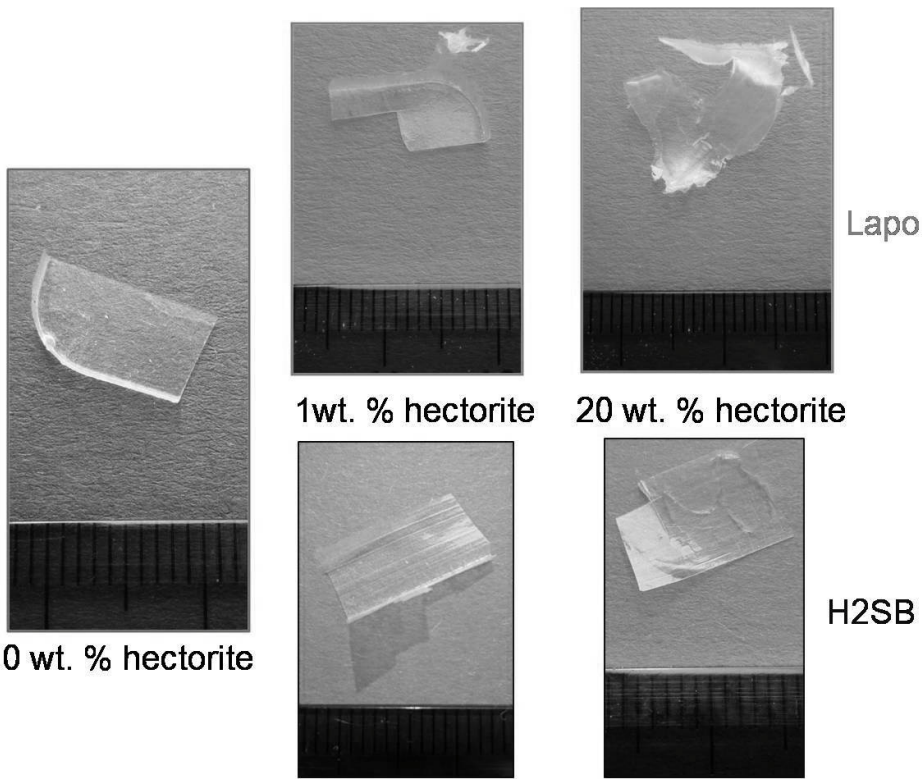


**Figure 5.3-6.** Composite films.Scale is in mm.

The integrity of the films between samples varied more with laponite was than with H2SB, suggesting homogeneity of clay dispersion in Laponite composite samples was lower than in H2SB. The need to drive off large quantities of solvent when producing the films may lead to cracks in the samples prepared with Laponite. It was not possible to obtain a coherent film 20 wt. % Laponite.

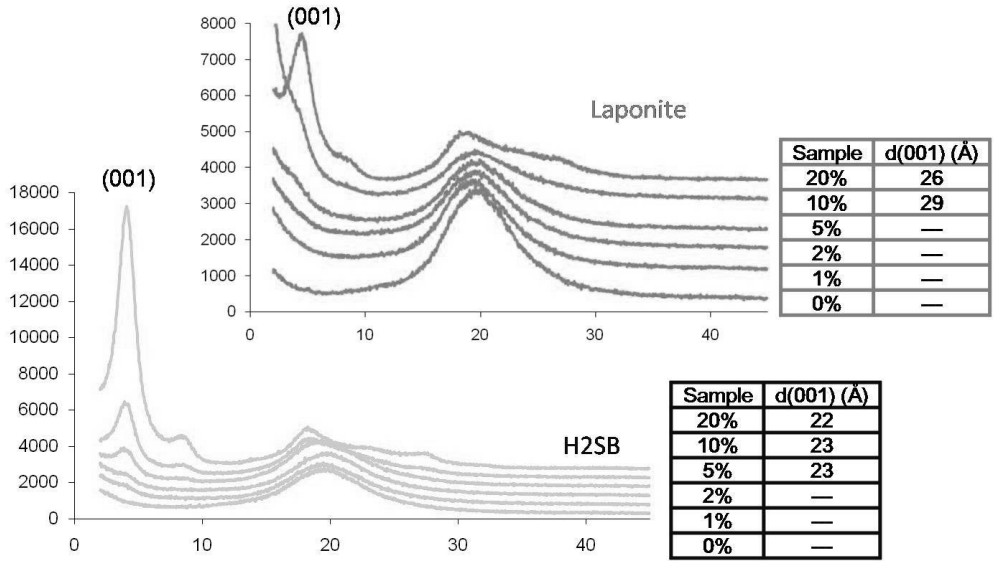


**Figure 5.3-7.** XRD patterns of composite samples prepared with HSB and Laponite.

Figure 5.3-7 shows the XRD patterns of the composite samples. H2SB appeared to be more oriented in polyurethane than laponite since (00l) reflections due to the hectorite phase were observed in H2SB composites at lower clay wt. % (10 wt. % and 20 wt. % for H2SB and laponite composites, respectively). Those (00l) reflections were not observed for ≤ 20 wt % polyurethane-Laponite composites found in the bibliography. At higher clay concentrations (> 2wt% for H2SB and > 5 wt% for laponite) an intercalated system is obtained whereas below these concentrations exfoliated clay may exist. An expansion of the clay layers by the polyurethane, at higher clay concentrations, was observed as in the PEG swollen H2SB and laponite described earlier.

The TGA curves, and their negative derivatives, of composite films are presented in Figure 5.3-8.

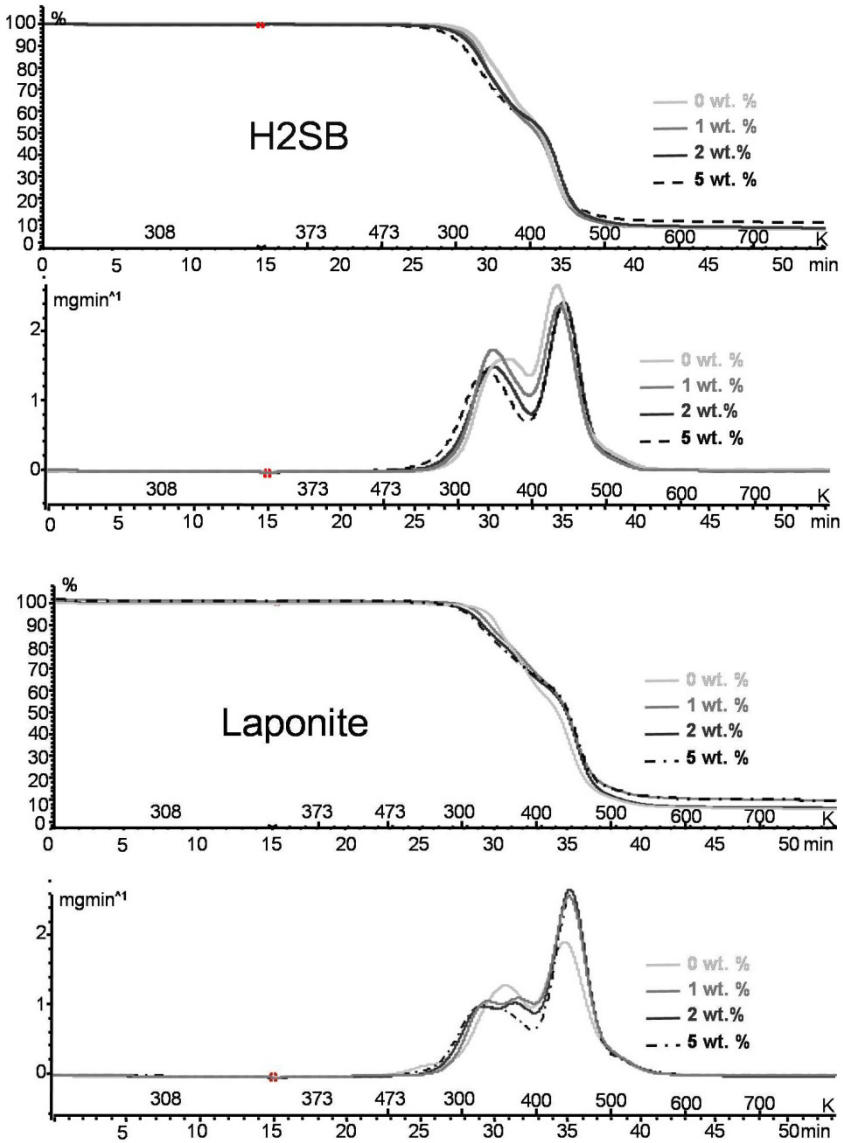


**Figure 5.3-8.** TGA and first derivative curves of composite samples prepared with H2SB and with Laponite.

All the derivatives showed two maxima at approximately 330 K and 430 K, respectively, confirming that neither H2SB nor the Laponite exerted any strong effect on the decomposition route. In both sets of composite samples, the temperature of the second maximum increased slightly when the hectorite wt. % increased in the composite. When Laponite was used for composite preparation the first maximum changed to produce two maxima suggesting two different thermal events were occurring, however, for H2SB composites the first maximum remained to suggest one thermal event.

Figure 5.3-9a) shows the storage modulus data of H2SB composite samples at various temperatures, plotted against the fraction of hectorite. The higher value of storage modulus at higher temperature observed when increasing hectorite fraction may indicate that this microwave synthesised hectorite increased the heat distortion temperature (HDT) of composite, i.e., the temperature at which the material deforms under load (Kumar et al., 2005).

However, in the case of Laponite samples (Figure 5.3-8b) the intersample variation between the results made it difficult to compare these results to those obtained with H2SB samples.

UNIVERSITAT ROVIRA I VIRGILI
SYNTHESIS OF HECTORITES AND SAPONITES WITH MICROWAVES AND THEIR APPLICATION IN CATALYSIS AND COMPOSI
Isabel Vicente Valverde
ISBN:/DL:T. 1033-2011

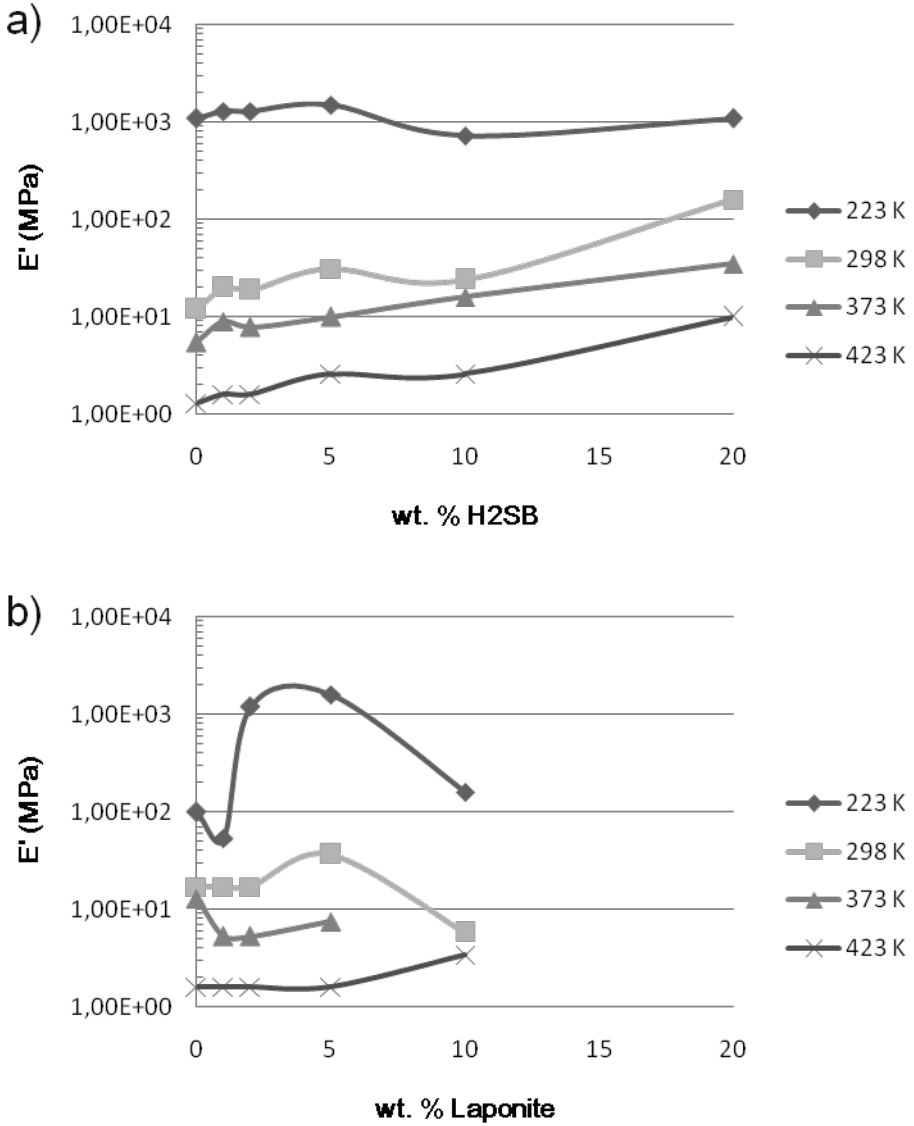


**Figure 5.3-9.** Storage modulus data at various temperatures of a)H2SB composites and b) Laponite composites.

UNIVERSITAT ROVIRA I VIRGILI
SYNTHESIS OF HECTORITES AND SAPONITES WITH MICROWAVES AND THEIR APPLICATION IN CATALYSIS AND COMPOSI
Isabel Vicente Valverde
ISBN:/DL:T. 1033-2011

Nevertheless, when the H2SB results were compared to those of McKinley et al. (2005, Figure 5.3-10), whose method was followed to synthesise our samples, the behaviour was quite similar.

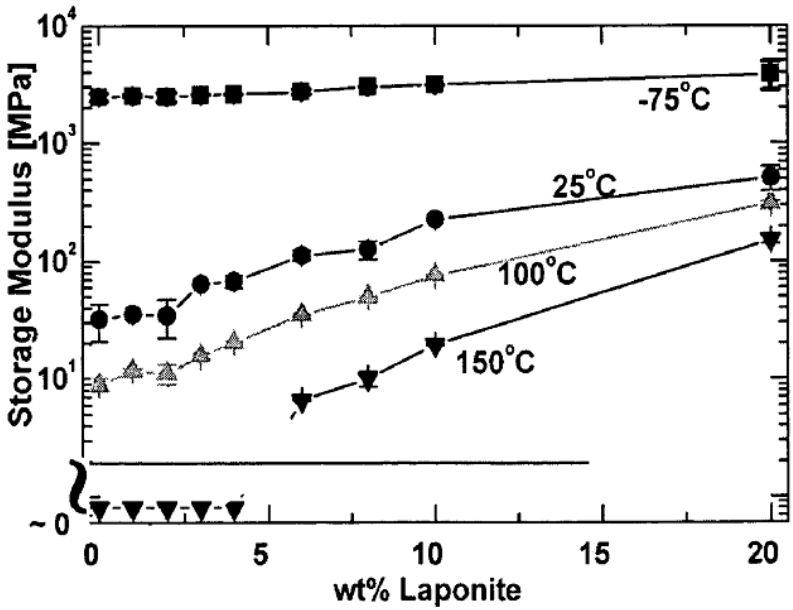


**Figure 5.3-10.** Storage modulus data at various temperatures (-75ºC= 198 K; 25 ºC= 298 K; 100 ºC= 373 K; 150 ºC= 423 K) of Laponite composites by Kumar et al., (2005).

The key difference between our samples and those of Kumar et al. (2005), is that they were able to dry their samples in a very controlled manner, which we were unable to replicate. Our samples were dried in an oven for shorter times and at higher temperature which were those feasible in our laboratories.

Figure 5.3-11 shows the Tan delta (loss modulus/ storage modulus) for the composite samples. The soft segment glass temperature ($T_g$) did vary significantly; however, a second peak appeared above the $T_g$ (about 300 k) at concentrations greater than 10 wt % of clay. The appearance of this peak,

together with a reduction in the intensity of the tan delta peak by increasing the clay content, indicated that the composite was becoming less rubbery as more clay was added. This is a normal behaviour because it is well known that adding clay makes a composite more brittle.

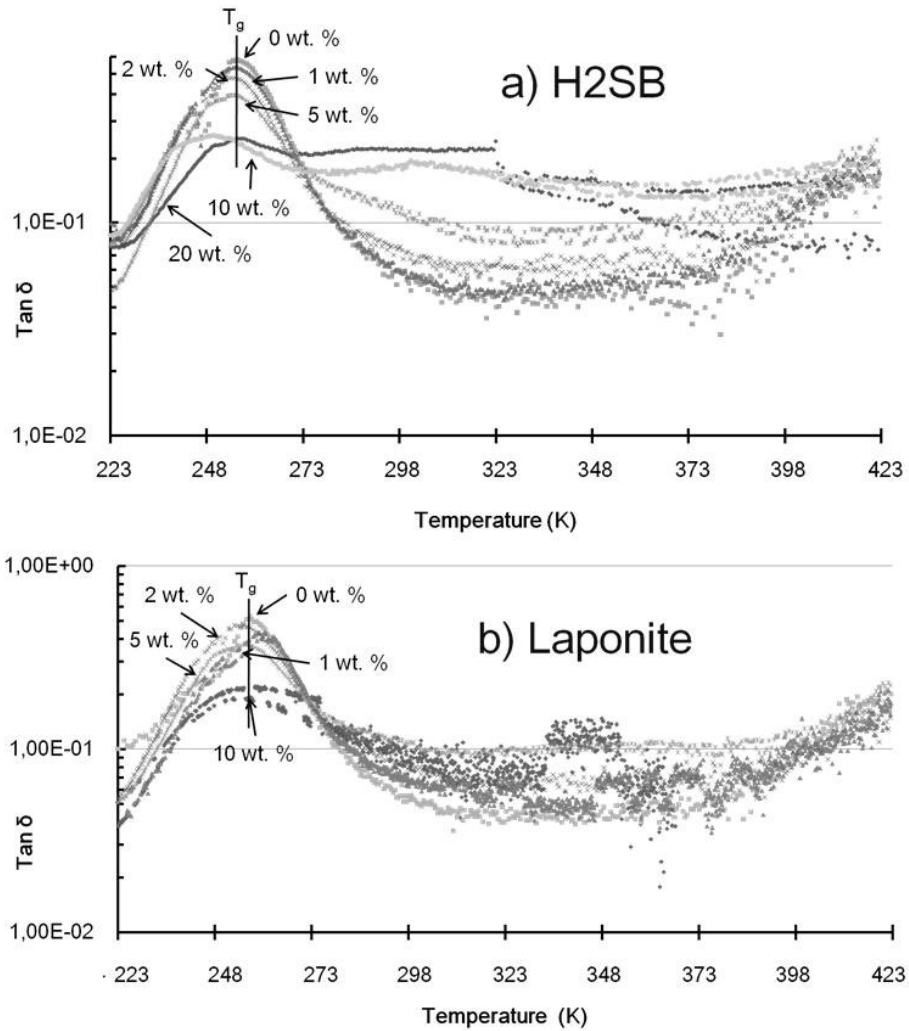


**Figure 5.3-11.** Tan delta (Tan δ) of a) H2SB and b) Laponite composites.

Again these results agreed with those obtained by Mc Kinley et al (2005, Figure 5.3-12)

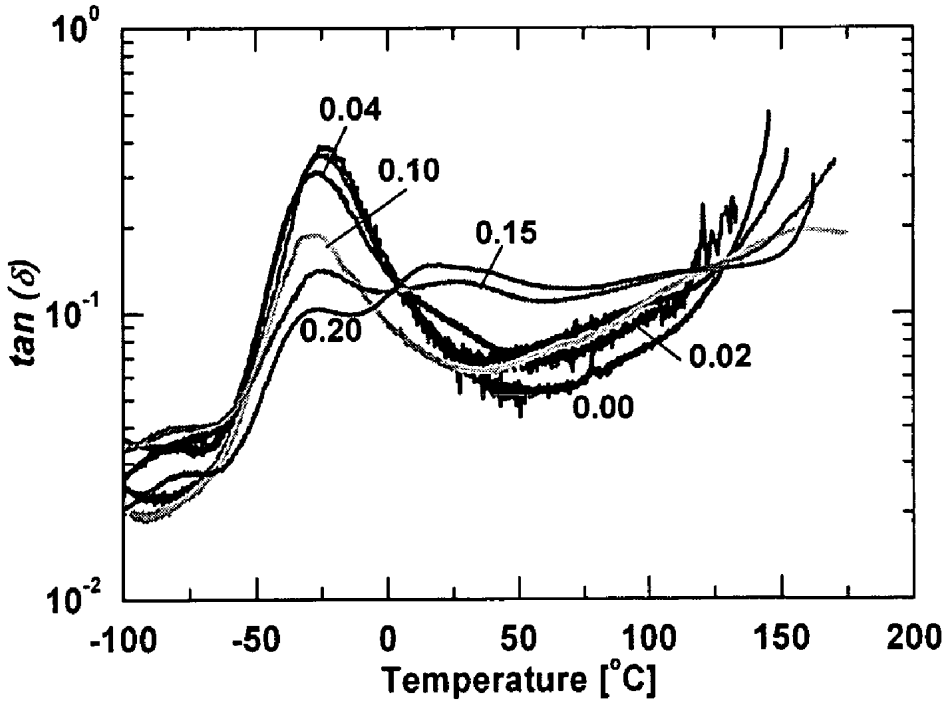


**Figure 5.3-12.** Tan delta (Tan (δ)) of Laponite composites by Kumar et al. In this case wt. clay content in composites is expressed in parts per unit. For example 0.04 in this diagram is equivalent to 4 wt%.

The original plan was to encourage the hectorite particles to interact preferentially with the hard segments in the PU taking advantage of the small diameter of hectorite particles, however, this did not seem to happen. The increasing stiffness with clay content suggests that the hectorite particles went into the soft segments. Nevertheless, the obtained results were similar to those obtained by Mc Kinley et al, using a more simple procedure.

## *5.4. Conclusions*

When using a microwave synthesised hectorite in the preparation of clay/polyurethane composite:

- Well dispersed clay into the polyurethane matrix composites were achieved using microwave synthesised hectorite but at lower clay loadings than when using Laponite (≤ 2 wt. % in front of ≤ 5 wt. %, respectively), as deduced from XRD results.

- The thermal stability of composites prepared with microwave synthesised hectorite and with Laponite did not significantly vary as observed by TG/DTG curves.

- From the thermomechanical analysis we observed that both microwave synthesised hectorite and Laponite not only interacted with the hard segments of polyurethane but unfortunately also with the soft segments.

- Composite prepared with microwave synthesised hectorite led to thermomechanical properties comparable to those found in the bibliography (Kumar et al., 2005).

## *5.5. Acknowledgments*

The authors are grateful for the financial support of the Ministerio de Educación y Ciencia of Spain and FEDER funds (CTQ2005-02384/ PPQ and CTQ2008-04433/PPQ) and for the FPU grant (AP2006-00835) and the fellowship for short stages also financed by the Ministerio de Educación y Ciencia of Spain.

# Chapter 6

## Conclusions

Since each study has their own conclusions, in this section some general conclusions will be exposed.

**When using microwaves to synthesise hectorites and saponites:**

- ✓ The hydrothermal microwave aging treatment provided faster synthesis of hectorites and saponites than those obtained by conventional heating. At longer times, an increase of clay phase content was also observed for both.

**Regarding hectorites:**

- ✓ The formation of the hectorite phase was faster when increasing the synthesis temperature from 373 K to 393 K, as observed by XRD, $N_2$ physisorption and CEC determination techniques.
- ✓ Hectorite with higher crystallinity was obtained when the fresh brucite $Mg(OH)_2$ reagent, which is supposed to act as crystallisation nuclei of hectorite, had higher crystallinity, as verified by XRD.
- ✓ Purer hectorites were obtained by treating the impure hectorite with $Na_2CO_3$ or by decreasing the silica content in the starting slurry, as confirmed by XRD and FTIR techniques.

**In the synthesis of saponites:**

- ✓ Higher crystallinity of the saponite phase with higher Al(Td)/Al(Oh) ratio was observed when increasing the pH of the initial slurry from 7 to 8. However, the amorphous $SiO_2$ content in the latter samples was also higher, as monitored by XRD, FTIR, CEC determination and $^{27}$Al-MAS-NMR.

- ✓ Higher content of higher crystalline saponite was achieved when $F^-$ was added to the initial slurry as observed by XRD, FTIR, CEC determination and $^{27}$Al-MAS-NMR techniques.

**When applying microwave synthesised clays as catalytic supports for the hydrogenation of styrene oxide:**

- ✓ High activity, high selectivity to 2-phenylethanol and high resistance to deactivation catalytic systems were obtained by impregnating microwave synthesised saponites and hectorites with nickel nitrate followed by calcination-reduction. The best catalytic results were achieved with 20 wt. % and 10 wt. % nickel for Ni/saponite and Ni/hectorite catalysts, respectively.

- ✓ Catalytic results were related to the presence of metal nickel sites with different activity since different NiO-support interactions were observed by TPR for their precursors.

ISBN:/DL:T. 1033-2011

- ✓ Ni/saponites and Ni/hectorites prepared by $Ni^{2+}$ cation exchange of hectorites and saponites showed lower conversion, lower selectivity to 2-phenylethanol and higher selectivity to phenylacetaldehyde than impregnated catalysts. This was explained by the lower coverage of support acid sites by metal sites due to the lower nickel content of the exchanged catalyst.

- ✓ The best result was achieved when using a 10 wt. % Ni/ microwave synthesised hectorite catalyst obtained by impregnation, with total activity and total selectivity to 2-phenylethanol at 1 h of reaction, and maintaining this behaviour after 3 runs.

**When impregnated Ni/saponites catalysts were used:**

- ✓ The presence of amorphous silica in higher or lower amounts in the synthesised saponites could not explain the different activity of the catalysts prepared at different initial pH. However, catalysts prepared with saponite obtained from a slurry with initial pH of 7 showed higher activity than the catalysts obtained from a slurry with initial pH= 8.

**When impregnated Ni/hectorites catalysts were used:**

- ✓ The use of conventional synthesised hectorite, acidified microwave synthesised hectorite or microwave hectorite synthesised with less silica content as catalytic supports, initially resulted in more active catalytic systems but they lost their activity faster than when using the microwaved synthesised hectorite as catalytic support.

**When using a microwave synthesised hectorite in the preparation of clay/polyurethane composites:**

- ✓ Well dispersed clays into the polyurethane matrix composites were obtained when hectorite loading was ≤ 2 wt. % as observed by XRD.
- ✓ The thermal stability of obtained composites (clay contents ≤ 20 wt. %) did not significantly vary as observed from TG/DTG curves.
- ✓ When thermomechanical analyses were performed, we observed that hectorite not only interacted with the hard segments of polyurethane but unfortunately also with the soft segments. Nevertheless, the composites prepared led to thermomechanical properties comparable to those found in the bibliography (Kumar et al., 2005).

# References

Aggarwal, V., Li, H., Boyd S. A., Teppen, B.J., 2006. Enhanced sorption of trichloroethene by smectite clay exchanged with $Cs^+$. Environ. Sci. Technol. 40(3), 894-9.

Alexandre, M., Dubois, P., 2000. Polymer-layered silicate nanocomposites: preparation, properties and uses of new class of materials. Mater. Sci. Eng., R Rep. 28, 1–63.

Andrew, E. R., Bradbury A., Eades R. G., 1959. Removal of Dipolar Broadening of Nuclear Magnetic Resonance Spectra of Solids by Specimen Rotation. Nature. 183(4678), 1802-1803.

Baird, T., Cairns-Smith, A. G., MacKenzie, D. W., Snell, D., 1971. Electron microscope studies of synthetic hectorite. Clay Miner. 9, 250-252.

Baird, T., Cairns-Smith, A. G., MacKenzie, D. W., 1973. An electron microscopic study of magnesium smectite synthesis. Clay Miner. 18, 17-26.

Barrer, R. M., Jones, D. L., 1970. Chemistry of soil minerals. Part VIII. Synthesis and properties of fluorhectorites. J. Chem. Soc. A. 1531-1537.

Bauer, K., Garbe, D. & Surburg, H., 2001. Common Fragrance and Flavor Materials Preparation, Properties and Uses, Holzminden: Wiley-VCH.

Békássy, S., Farkas, J., Agai, B., Figueras, F., 2000. Selectivity of C-versus O-acylation of diphenols by clay catalysts. I. Acylation of resorcinol with phenylacetyl chloride. Top. Catal. 13(3), 287–290.

Békássy, S., Ágai, B., Farkas, J., Gábor, E., Ferenczi, M., Figueras, F., 2007. An Environmentally Friendly Route for the Synthesis of Benzofurane Derivatives using Selective Ring Acylation of Resorcinol. Cat. Lett. 118(3-4), 219-223.

Bellefon, C., Tanchoux, N., Caravieilhes, S.,1998. New reactors and methods for the investigation of homogeneous catalysis. J. Organomet. Chem. 567, 143-150.

Benito, P., Labajos, F. M., Rocha, J., Rives, V., 2006. Influence of microwave radiation on the textural properties of layered double hydroxides. Micropor. Mesopor. Mat. 94, 148-158.

Benito, P., Labajos, F. M., Rives, V., 2009. Microwaves and layered double hydroxides: A smooth understanding. Pure and Applied Chemistry. 81(8), 1459-1471.

Bergadà, O., Vicente, I., Salagre, P., Cesteros, Y., Medina, F., Sueiras, J.E., 2007a. Microwave effect during aging on the porosity and basic properties of hydrotalcites. Microporous Mesoporous Mater. 101, 363–373.

Bergadà, O., Salagre, P., Cesteros, Y., Medina, F., Sueiras, J. E., 2007b. Effective catalysts, prepared from several hydrotalcites aged with and without microwaves, for the clean obtention of 2-phenylethanol. Appl. Catal. A: Gen., 331, 19-25.

Bergadà, O., Salagre, P., Cesteros, Y., Medina, F., Sueiras, J. E., 2008. Control of the basicity in Ni–MgO systems: influence in the hydrogenation of styrene oxide. Catal. Lett., 122, 259-266.

Bergadà. O., Boix. E., Salagre, P., Cesteros, Y., Medina, F., Sueiras, J. E., 2009. Acidity properties of Ni-exchanged mordenites prepared with and without microwaves. Appl. Catal. A: Gen., 368, 163-169.

Bergaya, F., Vayer, M., 1997. CEC of clays: measurement by adsorption of a copper ethylenediamine complex. Appl. Clay Sci. 12, 275–280.

Bisio, C., Gatti, G., Boccaleri, E., Marchese, L., Superti, G.B., Pastore, H.O., Thommes, M., 2008. Understanding physico-chemical properties of saponite synthetic clays. Microporous Mesoporous Mater. 107, 90–101.

Breu, J., Seidl, W., Stoll, A., 2003. Fehlordnung bei Smectiten in Abhängigkeit vom Zwischenschichtkation. Z. Anorg. Allg. Chem. 629, 503–515

Bujdák, J., Iyi, N., 2006. Molecular aggregation of rhodamine dyes in dispersions of layered silicates: influence of dye molecular structure and silicate properties. J. Phys. Chem. B. 110(5), 2180-2186.

Calvino-Casilda, V., Lopez-Peinado, A. J., Fierro, J. L. G., Martín-Aranda, R. M., 2003. Microwave assisted N-propargylation of imidazole using alkaline promoted carbons. Appl. Catal. A: Gen. 240(1-2), 287-293.

Calvino-Casilda, V., Martín-Aranda, R. M, López-Peinado, A, J., 2009. Microwave Assisted Green Synthesis of Long-chain 1-Alkylimidazoles and Medium-chain 1-alkyl-2-Methylimidazoles with Antiviral Properties Catalyzed by Basic Carbons. Catal. Lett.. 129(3-4), 281-286.

Campelo, J. M., Chekraborty, R., Marinas, J. M., 1996. Reductive Cleavage of Epoxides with Zinc Borohydride Supported on Aipo. Synth. Commum. 26(3), 415-421.

Carretero, M. I., Gomes, C. S. F., Tateo, F., 2006. Clays and human health. In: Bergaya, F., Theng, B.K.G., Lagaly, G. (Eds.), Handbook of Clay Science, vol.1. Elsevier, Amsterdam, pp. 765–787.

Carretero, M.I., Pozo, M., 2009. Clay and non-clay minerals in the pharmaceutical industry Part I. Excipients and medical applications. Appl. Clay Sci., 46(1), 73-80.

Casagrande, M., Storaro, L., Lenarda, M., Rossini, S., 2005. Solid acid catalysts from clays: oligomerization of 1-pentene on Al-pillared smectites. Catal. Commun. 6, 568–572.

Chang, J. H., Park, D. K., Ihn, K. J., 2001. Montmorillonite-based nanocomposites of polybenzoxazole: Synthesis and characterization (I). J. Polym. Sci. Part B: Polym. Phys. 39(5), 471-476.

Chattopadhyay, D., Raju, K., 2007. Structural engineering of polyurethane coatings for high performance applications☆. Progress in Polymer Science. 32(3), 352-418.

Cheary, R. W., Coelho, A. A., 1992. A fundamental parameters approach to X-ray line-profile fitting. J. Appl. Cryst. 25, 109-121.

Chen, K., Wilkie, C. A.., Vyazovkin, S., 2007. Nanoconfinement revealed in degradation and relaxation studies of two structurally different polystyrene-clay systems. J.Phys. Chem. B. 111(44), 12685-12692.

Chen, B., Evans, J. R. G., Greenwell, H. C., Boulet, P., Coveney, P. V., Bowden, A. A., Whiting, A., 2008. A critical appraisal of polymer-clay nanocomposites. Chem. Soc. Rev. 37(3), 568-94.

Chmielarz, L., Kustrowski, P., Drozdek, M. Dziembaj, R., Cool, P., Vansant, E., 2006. Selective catalytic oxidation of ammonia into nitrogen over PCH modified with copper and iron species. Catal. Tod., 114(2-3), 319-325.

Coelho, A.A., 2005. TOPAS v3.0. Bruker AXS.

Cohen, J. B.; Schwartz, L. H., 1977. Diffraction from Materials, Academic Press, New York.

Cseri, T., Békássy, S., Bódás, Z., Ágai, B., Figueras, F., 1996. Acetylation of B15C5 crown ether on Cu modified clay catalysts. Tetrahedron Lett. 37(9), 1473–1476.

Czímerová, A., J. Bujdák, Dohrmann, R., 2006. Traditional and novel methods for estimating the layer charge of smectites. Appl Clay Sci. 34, 2-13.

Decarrau, A., 1980. Cristallogène experimentale des smectites magnésiennes: hectorite, stévensite. Bull. Minéral. 103, 579–590.

De Lima, R B, Paganin, V, Iwasita, T, Vielstich, W. 2003. On the electrocatalysis of ethylene glycol oxidation. Electrochim. Acta, 49, 85-91.

Dimitry, O. I. H., Abdeen, Z. I., Ismail E. A., Saad, A. L. G., 2010. Preparation and properties of elastomeric polyurethane/organically modified montmorillonite nanocomposites. J. Polym. Res. 17(6), 801-813.

Eliel, E.L., Delmonte, D.W., 1956. A synthesis of optically active styrene oxide and other epoxides. J. Org. Chem., 21(5), 596-597.

Farkas, J., Békássy, S., Ágai, B., Hegedüs, M., Figueras, F., 2000. Acylation of Resorcinol on Clay Catalysts. Synthetic Comm. 30(14), 2479-2485.

Farkas, J., Békássy, S., Madarász, J., Figueras, F., 2002. Selective oxidation of benzylic alcohols to aldehydes with metal nitrate reagents catalyzed by BEA zeolites or clays. New J. Chem. 26(6), 750-754.

Fujitsu, H., Shirahama, S., Matsumura, E., Takeshita, K., Mochida, I., 1981. Catalytic hydrogenation of styrene oxide with cationic rhodium complexes. J. Org. Chem. 46, 2287-2290.

Furuichi, N., Kurokawa, Y., Fujita, K., Oya, A., Yasuda, H., Kiso, M., 1996. Preparation and properties of polypropylene reinforced by smectite. J. Mater. Sci., 1996, 31, 4307.

Gibson, C.A., Theiling, L.F., 1977. Hydrogenation of styrene oxide to produce 2-phenylethanol. US Patent 4,064,186.

González, M.D., Cesteros, Y., Salagre, P., Medina, F., Sueiras, J.E., 2009. Effect of microwaves in the dealumination of mordenite on its surface and acidic properties. Micropor. Mesopor. Mater. 118, 341-347.

Granquist, W.T., Pollack, S.S., 1959. A study of the synthesis of hectorite. Clays Clay Miner. 8, 150–169.

Grey, R. A., Pez, G. P., Wallo, A., 1981. Anionic metal hydride catalysts. 2. Application to the hydrogenation of ketones, aldehydes, carboxylic acid esters, and nitriles. J. Am. Chem. Soc. 103, 7536-7542.

Guerra, D.L., Viana R. R., Airoldi, C., 2010. Use of raw and chemically modified hectorites as adsorbents for Th(IV), U(VI) and Eu(III) uptake from aqueous solutions. Desal.; 260(1-3),161-171.

Guidotti, M., Psaro, R., Ravasio, N., Sgobba, M., Carniato, F., Bisio, C. Gatti, G., Marchese, L., 2009. An efficient ring opening reaction of methyl epoxystearate promoted by synthetic acid saponite clays. Green Chem., 11, 1173-1178.

Herney-Ramirez, J., Silva, A. M. T., Vicente, M. A., Costa, C. A., Madeira, L. M., In press. Degradation of Acid Orange 7 using a Saponite-based Catalyst in Wet Hydrogen Peroxide Oxidation: Kinetic Study with the Fermi's Equation. Appl. Catal. B., DOI: 10.1016/j.apcatb.2010.09.020.

Higashi, S., Miki, K., Komarneni, S., 2002. Hydrothermal synthesis of Zn-smectites. Clays Clay Miner. 50, 299–305.

Hölderich, W. H., Barsnick, U., 2001. Rearrangement of Epoxides. In: Sheldon, S. A; Van Bekkum, H., (Eds.), Fine Chemicals through Heterogeneous Catalysis., Wiley-VCH, Germany.

Hopff, H., Kuhn, H., Hoffmann, U., Homburg, B., 1958. Process for preparation of ß-phenyl ethyl alcohol. US Patent 2,682,466.

Jaber, M., Miéhé-Brendlé, J., 2005. Influence du milieu de synthèse sur la cristallisation de saponite: proposition de mécanisme réactionnel en milieux acide et basique, C.R. Chimie 8, 229–234.

Jaber, M., Miéhé-Brendlé, J., 2008. Synthesis, characterization and applications of 2:1 phyllosilicates and organophyllosilicates: contribution of fluoride to study the octahedral sheet. Microporous Mesoporous Mater. 107 (1–2), 121–127.

Kappe, C. O., 2004. Controlled microwave heating in modern organic synthesis. Angew. 43(46), 6250-84.

Kawasaki, T., Omine, T., Suzuki, K., Sato, H., Yamagishi, A.,Soai, K., 2009. Highly enantioselective asymmetric autocatalysis using chiral ruthenium complex-ion-exchanged synthetic hectorite as a chiral initiator. Org. Biomol. Chem. 7, 1073-1075.

Khaorapapong, N., Kuroda, K., Hashizume, H., 2001. Solid-state intercalation of 4,4'-bipyridine and 1,2-di(4-pyridine) ethylene into the interlayer spaces of Co(II), Ni (II)-, and Cu(II)-montmorillonites. Appl. Clay Sci. 19, 69-76.

Kingston, H. M., Haswell, S., J., 1997. Microwave-Enhanced Chemistry: Fundamentals, Sample Preparation and Applications. American Chemical Society, Washington DC.

Kirm, I., Medina, F., Rodríguez, X., Cesteros, Y., Salagre, P., Sueiras, J.E., 2005. Preparation of 2-phenylethanol by catalytic selective hydrogenation of styrene oxide using palladium catalysts. J. Mol. Catal. A: Chem. 239(1-2), 215-221.

Kirm, I., Medina, F., Sueiras, J. E., Salagre P., Cesteros, Y., 2007. Hydrogenation of styrene oxide in the presence of supported platinum catalysts to produce 2-phenylethanol. J. Mol. Catal. A: Chem. 261(1), 98-103.

Kloprogge, J.T., Breukelaar, J., Wilson, A.E., Geus, J.W., Jansen, B.H., 1994a. Solid-state nuclear magnetic resonance spectroscopy on synthetic ammonium/aluminiumsaponites. Clays Clay Miner. 42, 416–420.

Kloprogge, J.T., Breukelaar, J., Geus, J.W., Jansen, B.H., 1994b. Characterization of Mg saponites synthesised from gels containing amounts on $Na^{+}$, $K^{+}$, $Rb^{+}$, $Ca^{2+}$, $Ba^{2+}$, or $Ce^{4+}$ equivalent to CEC of the saponite. Clays Clay Miner. 42, 18–22.

Kloprogge, J.T., Komarneni E., Amonette, S. J., 1999. Synthesis of smectite clay minerals: A critical review. Clays Clay Miner., 47(5), 529-554.

Kloprogge, J.T., Frost, R.L., 2000. The effect of synthesis temperature on the FT-Raman and FT-IR spectra of saponites. Vib. Spectrosc. 23, 119–127.

Kochkar, H.; Clacens, J. M.; Figueras, 2002. Isomerization of Styrene Epoxide on Basic Solids. F. Catal. Lett. 78, 91-94.

Komarneni, S., Roy, R., Li, Q.H., 1992. Microwave–hydrothermal synthesis of ceramic powders. Mater. Res. Bull. 27, 1393–1405.

Komarneni, S., Li, Q.H., Roy, R., 1996. Microwave–hydrothermal processing of layered anion exchangers. J. Mater. Res. 11, 1866–1869.

Körosi, L., Németh, J., Dékány, I., 2004. Structural and photooxidation properties of SnO2/layer silicate nanocomposites. Appl. Clay Sci. 27, 29–40.

Krishnamurthy, S., Schubert, R. M., Brown, H. C., 1973. Lithium triethylborohydride as a convenient reagent for the facile reduction of both hindered and bicyclic epoxides prone to electrophilically induced rearrangement. JACS, 95(25), pp.8486-8487.

Kumar, N., Liff, S. M., McKinley, G. H., 2005. Methods to disperse and exfoliate nanoparticles. US Patent App. 11/253,219.

Laudelout, H., 1987. In: Newman (Ed.), Chemistry of Clays and Clay Minerals. Longman Scientific and Technical, London.

Levin, E.M., Hou, S.S., Bud'ko, S.L., Schmidth-Rohr, K., 2004. Magnetism and nuclear magnetic resonance of hectorite and montmorillonite layered silicates. J. Appl. Phys. 96, 5085–5092.

Li, Z., Han, C., Shen, J. 2006. Reduction of $Ni^{2+}$ by hydrazine in solution for the preparation of nickel nano-particles. J. Mater. Sci., 41, 3473-3480.

Liff, S. M., Kumar N., McKinley G. H., 2007. High-performance elastomeric nanocomposites via solvent-exchange processing. Nature Mat., 6(1), 76-83.

Liu, X., Breen, C., 2005. High-temperature crystalline phases in nylon-6/clay nanocomposites. Macromol. Rapid Commun. 26, 1081–1086.

Lowe, I., 1959. Free induction decays of rotating solids. Phys. Rev. Lett. 2(7), 285–287.

Ma, J., Jia Y., Jing, Y., Yao, Y., Sun, J., 2010. Synthesis and photocatalytic activity of $TiO_2$-hectorite layer-by-layer thin films. Appl. Clay Sci., 47(3-4), 433-437.

Martin D. J., Meijs, G. F., Gunatillake, P. A., Yozghatlian, S. P., Renwick G. M., 1999. The influence of composition ratio on the morphology of biomedical polyurethanes. J. Appl. Polym. Sci. 71(6), 937-952.

Martín-Aranda, R. M., Vicente-Rodríguez M. A., López-Pestaña J. M., López-Peinado, A. J., Jerez, A., De López-González, J. D., Bañares-Muñoz, M.A., 1997. Application of basic clays in microwave activated Michael additions: Preparation of N-substituted imidazoles. J. Mol. Catal. A: Chem. 124, 115-121.

McKeown, N.K., Bishop, J.L., Noe Dobrea, E.Z., Ehlmann, B.L., Parente, M., Mustard, J.F., Murchie, S.L., Swayze, G.A., Bibring, J.-P., Silver, E.A.., 2009. Characterization of phyllosilicates observed in the central Mawrth Vallis region, Mars, their potential formational processes, and implications for past climate. J. Geophys. Res., 114 (11), E00D10, 20 PP.

Mingos, D. M. and D.R. Baghurst., 1997. Applications of Microwave Dielectrc Heating Effects to Synthetic Problems in chemistry. In: H.M. Kingston and S. J. Haswell (Ed.), Microwave-Enhanced Chemistry: Fundamentals, Sample Preparation and Applications. American Chemical Society, Washington, DC.

Mitsui, S.; Imaizumi, S.; Hisashige, M.; Sugi, Y. The deoxygenation in the catalytic hydrogenolysis of styrene oxides. 1973. Tetrahedron. 29, 4093-4097.

Mochida, I., Shirahama, S., Fujitsu, H., Takeshita, K., 1977. Catalytic activities of cationic rhodium complexes for the hydrogenation of styrene oxide Chem. Lett. 4(1977) 421-422.

Mookherjee, B.D., Wilson, R.A. & Kirk, R.E. eds., 1996. Encyclopedia of Chemical Technology, New York: Jonh Wiley.

Moncada, E., Quijada, R., Retuert, J., 2007. Comparative effect of metallocene and Ziegler-Natta polypropylene on the exfoliation of montmorillonite and hectorite clays to obtain nanocomposites. J. Appl. Polym. Sci. 103(2), 698–706.

Moreno, S., Kou, R.S., Poncelet, G., 1996. Hydroconversion of heptane over Pt/Al-pillared montmorillonites and saponites. A comparative study. J. Catal., 162, 198-208.

Nagendrappa, G., In press. Organic synthesis using clay and clay-supported catalysts. Appl. Clay Sci., DOI: 10.1016/j.clay.2010.09.016.

Newalkar, B.L., Olanrewaju, J., Komarneni, S., 2001. Microwave–hydrothermal synthesis and characterization of zirconium-substituted SBA-15 mesoporous silica. J. Phys. Chem. B 105, 8356–8360.

Nomura, K., Ogura, H., Imanishi, Y., 2001. Direct synthesis of 2-phenylethanol by hydrogenation of methyl phenylacetate using homogeneous ruthenium-phosphine catalysis under low hydrogen pressure. J. Mol. Cat. A: Chem. 166(2), 345–349

Nielsen, L. E., Landel, R. F. (Eds.), 1994. Mechanical properties of polymers and composites. Marcel Dekker, Inc, New York.

Okada, A., Usuki, A., 2006. Twenty Years of Polymer-Clay Nanocomposites. Macromol. Mater. Eng. 291(12), 1449-1476.

Petit, S., 2006. Fourier Transform Infrared Spectroscopy. In: Bergaya, F., Theng, B. K. G., Lagaly, G. (Eds.), Handbook of Clay Science, vol.1. Elsevier, Amsterdam, pp. 919–938

Perozo-Rondon, E., Costarrosa, L., Martin-Aranda, R., Rojas-Cervantes, M., Vicente-Rodríguez M. A., 2006. Microwave enhanced synthesis of N-propargyl derivatives of imidazole. A green approach for the preparation of fungicidal compounds. Appl. Surf. Sci. 252(17), 6067-6070.

Pieper, H., Bosbach, D., Panak, P.J., Rabung, T., Fanghanel, T., 2006. Eu(III) coprecipitation with the trioctahedral clay mineral hectorite. Clays Clay Miner. 54, 45–53.

Pilter, Z., Szabó, S., Hasznos-Nezdei, M., Pallai-Varsányi, E., 2000. X-ray diffraction study of the effect of microwave treatment of zeolite Na-A. Microporous Mesoporous Mater. 40, 257–262.

Pinnavaia, T. J., 1983. Intercalated Clay Catalysts. Science., 220, 365-371.

Pinnavaia, T. J., Beall G. W., 2000. Polymer-Clay Nanocomposites. John Wiley & Sons, Chichester.

Porter, D., Vollrath, F., Shao, Z., 2005. Predicting the mechanical properties of spider silk as a model nanostructured polymer. Eur. Phys. J. E. 16(2), 199-206.

Prikhod'ko, R.V., Sychev, M.V., Sychev, M.V., Astrelin, I.M., Erdmann, K., Hensen, E.J.M., van Santen, R.A., 2003. Nonhydrothermal synthesis and properties of saponite-like materials. Russ. J. Appl. Chem. 76 (5), 700–705.

Pruski, M.; Amoureux, J. P.; Fernandez, C. Progress, 1976. High resolution solid state NMR of quadrupolar nuclei. Applications to porous materials and catalysts. In Magnetic Resonance in Colloid and Interface Science, Resing H. A.; Wade, C. G. Eds. ACS Symposium Series: San Francisco. vol. 76, p. 107.

Pshinko, G. N., Kobets, S. A., Bogolepov, A. A., Goncharuk, V. V., 2010. Treatment of Waters Containing Uranium with Saponite Clay. J. Water Chem. Technol., 32(1), 10-16.

Ranu, B. C., Das, A. R., 1990. Regio- and stereo-selective reductive cleavage of epoxides with zinc borohydride supported on silica gel J. Chem. Soc., Chem. Commun. 19, 1334-1335.

Rico, E., Trujillano, R., Vicente, M.A., Rives, V., Gil, A., Korili, S.A., 2008. Preparación de saponitas sintéticas mediante tratamiento hidrotérmico usando radiación microondas. Macla 9, 203–204.

Rivera, A., Fetter, G., Bosch, P., 2006. Microwave power effect on hydrotalcite synthesis. Microporous Mesoporous Mater. 89, 306–314.

Robertson, J., Bandosz, T. J., 2006. Photooxidation of dibenzothiophene on $TiO_2$/hectorite thin films layered catalyst. J. Coll. Interface Sci.; 299(1), 125-35.

Rode, C. V., Telkara, M. M., Chaudhar, R. V. 2000. Alkali promoted regio-selective hydrogenation of styrene oxide to β-phenethyl alcohol, in: Corma, A., Melo, F. V., Mendioroz, S., Fierro, J. L. G. (Eds), Studies in Surface Science and Catalysis, Elsevier, Amsterdam, 130 A, pp. 533-538.

Rode, C. V., Telkar, M.M., Jaganathan, R., Chaudhari, R.V. 2003. Reaction kinetics of the selective liquid phase hydrogenation of styrene oxide to β-phenethyl alcohol. J. Mol. Catal. A: Chem. 200, 279-290.

Romero, M.D., Gómez, J.M., Ovejero, G., Rodríguez, A., 2004. Synthesis of LSX zeolite by microwave heating. Mater. Res. Bull. 39, 389–400.

Rusell, J.D., Fraser, A.R., 1994. Infrared methods. In: Wilson, M.J. (Ed.), Clay Mineralogy: Spectroscopic and Chamical Determinative Methods. Chapman & Hall, London.

Sakamoto, K., Nakamura, T., Noguchi, T., Tsuchiyama, 2010. A. A new variant of saponite-rich micrometeorites recovered from recent Antarctic snowfall. Meteoritics and Planetary Science, 45 (2), 220-237.

Salla, I., Bergadà, O., Salagre, P., Medina, F., Sueiras, J. E., Montanari, T. 2005. Isomerisation of styrene oxide to phenylacetaldehyde by fluorinated mordenites using microwaves. J. Catal. 232, 239-245.

Sanz, J., 2006. Nuclear Magnetic Resonance Spectroscopy. In: Bergaya, F., Theng, B. K. G., Lagaly, G. (Eds.), Handbook of Clay Science, vol.1. Elsevier, Amsterdam, pp. 919–938.

Schlegel, M. L., Descostes, M., 2009. Uranium Uptake by Hectorite and Montmorillonite: A Solution Chemistry and Polarized EXAFS Study. Environ. Sci. Technol.; 43(22), 8593-8598.

Sendovski M, Nir N, Fishman A., 2010. Bioproduction of 2-phenylethanol in a biphasic ionic liquid aqueous system. J. Agricult. Food Chem. 58(4), 2260-2265.

Sento, T., Shimazu, S., Ichikuni, N., Uematsu, T., 1999. Asymmetric hydrogenation of itaconates by hectorite-intercalated Rh-DIOP complex. J. Mol. Catal. A., 137(1-3), 263-267.

Seydibeyoğlu, M. Ö., Işçi, S., Güngör, N., Ece, O. I., Güner, F. S., 2010. Preparation of polyurethane/hectorite, polyurethane/montmorillonite, and polyurethane/laponite nanocomposites without organic modifiers. J. Appl. Polym. Sci., 116(2), 832-837.

Shah, R., Paul, D., 2006. Organoclay degradation in melt processed polyethylene nanocomposites. Polym. 47(11), 4075-4084.

Shen, Z., Simon, G.P., Cheng, Y. B., 2002. Comparison of solution intercalation and melt intercalation of polymer–clay nanocomposites. Polymer. 43(15), 4251-4260.

Smith, B. L., Schaffer, T. E., Viani, M., Thompson, J. B., Frederick, N. A., Kindt, J., Belcher, A., Stucky, G. D., Morse, D. E., Hansma, P. K., 1999. Molecular mechanistic origin of the toughness of natural adhesives, fibres and composites. Nature. 399, 761–763.

Spagnuolo, M., Martínez, C. E., Jacobson, A.R., Baveye, P., McBride, M. B., Newton, J., 2004. Coprecipitation of trace metal ions during the synthesis of hectorite. Appl. Clay Sci., 27(3-4), 129-140.

Sreekumar, R., Padmakumar, R., Rugmini, P., 1998. One-pot synthesis of nitroolefins using zeolite. Tetrahedron Lett., 39(18), 2695-2696.

Srodon, J., 2006. Identification and quantitative analysis of clay minerals. In: Bergaya, F., Theng, B.K.G., Lagaly, G. (Eds.), Handbook of Clay Science, vol.1. Elsevier, Amsterdam, pp. 765–787.

Stepkowska, E.T., J. L. Pérez-Rodríguez, C. Maqueda and E. Starnawska, 2004. Variability in water sorption and in particle thickness of standard smectites. Appl Clay Sci. 24, 185-199.

Stokes, A. R., Wilson, A. J. C., eds., 1942. A method of calculating the integral breadths of Debye-Scherrer lines. Proc.Camb.Phil.Soc., 38, pp 313-322.

Suquet, H., de La Calle, C., Pezerat, H., 1975. Swelling and structural organization of saponite. Clays Clay Miner. 23, 1–9.

Suquet, H., Malard, C., Copin, E., Pezerat, H., 1981. Variation du parameter b et de la distance basale d(001) dans une serie de saponites a charge croissante. I. Etats hydrates. Clay Miner. 16, 53–67.

Tichit, D., Rolland, A., Prinetto, F., Fetter, G., Martínez-Ortíz, M.J., Valenzuela, M.A., Bosch, P., 2002. Comparison of the structural and acid-base properties of Ga- and Al containing layered double hydroxides obtained by microwave irradiation and conventional ageing of synthesis gel. J. Mater. Chem. 12, 3832–3838.

Tompsett, G. A., Conner W. C., Yngvesson K. S., 2006. Microwave synthesis of nanoporous materials. Chemphyschem. 7(2), 296-319.

Trujillano, R., Rico, E., Vicente, M. A., Herrero, M., Rives, V., 2010. Microwave radiation and mechanical grinding as new ways for preparation of saponite-like materials. Appl Clay Sci. 48, 32-38.

Trujillano, R., Rico, E., Vicente, M. A.., Rives, V., Ciuffi, K. J., Cestari, A., Gil, A., Korili, S. A.., In press. Rapid microwave-assisted synthesis of saponites and their use as oxidation catalysts. Appl. Clay Sci. DOI: 10.1016/j.clay.2010.12.005.

Urbanczyk, L., Hrobarikova, J., Calberg, C., Jérôme, R., Grandjean, J., 2006. Motional Heterogeneity of Intercalated Species in Modified Clays and Poly(ε-caprolactone)/Clay Nanocomposites. Langmuir. 22(10), 4818-4824.

Vaccari A., 1998. Preparation and catalytic properties of cationic and anionic clays. Catal. Today ,41(1-3),53–71.

Vaccari A., 1999. Clays and catalysis: a promising future. Appl. Clay Sci., 14, 161-198.

Van Santen, R. A., Van Leeuwen, P: W. N. M., Moulyn, J. A., Averill, B. A., 2000. Studies in Surface Science and Catalysis: Catalysis an integrated approach. Elsevier, Amsterdam.

Varma R. S., 2002. Clay and clay-supported reagents in organic synthesis. Tetrahedron., 58(7), 1235–1255.

Vicente, I., Salagre, P., Cesteros, Y., Guirado, F., Medina, F., Sueiras, J.E., 2009. Fast microwave synthesis of hectorite. Appl. Clay Sci. 43, 103–107.

Vicente, I., P. Salagre, Y. Cesteros, F. Medina and J. E. Sueiras, 2010. Microwave-assisted synthesis of saponite. Appl. Clay Sci. 48, 26-31.

Vicente, I., P. Salagre, Y. Cesteros, In press. Ni nanoparticles supported on microwave-synthesised saponite for the hydrogenation of styrene oxide. Appl. Clay Sci. DOI:10.1016/j.clay.2010.12.025.

Vico, L., Acebal S., 2006. Some aspects about the adsorption of quinoline on fibrous silicates and Patagonian saponite. Appl Clay Sci., 33(2), 142-148.

Viseras, C., Cerezo, P., Sanchez, R., Salcedo, I., Aguzzi, C., 2010. Current challenges in clay minerals for drug delivery. Appl. Clay Sci.; 48(3), 291–295.

Vogels, R.J.M.J., Breukelaar, J., Kloprogge, J.T., Jansen, J.B.H., Geus, J.W., 1997. Hydrothermal crystallisation of ammonium-saponite at 200 ºC and autogeneous water pressure. Clays Clay Miner. 45, 1–7.

Vogels, R.J.M.J., Kloprogge, J.T., Geus, J.W., 2005. Catalytic activity of synthetic saponite clays: effects of tetrahedral and octahedral composition. J. Catal. 231, 443–452.

Vollrath, F., Knight, D. P., 2001. Liquid crystalline spinning of spider silk. Nature 410(6828), 541-548.

Wang, W. J., Chin, W. K., Wang, W. J., 2002. Synthesis and structural characterizations of [chromophore]+-saponite/polyurethane nanocomposites. J. Polym. Sci. B: Polym Phys. 40(15), 1690-1703.

Wilson, R. 1991. Kirk-Othmer Encyclopedia of Chemical Technology, John Wiley & Sons, New York, 4.

Wood, T. F., Clifton, N. J., 1950. Process for preparing beta-phenyl ethyl alcohol. U. S. Pat 2524096.

Xu, M., Choi, Y. S., Kim, Y. K., Wang, K. H., Chung, I. J., 2003. Synthesis and characterization of exfoliated poly(styrene-co-methyl methacrylate)/clay nanocomposites via emulsion polymerization with AMPS. Polym. 44(20), 6387-6395.

Xue, S., Pinnavaia, T.J., 2008. Porous synthetic smectic clay for the reinforcement of epoxy polymers. Microporous Mesoporous Mater. 107, 134–140.

Yadav V. G., Chandalia S. B., 1998. Synthesis of Phenethyl Alcohol by Catalytic Hydrogenation of Styrene Oxide. Org. Proc. Res. Dev. 2(5), 294-297.

Yao, M., Liu, Z.Y., Wang, K.X., Zhu, M.Q., Sun, H.J. 2005. Application of FTIR technique in microwave-hydrothermal synthesis of saponite. Guang Pu Xue Yu Guang Pu Fen Xi, 25, 870-873.

Zhang, J., Wilkie, C. A., 2004. A carbocation substituted clay and its styrene nanocomposite. Polym. Degrad. Stab. 83(2), 301-307.

Zhang, D., Zhou, C. H., Lin, C. X., Tong, D. S., Yu, W. H. 2010. Synthesis of clay minerals. Appl. Clay Sci. 50, 1-11.

Zhao, Q., Samulski, E. T., 2006. A comparative study of poly(methyl methacrylate) and polystyrene/clay nanocomposites prepared in supercritical carbon dioxide. Polym. 47(2), 663-671.

Zhou, C. H., 2010. Emerging trends and challenges in synthetic clay-based materials and layered double hydroxides. Appl. Clay Sci. 48, 1-4.

Zhu Y. J., Zhou, H. T., Hu, Y. H., 2011. Antityrosinase and antimicrobial activities of 2-phenylethanol, 2-phenylacetaldehyde and 2-phenylacetic acid. Food Chemistry. 124, 298-302.

Zielke, R.C., Pinnavaia, T.J., 1988. Modified clays for the adsorption of environmental toxicants: binding of chlorophenols to pillared, delaminated, and hydroxy-interlayered smectites. Clays Clay Miner. 36(5), 403–408.